Halvor Lund

Relaxation models for two-phase flow with applications to CO$_2$ transport

Halvor Lund

Doctoral Thesis

NTNU – Trondheim
Norwegian University of
Science and Technology

NTNU – Trondheim
Norwegian University of
Science and Technology

NTNU

Halvor Lund

Relaxation models for two-phase flow with applications to CO$_2$ transport

Thesis for the degree of Philosophiae Doctor

Trondheim, August 2013

Norwegian University of Science and Technology
Faculty of Engineering Science & Technology
Department of Energy and Process Engineering

NTNU – Trondheim
Norwegian University of
Science and Technology

NTNU
Norwegian University of Science and Technology

Thesis for the degree of Philosophiae Doctor

Faculty of Engineering Science & Technology
Department of Energy and Process Engineering

Abstract

This thesis presents mathematical models for two-phase pipeline flow, with an emphasis on applications to CO_2 pipeline flow, as well as numerical methods suitable for solving these models. The considered models form a hierarchy of homogeneous (single-velocity) two-phase flow models with *relaxation terms* that account for transfer processes between the two phases. The relaxation terms model heat, mass and volume transfer caused by differences in temperature, chemical potential and pressure, respectively.

The basis of the model hierarchy is a six-equation model with all three relaxation processes present. The rest of the hierarchy is then derived by assuming that one or more of the relaxation processes are infinitely rapid, which results in equilibrium in pressure, temperature and/or chemical potential, which makes a total of eight models. The models are formulated using conservation laws for mass, momentum and energy as well as an advection equation for the gas volume fraction. It is shown that the subcharacteristic condition, which is related to the stability of such models, translates to the requirement that the speed of sound is reduced when a new equilibrium condition is introduced. Expressions for the speeds of sound in the eight models are derived and proven to satisfy the subcharacteristic condition.

A mass-transfer model for pipeline flow based on statistical rate theory is derived and formulated as a chemical-potential relaxation term in the pressure-temperature equilibrium model of the hierarchy. The model is used to simulate depressurization of a CO_2 pipeline, and the results are found to be quite close to those of the full-equilibrium model. An exponential time-differencing scheme tailor-made for relaxation terms is applied to the model and compared to the Backward Euler method. The exponential time-differencing scheme is an explicit method, but it relies on knowledge of the equilibrium of the relaxation process. The mass-transfer equilibrium value has to be calculated using a Newton-Raphson iteration, which essentially makes both methods implicit, and comparable in both computational cost and accuracy.

Finally, the Rankine-Hugoniot-Riemann (RHR) solver is presented, which aims to solve multidimensional conservation laws with source terms. The solver introduces the novel idea of treating flux gradients in other dimensions as additional source terms. The source term and cross-flux term is placed as a singular source in the centre of each cell, which causes a jump in the solution according to a Rankine-Hugoniot condition. The states on

either side of a cell interface then define a Riemann problem that is solved by an approximate Riemann solver. The RHR solver is shown to be of second order in space for a 2D scalar advection equation, the 2D isothermal Euler equations and the 2D shallow water equations.

Preface

The work presented in this thesis was carried out in the period September 2010 to June 2013, at the Department of Energy and Process Engineering at the Norwegian University of Science and Technology (NTNU). Professor Bernhard Müller has been my main supervisor, and Svend Tollak Munkejord at SINTEF Energy Research and Tore Flåtten at SINTEF Energy Research/SINTEF Materials and Chemistry have been co-supervisors.

My main supervisor, Bernhard Müller, deserves thanks for always being friendly, very knowledgeable on computational fluid mechanics, and very thorough whenever giving me feedback. He has allowed me the freedom I needed to pursue my own ideas, while still ensuring that I was on track so that I finished my PhD work on time, which I am very grateful for.

Bernhard Müller also contributed to making it possible for me to work with Patrick Jenny's group at ETH Zürich in Switzerland from January till August 2012, which I very much enjoyed. Professor Patrick Jenny and his group deserve many thanks for allowing me to visit and for including me in their group, which made my visit fruitful both at work and off work.

I would like to thank Tore Flåtten for encouraging me to go my own ways, for many interesting discussions on relaxation systems, and for recognizing the potential of my work when I didn't. Svend Tollak Munkejord also deserves credit for introducing me to the field of two-phase flow and finite-volume numerics, giving good feedback on my articles, as well as arranging the financial support of my PhD project as the project leader of CO_2 Dynamics.

As office mates during two of the last three years, Karl Yngve Lervåg and I have shared many of the sorrows and joys of the life as PhD students, and thanks to him, my work has felt far less lonely than it could have felt. Last, but not least, I would like to thank all my other colleagues at the department.

<div style="text-align: right">

Trondheim, May 2013
Halvor Lund

</div>

Contents

Il n'existe pas de sciences appliquées, mais seulement des applications de la science.

Louis Pasteur (1822–1895)

1 Introduction

Flow of gas and liquid, known as two-phase flow, has a large range of industrial applications. Such applications include heat exchangers [42], water-steam flow in the cooling system of nuclear reactors [12], flow of oil, gas and water in petroleum production [79], and CO_2 pipeline transport in a carbon capture and storage (CCS) infrastructure [3, 10, 22, 37]. The latter has been the motivation for the present thesis.

Carbon dioxide capture and storage will potentially be an important contribution to reducing the emissions of carbon dioxide from stationary sources. In the two-degree scenario (2DS) [36] of the International Energy Agency (IEA), CCS will account for a reduction of carbon dioxide emissions of seven gigatonnes per year in 2050. CCS aims to capture CO_2 from, for example, the flue gas from a power plant or chemical processing plant, and then store it in geological formations. Since the point of capture and point of storage may be far apart, some form of transport is necessary, and due to the large volumes to be transported, pipelines are often the most viable option [37].

For four decades, pipelines have been used to transport CO_2 from various natural and anthropogenic (man-made) sources and used for enhanced oil recovery (EOR), most notably in the United States. However, CO_2 transported in a CCS infrastructure may be subject to other standards than those that apply to EOR, such as requirements on the chemical composition

of the mixture transported, and on pipeline safety [37]. Transport of CO_2 will typically take place at high pressure, at conditions where CO_2 is in its dense (supercritical) phase. However, incidents like a controlled or uncontrolled depressurization may cause CO_2 to enter the two-phase region, with gas and liquid coexisting. When the pressure drops, liquid will evaporate to gas, causing a temperature drop, which in turn may cause the pipe steel to turn brittle and break more easily [10].

To predict the behaviour of two-phase flow in pipes, one needs good mathematical models. This has been the subject of research for decades [24, 38, 76], and has to a large extent been focused on the nuclear industry and petroleum production. Chapter 2 provides an overview of the research on such models. Since these models typically are too complex to solve analytically, numerical methods are necessary. The first methods for fluid dynamics were developed in the 1960s [32], and since then numerical methods have become more and more important as the available computational capacity has increased dramatically. A wide range of methods has emerged, which is discussed in Chapter 3.

There are already a number of simulation tools for multiphase flow available, especially in the nuclear and oil and gas industries. For safety analysis for nuclear reactors, the CATHARE [11] and RELAP5 [13] codes are of the most common, while the oil and gas industry has developed tools such as OLGA [8] and LedaFlow [21]. These codes are typically tailor-made for certain situations, with a number of empirically based correlations and considerations, thus they may not be suitable for applications for which they were not specifically designed, such as CO_2 pipeline transport.

This thesis follows a more fundamental path, by developing models based on the basic principles of physics as much as possible, which in turn may lead to more rigorous engineering models in the future. For incidents such as depressurization of a CO_2 pipeline and similar two-phase flow situations, it is important to be able to predict how heat and mass is transferred between the two phases, for example, how fast the liquid evaporates, and how each phase expands due to pressure differences. Other relevant physical processes are friction that the fluid experiences from the pipe walls, and heat transferred through the pipe walls to the surroundings. This may often be modelled using *relaxation terms*, which is a recurring theme in the work presented in this thesis. The relaxation processes considered are heat, mass and volume transfer, which are caused by differences in temperature, chemical potential and pressure, respectively, bringing the two phases back to equilibrium. This is explained more closely

in Section 2.2.

1.1. Goals

The main goal of this work has been to investigate how interactions between the gas and liquid phases in a two-phase flow model affect the wave velocities of that model. More specifically, the thesis considers how transfer of mass, heat and volume between the two phases affects the speed of sound, and how the speeds of sound in different models relate to each other. The transfer processes were expressed as *relaxation terms*. In addition, we aimed to develop a two-phase flow model with a mass transfer term based on basic physical principles rather than empirical correlations.

Another important goal was to develop robust finite-volume methods that were able to deal with source terms due to relaxation processes. These new numerical methods were necessary to solve the developed models accurately and reliably.

1.2. Thesis outline

The thesis is organized as follows: Chapter 2 gives an introduction to the modelling of two-phase flow, and introduces a hierarchy of two-phase flow models with different combinations of relaxation processes included. Two of the models are described in more detail, and the need for thermodynamic relations in the form of equations of state is also addressed. Next, Chapter 3 gives an overview of numerical methods for solving two-phase flow equations, and gives a short introduction to finite-volume methods. It then introduces the Rankine-Hugoniot-Riemann solver, which is constructed to solve general multidimensional conservation laws with source terms, and an exponential time-differencing scheme (similar to an exponential integrator) used to solve a relaxation model in time. Chapter 4 summarizes the results from each of the papers included in the thesis, and gives a brief description of my contribution to each paper. Finally, Chapter 5 summarizes and concludes the work, and outlines possibilities for further work. The full-text research papers are included in Appendix A at the end of the thesis.

The purpose of models is not to fit the data
but to sharpen the questions.

   Samuel Karlin (1924–2007)

2
Two-phase flow modelling

To provide a formal description of physical phenomena such as two-phase flow, we construct mathematical models that incorporate the most important properties of the phenomenon we wish to study. For single-phase flow, well-proven mathematical models exist, such as the Navier-Stokes equations (for viscous flow) or the Euler equations (for inviscid flow). For two-phase flow, however, constructing a model which incorporates all the relevant physics is a far more complex task. On the one hand, we seek a model which describes the physical reality as accurate as possible. On the other hand, a simpler model is often easier to treat mathematically and to implement, and computationally less expensive.

Two-phase (and multiphase) flow modelling has been subject to an increasing amount of research for half a century [24, 38, 76]. Such modelling is particularly challenging much due to the need to resolve the possibly complex movement and shape of the interface between the two phases, and the heat and mass transfer across it. In situations where the exact shape of the interface is of little importance, one can use the process of *averaging* (cf. Drew and Passman [25]), which averages the full model over an ensemble or a certain volume or time span. This leads to new systems of equations that allow gas and liquid to coexist at each location, without any notion of an interface.

Ishii [38, 39] introduced one of the first and most well-known averaged

two-phase flow models, which was time-averaged. Later, Baer and Nunziato [4] presented a comprehensive two-fluid model for the detonation-to-deflagration transition (DDT), where the two phases are solid and gas, while Stewart and Wendroff [77] derived a range of two-phase flow models for liquid-gas flow. In the last decades, a wide range of averaged two-phase flow models have been developed, and the following sections will provide an overview of the fluid-mechanical and thermodynamical aspects of such models.

2.1. Fluid dynamics

Fluid-mechanical models for two-phase flow are, as mentioned in the previous section, often averaged over a certain area or volume, or averaged over an *ensemble* (see Drew and Passman [25]) of realizations of a system. This removes the need to explicitly track or otherwise resolve the interface between the two phases. However, it introduces the need to model such phenomena as interfacial friction, the relation between the velocity of the gas and liquid, and heat and mass transfer using more empirical relations rather than first principles.

In the following, we will mostly consider one-dimensional flow models. This is justified by the fact that pipeline flow, which is our main interest, can be considered to be one-dimensional, because the flow varies much more in the axial direction of the order of kilometres than in the cross-section for diametres of the order of 1 meter.

There exist two main classes of averaged two-phase flow models: two-fluid models and drift-flux models. The two-fluid models allow the two phases to have independent velocities, and model the interaction through a relation for interfacial friction (see e.g. Refs. [4, 54, 70, 91]). Classical two-fluid models (see e.g. Refs. [8, 11, 77, 87]) are often *ill-posed* or non-hyperbolic, that is, they possess complex eigenvalues, thus their solutions do not depend continuously on initial values [44, 77, 82]. Two-fluid models are outside the scope of this thesis, and will not be discussed in more detail.

Drift-flux models, on the other hand, let the phase velocities depend explicitly on each other using a *slip relation*. They are most often hyperbolic, that is, possess real eigenvalues, which makes them more mathematically tractable. The hyperbolicity may be lost if the velocity difference is too large, see e.g. Flåtten and Munkejord [29]. The research of drift-flux models

can be said to have been initiated by Zuber and Findlay [92]. The Baer and Nunziato [4] model has been influential also for drift-flux models. Kapila et al. [43] developed two no-slip (single-velocity) drift-flux models for DDT, based on the Baer and Nunziato [4] model, which were also considered by Saurel et al. [73] and Pelanti and Shyue [66]. The numerical code TACITE [65] uses a drift-flux model for pipeline simulation, with a range of slip relations for different flow regimes. Numerical methods specifically made for drift-flux models include those of Romate [69], Baudin et al. [6, 7], and Flåtten and Munkejord [29].

Drift-flux models take advantage of the fact that the velocities of the gas and the liquid in a two-phase flow are often closely related. This relation may be expressed using a slip relation,

$$v_{\mathrm{g}} - v_{\ell} = \Phi(\alpha_{\mathrm{g}}, p, T, v_{\mathrm{g}}),$$

where v_{g} and v_{ℓ} are the velocities of the gas and liquid, respectively, p is the pressure and T is the temperature. The gas volume fraction is defined as

$$\alpha_{\mathrm{g}} = \frac{V_{\mathrm{g}}}{V}, \tag{2.1}$$

where V_{g} is the volume occupied by gas and V is the total volume.

The empirical relation Φ then gives an expression for the velocity difference as a function of the flow variables. One commonly used slip relation is the Zuber-Findlay [92] relation, which is based on empirical measurements of bubbly flow. Evje and Flåtten [27] give an interesting derivation of how a drift-flux model with a slip relation can be transformed into an equivalent two-fluid model with an interfacial friction term.

Choosing the right slip relation for a given flow situation is not straightforward, and doing rigorous analysis of models including a slip relation is generally harder. So in the following we will consider only models with no slip, that is, $v_{\mathrm{g}} = v_{\ell} = v$. Such models are also known as *homogeneous* flow models. Section 2.2 gives a more thorough description of the drift-flux models used in this work.

2.2. Hierarchy of drift-flux models

In an averaged two-phase flow model which is as general as possible, one may expect the two phases to have their own velocities, pressures, temperatures and chemical potentials. The interaction between the two

phases can then be modelled using *relaxation terms*, which serve to bring the two phases back to equilibrium. Velocity differences will cause transfer of momentum, temperature differences will cause heat transfer, differences in chemical potential will cause mass transfer (that is, condensation and evaporation), and pressure differences cause the phase with the highest pressure to expand, that is, volume transfer.

In papers L1 and L2, we consider a drift-flux model with the same velocity in each phase, also known as a *homogeneous* drift-flux model. We are then left with three relaxation processes, for heat, mass and volume transfer. To simplify the model further, each of these relaxation processes may be assumed to *always* be in equilibrium, so that the two phases have equal pressure, temperature and/or chemical potential. Each combination of such equilibrium assumptions will give rise to a model with other properties than the model with all the relaxation processes present. This can be interpreted as a *hierarchy* of relaxation models, which is illustrated in Figure 2.1.

In Figure 2.1, each circle symbolizes a model, identified by the variables that are in equilibrium, that is, equal in the two phases, in that particular model. An arrow denotes how one model is derived from another by assuming equilibrium in a variable. The left-most model (0) is the basic model in which all three relaxation processes are present. As we move rightward through the hierarchy, more and more equilibrium assumptions are added, which finally leads to the homogeneous equilibrium model ($pT\mu$). The work done in paper L1 is marked by dashed lines, while the work in paper L2 is shown with solid lines.

The models in this hierarchy were formulated as hyperbolic relaxation systems with source terms accounting for heat, mass and volume transfer between the phases, written generally in the form

$$\frac{\partial \mathbf{u}}{\partial t} + \mathbb{A}(\mathbf{u})\frac{\partial \mathbf{u}}{\partial x} + \frac{1}{\varepsilon}\mathbf{R}(\mathbf{u}) = \mathbf{0}, \tag{2.2}$$

where $\mathbf{u} \in \mathbb{R}^n$ is the vector of unknowns, and ε is a characteristic time for the relaxation processes described by $\mathbf{R}(\mathbf{u})$. For the model to be hyperbolic, we require the $n \times n$ matrix $\mathbb{A}(\mathbf{u})$ to be diagonalizable with real eigenvalues. Such relaxation systems have been analysed by Liu [52], Chen et al. [14] and Yong [90].

The following sections will first present the basic model, on which the hierarchy is based. Next, the notion of the subcharacteristic condition is explained, which is relevant for the stability of relaxation systems and
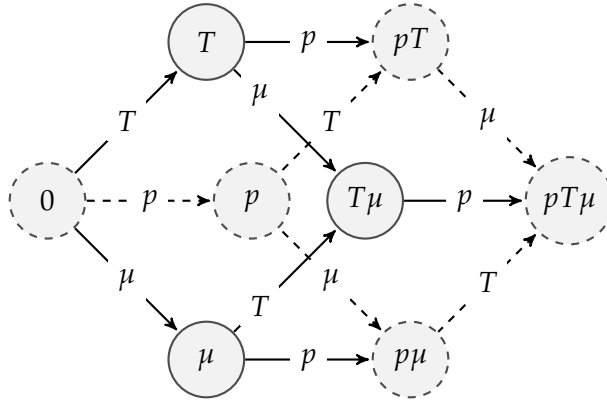
Figure 2.1.: Model hierarchy (adapted from Lund (L2)). Each circle symbolizes a two-phase flow model with equilibrium in zero or more of the variables p (pressure), T (temperature) and μ (chemical potential). An arrow represents a relaxation process of one variable, pointing in the direction of equilibrium in that variable. Dashed lines denote results from Flåtten and Lund (L1), while solid lines indicate results from Lund (L2).

which relates the wave velocities of different models to each other. Finally, two other models in the hierarchy are discussed, namely the pT- and $pT\mu$-models, since they have been used for simulations in papers L3 and L4.

2.2.1. The basic model

The basic model of the hierarchy was introduced by Flåtten and Lund [L1], and can be formulated using six equations that express conservation of momentum, balance of mass and energy, and advection of the gas volume fraction. The mass-balance equations are written as

$$\frac{\partial(\alpha_g\rho_g)}{\partial t} + \frac{\partial(\alpha_g\rho_g v)}{\partial x} = \mathcal{K}(\mu_\ell - \mu_g), \tag{2.3}$$

$$\frac{\partial(\alpha_\ell\rho_\ell)}{\partial t} + \frac{\partial(\alpha_\ell\rho_\ell v)}{\partial x} = \mathcal{K}(\mu_g - \mu_\ell), \tag{2.4}$$

where α_k is the volume fraction of phase k, ρ_k is the density of phase k and v is the velocity of the two phases. The right-hand-side relaxation term involves the chemical potential relaxation parameter $\mathcal{K} \geq 0$, and the chemical potential (or Gibbs free energy) μ_k of phase k. The chemical potential is a function of the pressure and temperature in the phase, given

by $\mu = e + p/\rho - Ts$ where s is the entropy. The relaxation term describes how mass is transferred between the two phases due to differences in chemical potential.

The advection equation for the gas volume fraction can be written as

$$\frac{\partial \alpha_g}{\partial t} + v \frac{\partial \alpha_g}{\partial x} = \mathcal{J}(p_g - p_\ell). \tag{2.5}$$

This follows from averaging and the assumption that in Lagrangian coordinates, only pressure differences will cause volume transfer between the phases. Such models have been used by a number of other authors, see e.g. Refs. [4, 70]. Here $\mathcal{J} \geq 0$ is the pressure-relaxation parameter, and p_k the pressure in phase k. In Lagrangian coordinates, we see that the relaxation term causes the phase with the highest pressure to expand at the cost of the other, as $p_g > p_\ell$ would cause the gas volume fraction to increase over time.

Next, the basic model can be expressed using a single momentum conservation equation, since the two phases have the same velocity. It is written as

$$\frac{\partial (\rho v)}{\partial t} + \frac{\partial (\rho v^2 + \alpha_g p_g + \alpha_\ell p_\ell)}{\partial x} = 0, \tag{2.6}$$

where $\rho \equiv \alpha_g \rho_g + \alpha_\ell \rho_\ell$ is the total density. The effective pressure is $p_{\mathrm{eff}} \equiv \alpha_g p_g + \alpha_\ell p_\ell$, which follows from the fact that the total force on a cross-section of the pipe is the sum of the forces exerted by the gas and the liquid.

Finally, the energy balance equations are written as

$$\frac{\partial E_g}{\partial t} + \frac{\partial (v E_g)}{\partial x} + \alpha_g p_g \frac{\partial v}{\partial x} + \frac{v}{\rho} \alpha_g \rho_g \frac{\partial (\alpha_g p_g + \alpha_\ell p_\ell)}{\partial x}$$
$$= \mathcal{H}(T_\ell - T_g) + p^* \mathcal{J}(p_\ell - p_g) + \left(\mu^* + \frac{1}{2} v^2 \right) \mathcal{K}(\mu_\ell - \mu_g), \quad (2.7)$$

$$\frac{\partial E_\ell}{\partial t} + \frac{\partial (v E_\ell)}{\partial x} + \alpha_\ell p_\ell \frac{\partial v}{\partial x} + \frac{v}{\rho} \alpha_\ell \rho_\ell \frac{\partial (\alpha_g p_g + \alpha_\ell p_\ell)}{\partial x}$$
$$= \mathcal{H}(T_g - T_\ell) + p^* \mathcal{J}(p_g - p_\ell) + \left(\mu^* + \frac{1}{2} v^2 \right) \mathcal{K}(\mu_g - \mu_\ell), \quad (2.8)$$

where $E_k \equiv \alpha_k \rho_k (e_k + \frac{1}{2} v^2)$ is the total energy per volume, and e_k the internal energy, of phase k. These were derived based on the assumptions that each relaxation process should conserve energy, and that in

Lagrangian coordinates, entropy is produced only by the relaxation terms. The first right-hand-side term is the heat-transfer term, governed by the temperature-relaxation parameter $\mathcal{H} \geq 0$, as well as the difference between the temperatures T_k of phase k. The pressure and chemical potential at the gas-liquid interface are denoted p^* and μ^*, respectively. These were expressed as convex combinations of the gas and liquid pressures and chemical potentials, respectively [L1].

The basic model was shown to satisfy the first and second laws of thermodynamics. It is very similar to models introduced by Kapila et al. [43] and discussed by Saurel et al. [73] and Pelanti and Shyue [66].

The relaxation parameters $\mathcal{K}$, $\mathcal{J}$ and $\mathcal{H}$ may depend on flow parameters. When it comes to the time scale of each relaxation process, which is directly related to the magnitude of the parameters $\mathcal{K}$, $\mathcal{J}$ and $\mathcal{H}$, Kapila et al. [43] and Zein et al. [91] give some interesting considerations, not for gas-liquid pipeline flow, but for the detonation-to-deflagration transition. They note that the velocity-relaxation length of the Baer and Nunziato [4] model is of the order of the grain size, which justifies the single-velocity assumption. Chinnayya et al. [15] and Petitpas et al. [67] discuss the velocity and pressure relaxation parameters in their models, and justify that these can be considered to be infinite for DDT cases. Petitpas et al. [67] also argue that the temperature relaxation parameter is much smaller than the ones for velocity and pressure.

By letting the relaxation parameters $\mathcal{K}$, $\mathcal{J}$ and/or $\mathcal{H}$ go to infinity, one can derive new models where the chemical potentials μ_k, pressures p_k and/or temperatures T_k, respectively, are in equilibrium. Significant parts of the papers L1 and L2 are devoted to relating the wave velocities of the different models. In this process, the *subcharacteristic condition* has been a central aspect, which will be explained more closely in the next section.

2.2.2. The subcharacteristic condition

The *subcharacteristic condition* is a concept that is closely related to the stability of relaxation systems in the form (2.2). In particular, Yong [90] introduced a certain stability requirement on the relaxation system (2.2) and showed that this requirement leads to *a)* convergence of the solution in the limit $\varepsilon \to 0$, and *b)* the subcharacteristic condition being fulfilled.

The formal definition of this condition can be found in papers L1 and L2, but it may be summarized as the requirement that the wave velocities $\tilde{\lambda}_i$ of an equilibrium system should be interlaced with the wave velocities λ_i of

the relaxation system. If the equilibrium and relaxation systems have k and n wave velocities, respectively, this means that $\lambda_i \leq \tilde{\lambda}_i \leq \lambda_{i+n-k}$. In the context of our hierarchy, this translates to the requirement that the speed of sound of an equilibrium system should be smaller than (or equal to) the speed of sound of the corresponding relaxation system. In other words, for each equilibrium assumption we make on the chemical potentials μ_k, pressures p_k or temperature T_k in the basic model in Section 2.2.1, the speed of sound cannot increase.

More specifically, we show in papers L1 and L2 how the speed of sound $\tilde{a}$ of an equilibrium model $\mathcal{X}$ and the corresponding relaxation (non-equilibrium) model $\mathcal{Y}$ can be written as

$$\tilde{a}_{\mathcal{X}}^{-2} = \tilde{a}_{\mathcal{Y}}^{-2} + Z_{\mathcal{X}}^{\mathcal{Y}}, \tag{2.9}$$

where $Z_{\mathcal{X}}^{\mathcal{Y}}$ is a non-negative term expressed using sums of squares. The speed of sound in two-phase models is of particular interest to us, since it determines how fast pressure waves propagate in industrially relevant cases such as a pipeline depressurization.

Conditions similar to the subcharacteristic condition have been discussed by Leray [47] and Whitham [88], but we follow the more recent work of Liu [52]. Many physical models satisfy this condition, and it is mentioned by a number of authors, e.g. Baudin et al. [6, 7] and Flåtten et al. [28].

2.2.3. The pT-model with phase transfer

This section will go into detail of the pT model with phase transfer, a model in which the two phases have the same pressure p and temperature T, but still with two mass balance equations to allow the effects of phase transfer to be included. In general, we can write this model as

$$\frac{\partial(\alpha_g \rho_g)}{\partial t} + \frac{\partial(\alpha_g \rho_g v)}{\partial x} = \Gamma_g, \tag{2.10}$$

$$\frac{\partial(\alpha_\ell \rho_\ell)}{\partial t} + \frac{\partial(\alpha_\ell \rho_\ell v)}{\partial x} = \Gamma_\ell, \tag{2.11}$$

$$\frac{\partial(\rho v)}{\partial t} + \frac{\partial(\rho v^2 + p)}{\partial x} = 0, \tag{2.12}$$

$$\frac{\partial E}{\partial t} + \frac{\partial[(E+p)v]}{\partial x} = 0, \tag{2.13}$$

where $E = E_g + E_\ell$ is the total energy per volume. This model may be argued to be one of the simplest possible two-phase flow models that

includes the effect of phase transfer, since such models would require at least two mass equations and a momentum equation. It has been discussed by Lund and Aursand [L3, L4], and also by Flåtten et al. [28].

There does not seem to be any common agreement in the literature upon how mass transfer should be modelled. A number of authors use models in a relaxation form, but by relaxing different variables. Chung et al. [16] model mass transfer with

$$\Gamma_{\mathrm{g}} = -\Gamma_{\ell} = \frac{\alpha_{\mathrm{g}}\alpha_{\ell}}{h_{\mathrm{g,s}} - h_{\ell,\mathrm{s}}} \left[\eta_{\ell}\rho_{\ell}c_{p,\ell}(T_{\ell} - T_{\mathrm{s}}) + \eta_{\mathrm{g}}\rho_{\mathrm{g}}c_{p,\mathrm{g}}(T_{\mathrm{g}} - T_{\mathrm{s}}) \right], \quad (2.14)$$

where $h_{k,\mathrm{s}} = e_k + \frac{p}{\rho_k}$ is the specific saturation enthalpy for phase k, T_{s} is the saturation temperature, $c_{p,k}$ is the specific heat capacity at constant pressure for phase k, and η_k are empirical constants.

A variant of this model is the one used by Cortes [18],

$$\Gamma_{\mathrm{g}} = -\Gamma_{\ell} = \frac{\alpha_{\mathrm{g}}\alpha_{\ell}}{h_{\mathrm{g,s}} - h_{\ell,\mathrm{s}}} \left[\eta_{\ell}\rho_{\ell}(h_{\ell} - h_{\ell,\mathrm{s}}) + \eta_{\mathrm{g}}\rho_{\mathrm{g}}(h_{\mathrm{g}} - h_{\mathrm{g,s}}) \right],$$

which is equivalent to (2.14) if we assume c_p to be constant. Toumi [82] also uses a similar model, but points out that it is not chosen for its physical validity, but rather for its simplicity.

Saurel et al. [72] model the mass transfer with relaxation of the chemical potential with the relaxation parameter $\mathcal{K}$,

$$\Gamma_{\mathrm{g}} = -\Gamma_{\ell} = \mathcal{K}(\mu_{\ell} - \mu_{\mathrm{g}}). \quad (2.15)$$

A similar formulation of mass transfer is discussed by Stewart and Wendroff [77].

Common for all these models is that they heavily depend on empirical constants whose correct value may be difficult to determine. With this in mind, we hoped to derive a mass transfer model which to a larger degree was based on first principles. In paper L3, we developed a new phase transfer model based on *statistical rate theory*, giving a model in the form (2.15), but with an explicit expression for $\mathcal{K}$ depending on the volume fractions, the gas density and the temperature. We applied the model to a CO_2 pipeline depressurization case, and compared it to a simpler model with a constant coefficient $\mathcal{K}$.

2.2.4. The homogeneous equilibrium ($pT\mu$) model

The homogeneous equilibrium model, denoted $pT\mu$ in Figure 2.1, has been used for a number of different two-phase flow applications, see e.g.

Refs. [17, 53, 72, 78]. Mathematically, it can be formulated just as the single-phase Euler equations, but with a more complex mixture equation of state for the pressure p. It may be derived by adding the two mass equations (2.10)–(2.11) in the pT-model, which together with the momentum equation (2.12) and the energy equation (2.13) read

$$\frac{\partial \rho}{\partial t} + \frac{\partial \rho v}{\partial x} = 0, \tag{2.16}$$

$$\frac{\partial (\rho v)}{\partial t} + \frac{\partial (\rho v^2 + p)}{\partial x} = 0, \tag{2.17}$$

$$\frac{\partial E}{\partial t} + \frac{\partial [(E + p)v]}{\partial x} = 0. \tag{2.18}$$

By also letting the chemical potential relaxation parameter $\mathcal{K}$ go to infinity, we know that the two chemical potentials are equal, $\mu_g = \mu_\ell$. Such an instant equilibrium in the mass transfer process is also known as flash evaporation or flash condensation.

To solve for the pressure p as a function of the known conserved variables, that is, density ρ, momentum density ρv and total energy E, one needs an equation of state. For the stiffened gas equation of state (which will be described in the next section) for each phase, this involves solving a transcendental equation, and is therefore done numerically, as described by Lund and Aursand [L4, Sec. 3].

Saurel et al. [72] showed that the speed of sound $c_{pT\mu}$ of the homogeneous equilibrium model can be written as

$$c_{pT\mu}^2 = \frac{1}{\rho} \left(\frac{\alpha_g}{\rho_g c_g^2} + \frac{\alpha_\ell}{\rho_\ell c_\ell^2} + T \left[\frac{\alpha_g \rho_g}{c_{p,g}} \left(\frac{\mathrm{d}s_g}{\mathrm{d}p} \right)^2 + \frac{\alpha_\ell \rho_\ell}{c_{p,\ell}} \left(\frac{\mathrm{d}s_\ell}{\mathrm{d}p} \right)^2 \right] \right)^{-1}, \tag{2.19}$$

where c_k is the speed of sound and s_k the entropy per mass of phase k. The entropy derivatives are evaluated at the boiling point. A peculiar property of this speed of sound is that it is *discontinuous* at the transition between a pure phase (gas or liquid) and a two-phase mixture. In other words, $c_{pT\mu}(\alpha_\ell = 1) \neq c_\ell$ and $c_{pT\mu}(\alpha_g = 1) \neq c_g$. This discontinuous behaviour has not been observed experimentally, see e.g. Kieffer [45] or Coste et al. [19], hence it is most probably not a real physical effect, but rather an indication that the modelling assumptions are somewhat crude. This may mean that the homogeneous equilibrium model is not ideal in cases where a correct value of the speed of sound is important. However, an advantage with this model is that no explicit modelling of phase transfer is needed.

The homogeneous equilibrium model has been used as a reference model by Lund and Aursand [L3], and was also used for simulation of depressurization of a CO_2 pipeline by Lund et al. [53].

2.3. Equation of state

To be able to relate state variables such as pressure (p), density (ρ), internal energy (e) and temperature (T) to each other, we need an *equation of state* (EOS). One of the simplest and most well-known equations of state is the ideal gas law, first stated by Clapeyron in 1834, which may be expressed as

$$p = \rho R T, \tag{2.20}$$

where R is the specific gas constant of the gas. The ideal gas law works well for gases at low pressure, but for liquids and higher pressures, it fails to give accurate predictions.

Later, more accurate and complex equations of state were suggested, such as the class of *cubic equations of state*. The first of this class was proposed by van der Waals in 1873, and may be written as [46]

$$\left(p + \frac{a}{V_m^2} \right) (V_m - b) = RT, \tag{2.21}$$

where V_m is the molar volume and a and b are constants specific for each material. This equation has a more realistic description of the behaviour of a substance, since it includes interactions between molecules and the volume of each molecule. More recently, the cubic equations of states have been developed further to give more accurate results, such as the Redlich-Kwong equation [68] and the Soave-Redlich-Kwong (SRK) equation. A thorough review of cubic EOS'es can be found e.g. in the work of Valderrama [85]. There exist a number of more advanced equations of state, such as those based on the (extended) corresponding state principle [41].

A slight disadvantage of cubic and more advanced equations of state, however, is that analytical, closed-form relations between the different thermodynamical variables are hard or impossible to obtain. Therefore, whenever an equation of state was needed in the works presented in this thesis, we have used the *stiffened gas* EOS (advocated by e.g. Menikoff [55, 56]), which may be seen as a linearization of a more complex EOS. It is mathematically similar to the ideal gas law, but has a stiffening term that allows a finite density at zero pressure, which is crucial to model liquids.

The stiffened gas pressure can be written as [55]

$$p(\rho, T) = \rho(\gamma - 1)c_v T - p_\infty. \tag{2.22}$$

With the stiffening pressure set to zero, $p_\infty = 0$, this pressure law is identical to the ideal gas law (2.20). In a more general (and complete) sense, the stiffened gas can be defined using its expression for the Helmholtz free energy, which is given by [55]

$$A(\rho, T) = c_v T \left(1 - \ln \left(\frac{T}{T_0} \right) + (\gamma - 1) \ln \left(\frac{\rho}{\rho_0} \right) \right) - s_0 T + \frac{p_\infty}{\rho} + e_*, \tag{2.23}$$

where c_v is the heat capacity at constant volume, $\gamma = c_p / c_v$ is the ratio of specific heats, p_∞ is a stiffening pressure, and e_* is a reference internal energy. T_0, ρ_0 and s_0 are the reference temperature, density and entropy, respectively. These constants can be determined using a more complex equation of state, or empirical measurements, such that the EOS is reasonably accurate in the range of pressures and temperatures that one wants to study.

All the relations between different thermodynamical properties can be derived rather trivially from the Helmholtz free energy, such as the pressure equation (2.22). Thus the stiffened gas EOS is a suitable choice if one wants to avoid the computational complexity associated with more advanced equations of state, but still requires reasonable accuracy for a certain temperature and pressure range. Comparisons of the stiffened gas EOS to experimental values can be found in e.g. the works of Saurel and Abgrall [71], and Menikoff and Plohr [55].

I hear and I forget.
I see and I remember.
I do and I understand.

    Confucius (551–479 BC)

3

Numerical methods

Equations for two-phase flow are typically far too complex to be solved analytically, at least for most relevant industrial applications. Thus we rather solve them *numerically*. The first step is to *discretize* the continuous problem at hand to make a discrete one. Next, one needs a *numerical method* to solve this discrete problem.

    The choice of numerical method is closely coupled to which model or equations one wants to solve. One of the first methods was the Marker-And-Cell method [32], which was developed by Harlow and collaborators at Los Alamos National Laboratory in the 1960s. This was designed to solve a one-fluid-model, which uses one set of equations for the whole domain, with density and viscosity fields that are discontinuous at the interface between the two phases. More recent methods to solve two-phase flow with an interface include the volume of fluid (VOF) method [33, 74], the level-set method [64] and the front-tracking method [83, 84]. Phase-field or diffuse-interface models (see e.g. Anderson et al. [1], Gonzalez-Cinca et al. [30]) have a smooth transition, rather than an abrupt one, between the two phases.

    One of the basic principles of physics is that certain quantities, like mass, momentum and energy, are conserved. This conservation property is reflected in many fluid-mechanical equations, such as the two-phase flow equations presented in Chapter 2. In general, we may write a multidimen-

sional conservation law as

$$\frac{\partial \mathbf{u}}{\partial t} + \nabla \cdot \mathcal{F}(\mathbf{u}) = \mathbf{0}, \tag{3.1}$$

where $\mathbf{u}$ is the vector of the conserved variables and $\mathcal{F}$ is the flux tensor, which describes the flux in multiple dimensions. With this in mind, we seek a numerical method that is able to numerically conserve those quantities that are conserved in the mathematical model (3.1).

Finite-volume methods are often used to solve fluid-mechanical problems, as they are conservative in the sense that changes in the integral of $\mathbf{u}$ over the domain are only caused by fluxes in and out of the domain. Such methods also allow for discontinuities in the solution. As explained by LeVeque [49], using a method based on the integral form of the equations, rather than the differential form, is essential to compute solutions with discontinuities correctly.

Finite-volume methods are based on dividing the physical domain into small volumes of finite size, and then keeping track of the average of the conserved quantities inside this volume. In one dimension, we can write Eq. (3.1) as

$$\frac{\partial \mathbf{u}(t)}{\partial t} + \frac{\partial \mathbf{f}(\mathbf{u})}{\partial x} = \mathbf{0}, \tag{3.2}$$

where $\mathbf{f}(\mathbf{u})$ is the flux vector. We then divide our domain into finite volumes (or grid cells) with size Δx, and we denote the i-th grid cell $\mathcal{C}_i = (x_{i-1/2}, x_{i+1/2})$ where $x_{i+1/2} = x_{i-1/2} + \Delta x$. By integrating (3.2) over a grid cell $\mathcal{C}_i$, and over a time step from t^n to $t^{n+1} \equiv t^n + \Delta t$, we get

$$\mathbf{U}_i^{n+1} = \mathbf{U}_i^n - \frac{\Delta t}{\Delta x}(\mathbf{F}_{i+1/2}^n - \mathbf{F}_{i-1/2}^n) = \mathbf{0}. \tag{3.3}$$

Here, $\mathbf{U}_i^n$ is some approximation of the average of $\mathbf{u}$ over cell $\mathcal{C}_i$ at time t^n,

$$\mathbf{U}_i^n \approx \frac{1}{\Delta x} \int_{x_{i-1/2}}^{x_{i+1/2}} \mathbf{u}(x, t^n) \mathrm{d}x. \tag{3.4}$$

The numerical fluxes are denoted $\mathbf{F}_{i+1/2}^n$ and approximate the flux at the interface between two grid cells from time t^n to t^{n+1},

$$\mathbf{F}_{i+1/2}^n \approx \frac{1}{\Delta t} \int_{t^n}^{t^{n+1}} \mathbf{f}(\mathbf{u}(x_{i+1/2}, t)) \mathrm{d}t. \tag{3.5}$$

The formulation (3.3) reveals the conservative nature of the finite-volume scheme, since changes in each cell are caused only by fluxes in and out
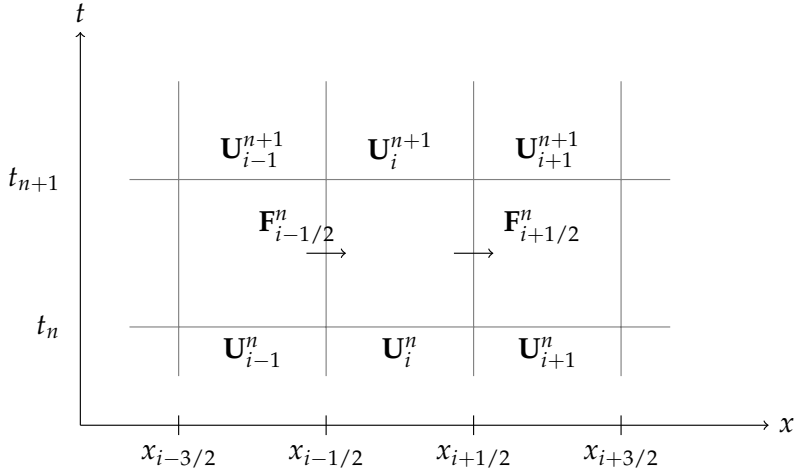
Figure 3.1.: Example of a finite-volume discretization in *x-t* space

of the cell. An illustration of the finite-volume discretization is shown in Figure 3.1.

When advancing the solution in time, we only know the values at the previous time step t^n, hence we cannot evaluate the integral (3.5) exactly. The challenge now lies in calculating the fluxes $\mathbf{F}^n_{i\pm1/2}$ knowing only the average of $\mathbf{u}$ in each cell at time t^n, $\mathbf{U}^n_i$. At the interface between two cells $\mathcal{C}_i$ and $\mathcal{C}_{i+1}$, where the flux $\mathbf{F}^n_{i+1/2}$ is to be calculated, there will be a discontinuity in $\mathbf{U}$ (if $\mathbf{U}^n_i$ and $\mathbf{U}^n_{i+1}$ differ). Calculating how the solution $\mathbf{u}$ evolves in time given a conservation law and a certain discontinuity is known as solving a *Riemann problem*. With the solution to the Riemann problem, we know the state $\mathbf{u}_{i+1/2}$ at the interface between the cells $\mathcal{C}_i$ and $\mathcal{C}_{i+1}$, which allows us to calculate the flux $\mathbf{F}^n_{i+1/2} = \mathbf{f}(\mathbf{u}_{i+1/2})$.

3.1. Solving the Riemann problem

One of the main characteristics of a finite-volume method, is that it allows for discontinuities in the solution, in the sense that the values of the solution in neighbouring cells (most often) are unequal, thus giving discontinuities at the cell interfaces. This implies one of the main challenges in constructing a finite-volume scheme, namely to find the numerical flux between two cells given a certain discontinuity. This problem is known as the *Riemann problem*. If it is solved exactly to determine $\mathbf{F}_{i\pm1/2}$ in Eq. (3.3), Godunov's

method is obtained (cf. Toro [81]). The Riemann problem can be solved approximately using centred schemes or upwind Riemann solvers.

An upwind scheme takes advantage of the fact that solutions to hyperbolic equations consist of waves propagating at finite speeds. It uses information about which direction the wave is travelling in and what information is transported with each wave to determine the solution to the Riemann problem. A centred scheme, on the other hand, does not take wave propagation into account, and treats all directions equally. There is a wide range of schemes available, cf. LeVeque [49] and Toro [81]. Here, only those are addressed which were used in the papers included in this thesis.

3.1.1. Centred schemes

The Lax-Friedrichs flux is a centred scheme, and can be written as [49]

$$\mathbf{F}^{\text{LF}}_{i+1/2} = \frac{1}{2}(\mathbf{f}(\mathbf{U}_i) + \mathbf{f}(\mathbf{U}_{i+1})) - \frac{\Delta x}{2\Delta t}(\mathbf{U}_{i+1} - \mathbf{U}_i). \tag{3.6}$$

The first term is simply a centred approximation to the flux at the interface, while the second term introduces numerical diffusion, which is necessary to make the method stable. However, this diffusion also causes the method to smear out the solution, so it has trouble preserving discontinuities sharply.

The first-order centred (FORCE) flux proposed by Toro [81] is a combination of the first-order Lax-Friedrichs flux and the second-order Richtmyer two-step Lax-Wendroff flux. The latter is given by defining an intermediate state

$$\mathbf{U}^{\text{Ri}}_{i+1/2} = \frac{1}{2}(\mathbf{U}_i + \mathbf{U}_{i+1}) - \frac{\Delta t}{2\Delta x}(\mathbf{f}(\mathbf{U}_{i+1}) - \mathbf{f}(\mathbf{U}_i)), \tag{3.7}$$

and then computing the flux vector at the intermediate state

$$\mathbf{F}^{\text{Ri}}_{i+1/2} = \mathbf{f}(\mathbf{U}^{\text{Ri}}_{i+1/2}). \tag{3.8}$$

The FORCE flux can then be expressed as

$$\mathbf{F}^{\text{FORCE}}_{i+1/2} = \frac{1}{2}(\mathbf{F}^{\text{LF}}_{i+1/2} + \mathbf{F}^{\text{Ri}}_{i+1/2}). \tag{3.9}$$

This flux has the advantage of being reasonably accurate, while still being simple enough to be computationally cheap and easy to implement.

The multi-stage (MUSTA) scheme of Toro [80] aims to be as simple as a centred scheme, while coming close to the accuracy of an upwind Riemann solver. It can be briefly described as follows:

1. Divide the domain around the cell interface at $x_{i+1/2}$ into a local grid with $2N$ cells, using the values $\mathbf{U}_i$ for the first N cells and $\mathbf{U}_{i+1}$ for the last N cells

2. Do M local time steps in each local grid, using the first-order centred FORCE flux (3.9)

3. Use the flux between cell N and $N+1$ in the local grid as the flux $\mathbf{F}_{i+1/2}$ in the original grid

In most cases, the MUSTA scheme is more accurate than the FORCE flux on which it is based, although computationally more expensive due to the need to do local time steps at each cell interface. The scheme was used in papers L3 and L4, where it is described more thoroughly.

3.1.2. Characteristic Riemann solvers

In paper L5, we use characteristic Riemann solvers (cf. Moretti [57] and Sesterhenn [75]) for a scalar linear advection equation, the 2D isothermal Euler equations and the 2D shallow water equations. The characteristic Riemann solver is an upwind Riemann solver, although the ones used in paper L5 are only approximate in the case of the Euler and shallow water equations. The main concept is to determine the properties propagated by waves to the cell interface, and from this determine the value $\mathbf{U}_{i+1/2}$ at the interface. The numerical flux is then simply given by $\mathbf{F}_{i+1/2} = \mathbf{f}(\mathbf{U}_{i+1/2})$.

In systems of hyperbolic PDEs, information is transported along rays called *characteristics*, along which the corresponding characteristic variables are constant. In the case of the scalar linear advection equation

$$\frac{\partial u}{\partial t} + a\frac{\partial u}{\partial x} = 0, \tag{3.10}$$

we may easily show that along the characteristic line $X(t) = x_0 + at$, the solution u is constant:

$$\frac{\mathrm{d}u(X(t),t)}{\mathrm{d}t} = \frac{\partial u(X(t),t)}{\partial t} + \frac{\partial u(X(t),t)}{\partial X}\frac{\partial X(t)}{\partial t} = \frac{\partial u}{\partial t} + a\frac{\partial u}{\partial x} = 0. \tag{3.11}$$

When solving the Riemann problem, this means that the solution $U_{i+1/2}$ at $x_{i+1/2}$ is equal to U_i (for $a > 0$), so the numerical flux is $F_{i+1/2} = aU_i$.

For a system of hyperbolic PDEs in the general form $\mathbf{u}_t + \mathbf{f}(\mathbf{u})_x = \mathbf{0}$, the process of calculating the characteristics is not as trivial. Here $(\cdot)_t$ and

$(\cdot)_x$ denote the partial derivatives with respect to t and x, respectively. To simplify matters, we write the system in a quasi-linear form,

$$\frac{\partial \mathbf{u}}{\partial t} + \mathbb{J}(\mathbf{u})\frac{\partial \mathbf{u}}{\partial x} = \mathbf{0}, \tag{3.12}$$

where $\mathbb{J}(\mathbf{u})$ is the Jacobian matrix of the flux function $\mathbf{f}(\mathbf{u})$. The system (3.12) is in a similar form as the linear advection equation (3.10), but for this system, the characteristic speeds are given by the eigenvalues of $\mathbb{J}$. The changes in the characteristic variables are the changes in conservative variables projected on the left eigenvectors of $\mathbb{J}$.

Figure 3.2 shows the characteristics for a two-equation system with eigenvalues $\lambda_1 < 0$ and $\lambda_2 > 0$, with the corresponding eigenvectors $\mathbf{w}_1$ and $\mathbf{w}_2$. Using the characteristics, one can determine that the state $\mathbf{U}_{i+1/2}$ at the interface $x_{i+1/2}$ is given by $\mathbf{w}_{1,R}$ and $\mathbf{w}_{2,L}$. Since the Jacobian matrix $\mathbb{J}(\mathbf{u})$ depends on $\mathbf{u}$, one has to choose where the Jacobian should be evaluated. One possible and reasonable option is to evaluate $\mathbb{J}$ at the point where the characteristic is coming from, which for the case in Figure 3.2 means to evaluate at $\mathbf{u}_R$ to calculate λ_1 and $\mathbf{w}_1$, and at $\mathbf{u}_L$ to calculate λ_2 and $\mathbf{w}_2$.
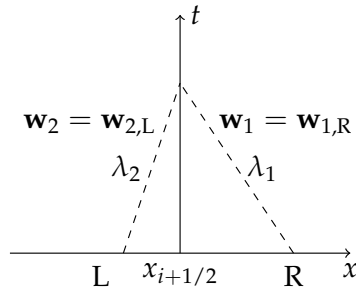
Figure 3.2.: A Riemann problem at $x_{i+1/2}$ for a two-equation system. The characteristics are shown by dashed lines.

In general, characteristic solvers may work well when we are dealing with smooth solutions or (close to) linear flux functions, but problems might occur when the eigenvalues change sign from one cell to the next. In paper L5, we show explicitly how to derive a characteristic solver for the isothermal Euler equations and the shallow water equations.

3.1.3. Higher order reconstruction

A common approach to achieve higher spatial order, is to use the monotone upstream-centred scheme for conservation laws (MUSCL), which is of second order for smooth solutions. It was proposed by van Leer [86], and is based on constructing a piecewise linear function $\tilde{\mathbf{U}}(x)$ using the discrete data $\{\mathbf{U}_i\}$. We introduce a linear slope $\sigma_{i,k}$ for the k-th variable in each cell, so that $\tilde{\mathbf{U}}(x)$ is given by

$$(\tilde{\mathbf{U}}_i(x))_k = (\mathbf{U}_i)_k + \sigma_{i,k}(x - x_i) \qquad \text{for } x_{i-1/2} \leq x < x_{i+1/2}, \qquad (3.13)$$

where $(\cdot)_k$ denotes the k-th component of a vector, and x_i is the centre of the i-th grid cell. To calculate the slope $\sigma_{i,k}$, one uses a slope-limiter function, of which many variants exist. Here, we only mention the minmod limiter, which is one of the more diffusive limiters, but which is also robust, and whose slope is given by

$$\sigma_{i,k} = \text{minmod}\left(\frac{(\mathbf{U}_i)_k - (\mathbf{U}_{i-1})_k}{\Delta x}, \frac{(\mathbf{U}_{i+1})_k - (\mathbf{U}_i)_k}{\Delta x}\right), \qquad (3.14)$$

where the minmod function can be written as

$$\text{minmod}(a, b) = \frac{1}{2}(\text{sign}(a) + \text{sign}(b)) \min(|a|, |b|) \qquad (3.15)$$

For discussion of other limiters, see e.g. LeVeque [49].

Given a certain slope, we can then construct the piecewise linear function $\tilde{\mathbf{U}}$ as illustrated in Figure 3.3. As seen in the figure, the Riemann problem at the interface between the cells $\mathcal{C}_i$ and $\mathcal{C}_{i+1}$ is now given by

$$(\tilde{\mathbf{U}}^L_{i+1/2})_k \equiv (\tilde{\mathbf{U}}_i(x_{i+1/2}))_k = (\mathbf{U}_i)_k + \frac{\Delta x}{2}\sigma_{i,k}$$

$$\text{and} \qquad\qquad (3.16)$$

$$(\tilde{\mathbf{U}}^R_{i+1/2})_k \equiv (\tilde{\mathbf{U}}_{i+1}(x_{i+1/2}))_k = (\mathbf{U}_{i+1})_k - \frac{\Delta x}{2}\sigma_{i+1,k}.$$

These states define a new Riemann problem, which can be solved by one of the methods described earlier in this section. It is worth noting that in many cases, it is common to apply the limiter to other variables than the conservative ones. For the 1D isothermal Euler equations, for example, the limited variables are most often the density ρ and the velocity u.

The MUSCL scheme was used as a reference scheme in paper L5 to assess the performance of the Rankine-Hugoniot-Riemann (RHR) scheme, which will be presented in the next section.
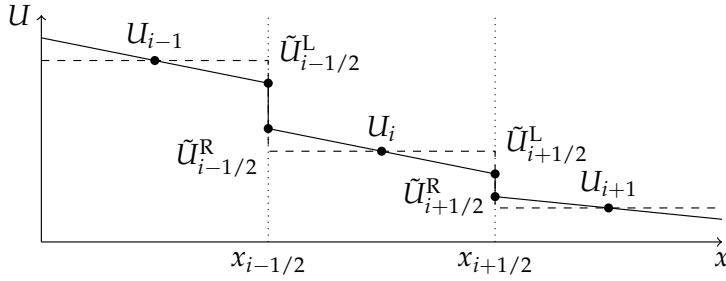
Figure 3.3.: Example of a piecewise linear reconstruction in a MUSCL scheme, for a scalar equation. The dashed lines show the constant reconstruction by the cell averages in each cell before the linear reconstruction (solid lines).

3.2. The Rankine-Hugoniot-Riemann solver

We consider a general multidimensional conservation law with source terms, in the form

$$\frac{\partial \mathbf{u}}{\partial t} + \nabla \cdot \mathcal{F}(\mathbf{u}) = \mathbf{q}(\mathbf{u}), \tag{3.17}$$

where $\mathcal{F}$ is a flux tensor and $\mathbf{q}(\mathbf{u})$ is a source term. Such systems of equations can describe a number of different flow applications, such as cavitation [72], fluid flow in a gravity field [51], combustion [40], multi-phase flow with mass or heat transfer between the phases [77][L3], and water/vapour flow in nuclear reactors [31], to mention a few.

Systems in the form (3.17) present a number of challenges to a numerical method. One such challenge is to resolve steady or quasi-steady states accurately, that is, cases where the magnitude of $\mathbf{u}_t$ is much smaller than that of the flux gradient or the source term. To see this more clearly, we look at Eq. (3.17) in two dimensions,

$$\frac{\partial \mathbf{u}}{\partial t} + \frac{\partial \mathbf{f}(\mathbf{u})}{\partial x} + \frac{\partial \mathbf{g}(\mathbf{u})}{\partial y} = \mathbf{q}(\mathbf{u}). \tag{3.18}$$

In steady state, $\mathbf{u}_t = \mathbf{0}$, the source term $\mathbf{q}$ may balance the flux terms on the left-hand side, or (if $\mathbf{q} = \mathbf{0}$) the two flux terms may balance each other.

One rather simple and often useful approach for solving equations in the form (3.18), are fractional-step methods. A typical fractional-step method, also known as Godunov splitting, divides the problem into two parts: one homogeneous conservation law, $\mathbf{u}_t + \mathbf{f}(\mathbf{u})_x + \mathbf{g}(\mathbf{u})_y = \mathbf{0}$, and one ODE

with the source term, $\mathbf{u}_t = \mathbf{q}(\mathbf{u})$. The two parts are then solved alternately. However, as LeVeque [49] points out, fractional-step methods often have trouble resolving steady or quasi-steady states.

Such steady or quasi-steady states typically require numerical schemes able to preserve these balances, which are known as *well-balanced* schemes. A number of authors have developed different variants of such schemes, including Bale et al. [5], Bermudez and Vazquez [9], Donat and Martinez-Gavara [23], Gosse [31], Hubbard and García-Navarro [35], and LeVeque [50, 48], Murillo and García-Navarro [59], Noelle et al. [61, 62, 63] and Xing et al. [89].

In 1997, Jenny and Müller [40] introduced a new approach to balancing flux gradients and source terms, named the *Rankine-Hugoniot-Riemann* solver. Their motivation was to solve a combustion case with a 2D premixed laminar flame, for which a traditional Riemann solver did not prove to be adequate. The novel ideas with the solver were first to include the source term $\mathbf{q}(\mathbf{u})$ in the flux computation in 1D, and second to treat the y-flux gradient $\mathbf{g}(\mathbf{u})_y$ as a source term when calculating the x-fluxes, and vice versa. In this way, the solver was especially suited to solve problems where the flux gradients balance each other.

We easily see that the y-flux may be seen as a source term by reformulating (3.18) as

$$\frac{\partial \mathbf{u}}{\partial t} + \frac{\partial \mathbf{f}(\mathbf{u})}{\partial x} = -\frac{\partial \mathbf{g}(\mathbf{u})}{\partial y} + \mathbf{q}(\mathbf{u}). \qquad (3.19)$$

By integrating this equation over a grid cell $\mathcal{C}_{i,j}$, we get

$$\frac{\partial \mathbf{U}_{i,j}}{\partial t} + \frac{\mathbf{F}_{i+1/2,j} - \mathbf{F}_{i-1/2,j}}{\Delta x} = -\frac{\mathbf{G}_{i,j+1/2} - \mathbf{G}_{i,j-1/2}}{\Delta y} + \mathbf{Q}_{i,j} \equiv \mathbf{Q}_{i,j,x}, \quad (3.20)$$

where $\mathbf{Q}_{i,j}$ is an approximation of the average of $\mathbf{q}$ over the grid cell, and $\mathbf{F}$ and $\mathbf{G}$ are the x- and y-flux approximations at the interfaces, respectively. In paper L5, we propose that the whole right-hand side $\mathbf{Q}_{i,j,x}$ can be treated as a singular source term located in the middle of the cell. In the original work by Jenny and Müller [40], the source term was placed at the cell interface rather than in the cell centre, which made it necessary to alter the Riemann solver. Here, we instead use the idea of LeVeque [48], who also places the source term in the cell centre, however without including the effect of cross-fluxes. If we go back to the PDE (3.19), we may express this as

$$\frac{\partial \mathbf{u}}{\partial t} + \frac{\partial \mathbf{f}(\mathbf{u})}{\partial x} = \Delta x \mathbf{Q}_{i,j,x} \delta(x - x_{i,j}), \qquad (3.21)$$

inside grid cell $\mathcal{C}_{i,j}$, where δ is the Dirac delta function. This now allows us to make a useful prediction of the solution $\mathbf{u}$ inside this grid cell, which is obtained by integrating the steady ($\mathbf{u}_t = \mathbf{0}$) version of (3.21) over x from $x < x_{i,j}$ to $x > x_{i,j}$. We obtain the Rankine-Hugoniot condition

$$\mathbf{f}(\mathbf{U}_{i,j,E}) - \mathbf{f}(\mathbf{U}_{i,j,W}) = \Delta x \mathbf{Q}_{i,j,x}, \tag{3.22}$$

where $\mathbf{U}_{i,j,E}$ and $\mathbf{U}_{i,j,W}$ denote the solution in the eastern ($x > x_{i,j}$) and western ($x < x_{i,j}$) part, respectively, of grid cell $\mathcal{C}_{i,j}$. To keep the method conservative, we ensure that the average over the grid cell is conserved,

$$\frac{\mathbf{U}_{i,j,E} + \mathbf{U}_{i,j,W}}{2} = \mathbf{U}_{i,j}. \tag{3.23}$$

(a) Condition (3.22) **(b)** Condition (3.23)
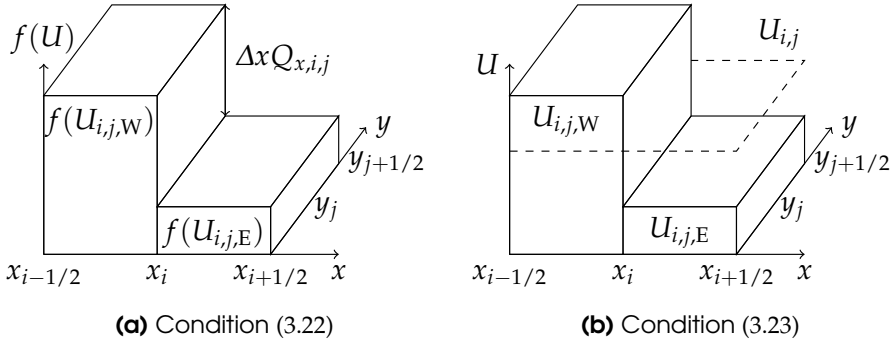
Figure 3.4.: Sketch of the conditions (3.22) and (3.23) to define $U_{i,j,W}$ and $U_{i,j,E}$, for a scalar case (adapted from Lund et al. (L5)).

The two equations (3.22) and (3.23) are illustrated in Figure 3.4 for a scalar case. They can be solved for $\mathbf{U}_{i,j,E}$ and $\mathbf{U}_{i,j,W}$, and two equivalent equations give the northern and southern states, $\mathbf{U}_{i,j,N}$ and $\mathbf{U}_{i,j,S}$. The Riemann problem at the interface between cells $\mathcal{C}_{i,j}$ and $\mathcal{C}_{i+1,j}$ is then given by the two states $\mathbf{U}_{i,j,E}$ and $\mathbf{U}_{i+1,j,W}$, and similarly the Riemann problem at the interface between cells $\mathcal{C}_{i,j}$ and $\mathcal{C}_{i,j+1}$ is given by $\mathbf{U}_{i,j,N}$ and $\mathbf{U}_{i,j+1,S}$.

As presented by Jenny and Müller [40], the RHR solver had some stability issues in two dimensions, resulting in spurious oscillations. This was handled by adding numerical diffusion to the source term, so that the source term used in the computations was

$$\mathbf{Q}^*_{i,j,x} = (1-\theta)\mathbf{Q}_{i,j,x} + \frac{\theta}{4}(\mathbf{Q}_{i-1,j,x} + \mathbf{Q}_{i+1,j,x} + \mathbf{Q}_{i,j-1,x} + \mathbf{Q}_{i,j+1,x}), \tag{3.24}$$

(and similarly for $\mathbf{Q}_{i,j,y}$) where θ is some empirical value, which was chosen to be $\theta = 0.04$ by Jenny and Müller [40]. This way of eliminating instabilities is rather arbitrary, and the chosen value of θ may not be suitable for other cases. This was addressed by Florian Müller in his Master's thesis [60], where he introduced a limiter instead of numerical diffusion.

In our paper [L5], we suggested a slightly different limiter than the one used by Müller [60]. The limiter ensures that the half-states calculated from Eqs. (3.22)–(3.23) lie between the values in the neighbour cells, so that no new maxima or minima are created, satisfying a total-variation diminishing (TVD) criterion. The limited value of $\mathbf{U}_{i,j,\mathrm{E}}$ may be written as [L5]

$$(\mathbf{U}^{\mathrm{L}}_{i,j,E})_k = \min\left[\max\left[(\mathbf{U}_{i,j,E})_k - (\mathbf{U}_{i,j})_k, -|\delta_k|\right], |\delta_k|\right] + (\mathbf{U}_{i,j})_k, \quad (3.25)$$

where $\delta_k = \mathrm{minmod}((\mathbf{U}_{i+1,j})_k - (\mathbf{U}_{i,j})_k, (\mathbf{U}_{i,j})_k - (\mathbf{U}_{i-1,j})_k)$. Here $(\cdot)_k$ denotes the k-th variable, and $\mathbf{U}_{i,j,\mathrm{E}}$ is the unlimited eastern state, and the minmod function is given by Eq. (3.15). The limiting procedure is illustrated in Fig. 3.5.

The limiter allows jumps $\mathbf{U}^{\mathrm{L}}_{i,\mathrm{E}} - \mathbf{U}^{\mathrm{L}}_{i,\mathrm{W}}$ which have the opposite sign of $\mathbf{U}_{i+1} - \mathbf{U}_{i-1}$, as seen in Figs. 3.5c–d, in contrast to limiters in a MUSCL scheme, for example. Such opposite jumps were not admitted by the limiter of Müller [60], but allowing such jumps seemed to give better results. For more details on the limiter, see paper L5, where we also show that the RHR solver is of second spatial order, and demonstrate this by applying it to a 2D scalar advection equation, the 2D isothermal Euler equations and the 2D shallow water equations.

3.3. Exponential time-differencing method

As was mentioned in Section 2.2, relaxation terms can be used to describe a number of physical processes, such as heat and mass transfer in a two-phase flow model. These terms drive the system towards some equilibrium state, in which the relaxation term tends to zero. As an example, heat transfer is caused by a temperature relaxation term, and the equilibrium point is where the two phases have the same temperature, so that heat no longer flows. As an isolated process, a relaxation term will typically cause an exponential decay over time towards an equilibrium state, as illustrated in Figure 3.6.
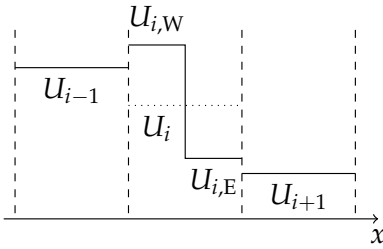
(a) Before limiting. $U_{i,\mathrm{W}}$ lies outside the interval $[U_{i+1}, U_{i-1}]$ and needs to be limited.
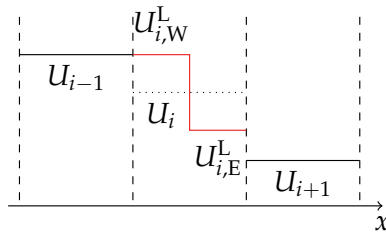
(b) After limiting. $U_{i,\mathrm{W}}$ is reduced, and $U_{i,\mathrm{E}}$ is increased accordingly to conserve U_i, as stated in Eq. (3.23).
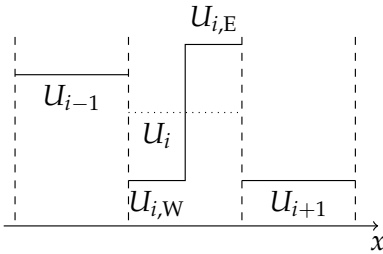
(c) Before limiting. $U_{i,\mathrm{E}}$ lies outside the interval $[U_{i+1}, U_{i-1}]$ and needs to be limited.
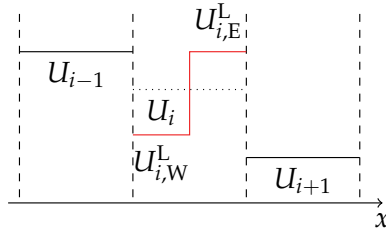
(d) After limiting. $U_{i,\mathrm{E}}$ is reduced, and $U_{i,\mathrm{W}}$ is increased accordingly to conserve U_i, as stated in Eq. (3.23).

Figure 3.5.: Illustration of the RHR limiting procedure for a scalar equation, for two different cases (adapted from Lund et al. (L5)).
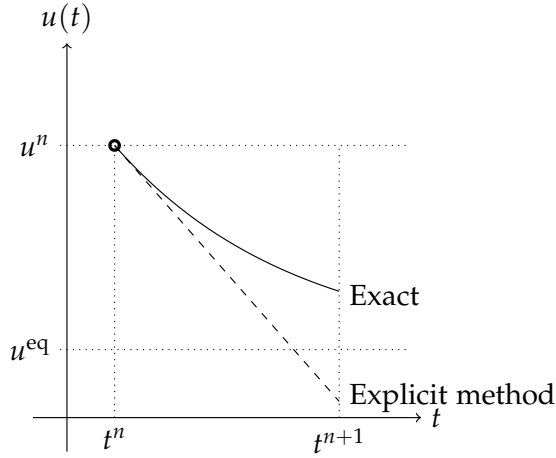
Figure 3.6.: Illustration of a relaxation process (3.26) over time towards an equilibrium state u^{eq}.

Figure 3.6 illustrates a simple relaxation ODE,

$$\frac{\mathrm{d}u}{\mathrm{d}t} = \frac{1}{\varepsilon}(u^{eq} - u), \tag{3.26}$$

where ε is the time scale of the relaxation process. The time scales of the fluid-mechanical conservation law, on the other hand, are of the order of the grid cell size divided by the wave speeds. If the time scales associated with the relaxation process are significantly smaller than those associated with the conservation law, we require careful numerical treatment to avoid instabilities. For reasons of efficiency and simplicity, we wish to resolve the solution of the relaxation ODE on the same time scale as that of the conservation law. However, if these time steps Δt are too large, we realize from Figure 3.6 that an explicit method like Forward Euler will possibly overshoot the equilibrium value.

In general, we wish to solve a relaxation ODE formulated as

$$\frac{\mathrm{d}u}{\mathrm{d}t} = s(u), \tag{3.27}$$

which has an equilibrium point u^{eq} defined by

$$s(u^{eq}) = 0. \tag{3.28}$$

For first-order accuracy, a natural and common choice for solving (3.27) is to use the Backward Euler scheme, which is given by

$$u^{n+1} = u^n + s(u^{n+1})\Delta t, \tag{3.29}$$

where Δt is the time step size. However, a crucial disadvantage of the Backward Euler scheme is its implicitness, which means that Eq. (3.29) often has to be solved using an iterative scheme such as the Newton–Raphson method.

A popular approach to solving ODEs in the form (3.27) has been the use of exponential integrators [20, 34]. This method utilizes the fact that such systems typically move exponentially towards some equilibrium point where $s(u) = 0$, so that the solution can be approximated using an exponential. Although exponential integrators often are a better approach than explicit methods, most exponential integrators linearize the source term $s(u)$, which may cause errors and overshooting of the equilibrium point. Recently, however, Aursand et al. [2] proposed a related exponential time-differencing method, tailor-made for relaxation systems, that never overshoots the equilibrium. In this way, the stability restriction on the time step is lifted. The first-order scheme, referred to as ASY1 (monotonically asymptotic exponential integration), is given by

$$u^{n+1} = u^n + (u^{\text{eq}} - u^n)\left[1 - \exp\left(-\frac{\Delta t}{\tau}\right)\right], \tag{3.30}$$

where u^{eq} is the equilibrium state and

$$\tau = \frac{u^{\text{eq}} - u^n}{s(u^n)} \tag{3.31}$$

is the time scale. The ASY1 scheme (3.30) is now unconditionally stable by construction, and the solution decays exponentially towards the equilibrium state u^{eq}. It is (in itself) an explicit scheme, removing the need to solve an implicit equation like the one in the Backward Euler scheme (3.29). However, it requires a priori knowledge of the equilibrium state u^{eq} given by Eq. (3.28), which may be trivial or cumbersome to calculate, depending on the nature of the relaxation source term. In the case of the simple relaxation ODE in Eq. (3.26), the first-order ASY1 scheme would solve the ODE *exactly*, regardless of the size of the time step Δt.

In paper L4, we demonstrate how the ASY1 scheme can be applied to a mass transfer term in the form of a chemical potential relaxation term.

The scheme can also be useful for a number of other relaxation processes in two-phase flow, such as heat transfer, interfacial friction or wall friction, to name a few.

The most exciting phrase to hear in science,
the one that heralds new discoveries, is not
"Eureka!", but "That's funny ..."

<div align="center">Isaac Asimov (1920–1992)</div>

4

Results

This chapter briefly reviews the most important results in my papers L1–L5 given in the appendix.

4.1. A hierarchy of relaxation two-phase flow models and the subcharacteristic condition

Paper L1: Tore Flåtten and Halvor Lund. Relaxation two-phase flow models and the subcharacteristic condition, *Mathematical Models and Methods in Applied Sciences*, 21(12), pp. 2379–2407, 2011.
Paper L2: Halvor Lund. A hierarchy of relaxation models for two-phase flow, *SIAM Journal of Applied Mathematics*, 72(6), pp. 1713–1741, 2012.

In paper L1, we introduce a hierarchy of relaxation two-phase flow models with relaxation transfer terms, as described in Section 2.2. These terms account for mass, heat and volume transfer from one phase to the other, driven by differences in chemical potential, temperature and pressure, respectively, between the two phases. We start by introducing a six-equation basic model with homogeneous flow, that is, the two phases have the same velocity. In the basic model, all three transfer terms are present, and it forms the base of the hierarchy. By assuming equilibrium in one or more of the transfer processes, one can derive a total of seven other

models. We express each of these eight models explicitly using equations for conservation of mass, momentum, and energy, as well as an advection equation for the gas volume fraction.

The concept of the subcharacteristic condition is important when it comes to relating the wave velocities of a relaxation model to an equilibrium model. In the context of our hierarchy, this translates to the condition that adding an equilibrium assumption cannot increase the two-phase speed of sound. This is expressed by

$$\tilde{a}_{\mathcal{X}}^{-2} = \tilde{a}_{\mathcal{Y}}^{-2} + Z_{\mathcal{X}}^{\mathcal{Y}}, \tag{4.1}$$

where $\tilde{a}_{\mathcal{X}}$ and $\tilde{a}_{\mathcal{Y}}$ are the two-phase speeds of sound for the equilibrium model and the corresponding relaxation (non-equilibrium) model, respectively. $Z_{\mathcal{X}}^{\mathcal{Y}}$ is a non-negative term that we expressed using sums of squares, which means that $\tilde{a}_{\mathcal{Y}} > \tilde{a}_{\mathcal{X}}$. Figure 4.1 shows the two-phase speed of sound for CO_2 at 50 bar for each of the eight models in the hierarchy. We note that the two-phase speed of sound is greatly affected by which equilibrium assumptions we make. In particular, the homogeneous equilibrium model (the $pT\mu$-model) is seen to be discontinuous at the transition between single-phase and two-phase flow. In other words, the two-phase speed of sound $\tilde{a}_{pT\mu}$ is not equal to the liquid speed of sound c_ℓ where the gas volume fraction is zero ($\alpha_g = 0$).
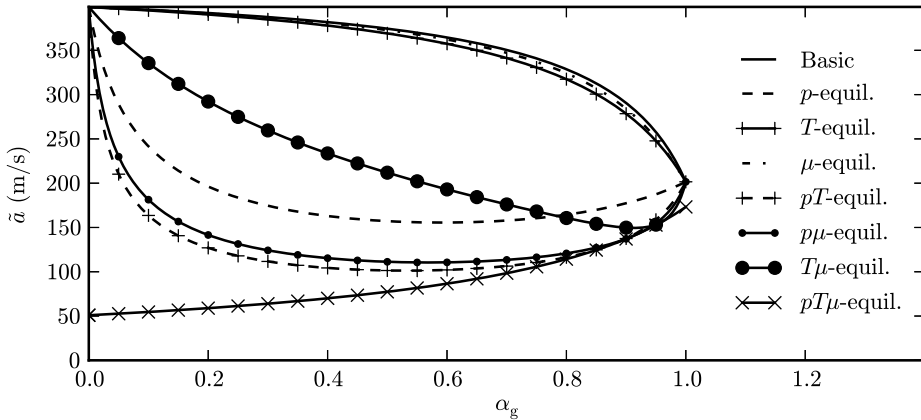
Figure 4.1.: Two-phase speed of sound for CO_2 at 50 bar as a function of gas volume fraction (L2). The single-phase speeds of sound are $c_\ell = 398.9$ m/s and $c_g = 201.5$ m/s.

In paper L1, we derive the basic model and the four models with pressure

equilibrium in an explicit form, that is, the p-, pT-, $p\mu$- and $pT\mu$-models. We also explicitly calculate the term Z_{χ}^{y} to show that the subcharacteristic condition is fulfilled for these models. Paper L2 completes the hierarchy by deriving the three last models and the subcharacteristic conditions related to these models.

Personal contribution: My contribution to the first paper [L1] was to derive the pressure-material relaxation model (the $p\mu$-model) and the subcharacteristic condition with respect to this model, as well as verifying and correcting some errors in the analysis of the other models. I also implemented the expression for the speed of sound and produced the plots and figures used in the paper. The second paper [L2] extends the hierarchy introduced in the first one, and was done solely by me, but with useful comments from Tore Flåtten.

4.2. Two-phase flow of CO_2 with phase transfer

Paper L3: Halvor Lund and Peder Aursand. Two-phase flow of CO_2 with phase transfer. *Energy Procedia*, 23, pp. 246–255, 2012.

In this paper, we aim to develop a two-phase flow model with a phase transfer term to account for evaporation and condensation between the liquid and gas phases of a CO_2 pipeline flow. We use the pT-model (2.10)–(2.13) as the fluid-mechanical model, since it includes a phase transfer term while still being relatively simple. The phase transfer term is expressed using two different models: One having a simple linear dependence on the difference in chemical potential between the two phases, and the other using statistical rate theory (SRT), based on transition probabilities from quantum mechanics and the Boltzmann definition of entropy. We develop the SRT theory to derive a phase transfer term $\Gamma_g = -\Gamma_\ell$ (cf. Eqs. (2.10)–(2.11)) for stratified pipeline flow, which is expressed as

$$\Gamma_g = -\Gamma_\ell = \begin{cases} \frac{32\rho_g(\alpha_g+\delta)\alpha_\ell}{\pi D}\sqrt{\frac{m}{2\pi k_B T}}(\mu_\ell - \mu_g) & \text{if } \mu_g < \mu_\ell, \\ \frac{32\rho_g\alpha_g(\alpha_\ell+\delta)}{\pi D}\sqrt{\frac{m}{2\pi k_B T}}(\mu_\ell - \mu_g) & \text{if } \mu_\ell \le \mu_g, \end{cases} \tag{4.2}$$

where D is the pipe diameter, k_B is the Boltzmann constant, and m is the molecular weight. The only empirical, undetermined factor in this model is the *initial volume fraction*, δ, which governed the speed of the nucleation process in the presence of only one phase. Thermodynamics are modelled using the stiffened gas equation of state. The system of

partial differential equations (PDEs) (2.10)–(2.13) is solved using a Godunov splitting approach, where we solve the homogeneous PDE system using a multi-stage (MUSTA) finite volume scheme, and the ordinary differential equation (ODE) describing the phase transfer relaxation term using the Backward Euler method to ensure stability.
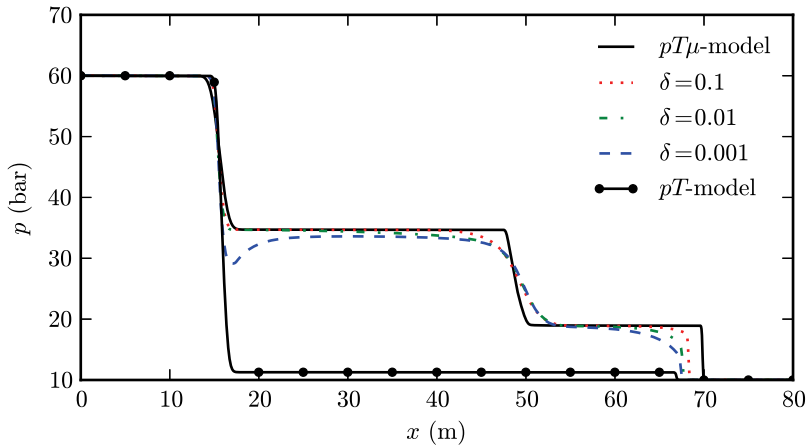
Figure 4.2.: Pressure during a CO_2 pipeline depressurization for the $pT\mu$-model, and the pT-model with and without the SRT phase transfer model (adapted from Lund and Aursand (L3)).

We compare the pT-model with the linear mass transfer model, with the SRT mass transfer model, and without mass transfer, and the homogeneous equilibrium model (HEM or $pT\mu$-model) with instantaneous phase transfer, for a CO_2 pipeline depressurization case. The results for the three latter models are shown in Figure 4.2. We note that the SRT model gives results that are quite similar to those of the HEM model. Adjusting the initial volume fraction gave qualitatively rather similar results, although a lower initial volume fraction led to a more significant pressure dip at the onset of liquid evaporation. The simple linear model, on the other hand, is very sensitive to the magnitude of its coefficient. However, it should be noted that the SRT model for pipeline flow has not yet been compared to experiments.

Personal contribution: My contribution to this work was to derive and implement the phase-transfer model based on SRT, run simulations and write most of the paper. I presented the work at the Trondheim CCS conference in June 2011.

4.3. Splitting methods for relaxation two-phase flow models

Paper L4: Halvor Lund and Peder Aursand. Splitting methods for relaxation two-phase flow models. *International Journal of Materials Engineering Innovation*, 4(2), pp. 117–131, 2013.

In this paper, we go into more detail on how to solve the relaxation ODE that describes the phase transfer term introduced in paper L3. We use a Godunov splitting scheme to solve the hyperbolic fluid-mechanical equation system and the relaxation term separately.

The relaxation phase transfer term acts to transfer mass between the two phases to reach some equilibrium point. It is crucial to solve this term accurately, since there is a risk of *overshooting* the equilibrium. This may happen if one uses an explicit method with too large time step, which may lead to physically nonsensical values, for example, negative mass in one of the phases. The relaxation ODE is solved using two approaches: one using the Backward Euler method, and one using an exponential time-differencing scheme.

Aursand et al. [2] have developed an exponential time-differencing scheme (similar to an exponential integrator, see Section 3.3) for use with relaxation systems, and verified that this method will not overshoot an equilibrium. The method has the advantage that it is an explicit method (if the equilibrium point is known), hence it does not need to find the solution iteratively to ensure stability, like the Backward Euler method must. We compare the solution and performance using the Backward Euler method and the exponential time-differencing ASY1 scheme, given by Eq. (3.30), for the CO_2 pipeline depressurization case introduced in paper L3. The time step was chosen according to the CFL condition, with a CFL number of 0.5. Figure 4.3 shows the temperature for this case, for the two different methods and different grid sizes. We see that the ASY1 scheme is slightly more diffusive for the very coarse 32 cell grid, but otherwise the two methods give comparable results.

In our case, the equilibrium point of the phase transfer process has to be calculated iteratively using a Newton-Raphson method for each time step, which leads to the two methods having a comparable computational cost. For a relaxation process with an easy-to-compute equilibrium value, one can expect the ASY1 scheme to be more efficient than the Backward Euler method.
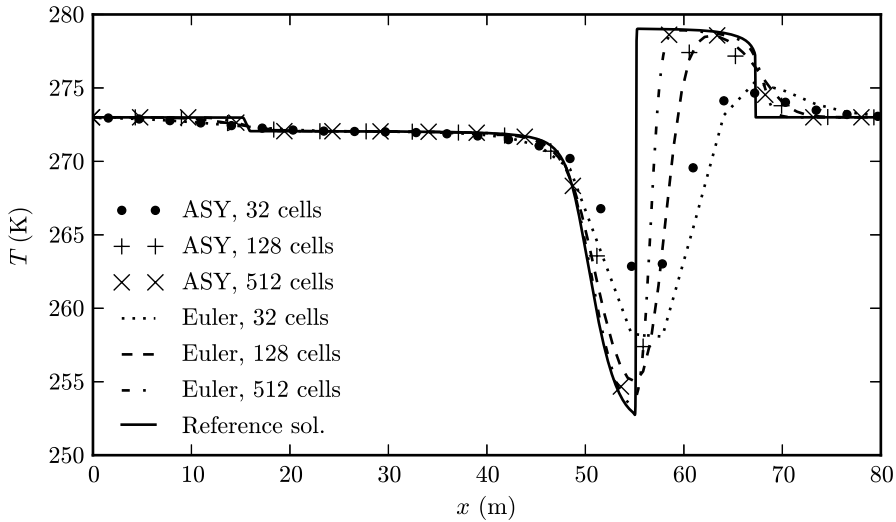
Figure 4.3.: Temperature during a CO_2 pipeline depressurization at time $t = 0.08$ s, for the test case described in papers L3 and L4 (adapted from Lund and Aursand (L4)).

Personal contribution: My contribution to this work was to implement the SRT model and do the calculations for finding the equilibrium state for the mass transfer process, run simulations and write most of the paper. I presented the work at the ECCOMAS Young Investigators Conference in Aveiro, Portugal in 2012.

4.4. The Rankine-Hugoniot-Riemann solver

Paper L5: Halvor Lund, Florian Müller, Bernhard Müller, and Patrick Jenny. Rankine-Hugoniot-Riemann solver for steady multidimensional conservation laws with source terms. Submitted for publication in *Journal of Computational Physics*, 2013.

The *Rankine-Hugoniot-Riemann* (RHR) solver was originally developed by P. Jenny and B. Müller [40] in 1997 to solve multidimensional conservation laws with source terms, more specifically to solve combustion cases with 1D and 2D premixed laminar flames. The solver uses a new approach to take the source into account for the flux evaluation in 1D, and to interpret cross fluxes as source terms. In the present work, these new source terms are imposed as delta functions in the middle of each cell, which leads to

(a) Without limiter.　　　　　　　　**(b)** With limiter.
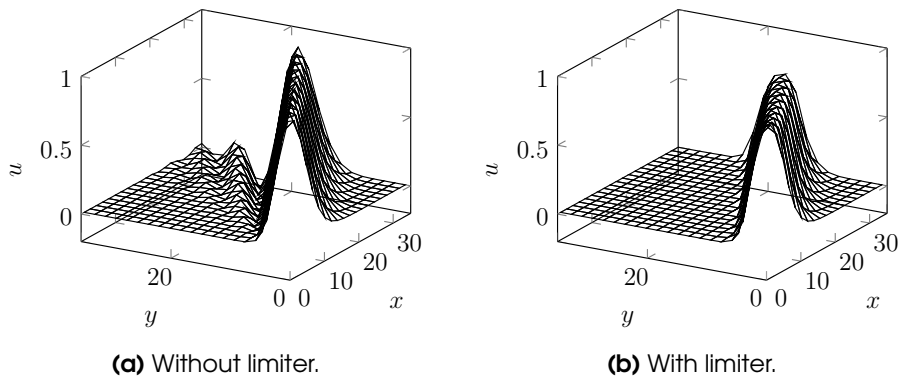
Figure 4.4.: Results for advection of a scalar using the RHR solver (L5).

jumps in the solution, according to a Rankine-Hugoniot condition. The new Riemann problems on the cell interfaces are then solved by a conventional (one-dimensional) Riemann solver.

Jenny and Müller [40] experienced some stability issues with the RHR solver in two dimensions, which were handled by adding numerical diffusion. In 2010, Florian Müller [60] introduced a limiter to eliminate these instabilities. The limiter ensures that the new states calculated by the Rankine-Hugoniot condition never exceed the states in the neighbour cells. Figure 4.4 illustrates the effect of the limiter on a scalar advection equation $u_t + au_x + bu_y = 0$, where the spurious oscillations in Fig. 4.4a are eliminated in Fig. 4.4b by using a limiter.

We are able to prove analytically that the solver is of second order for rectangular grids and the 2D scalar advection equation, and confirm this with numerical results for the 2D scalar advection equation, the 2D isothermal Euler equations and the 2D shallow water equations. Figure 4.5 shows the L^2 norm of the density error for a 2D isothermal Euler case (described in paper L5), and confirms that the RHR solver is of second order spatially, and more accurate than a MUSCL scheme with MC limiter by a factor of about two. The RHR solver is also found to be more accurate than the MUSCL scheme for the scalar advection equation and the 2D shallow water equations. However, the RHR solver has a slightly higher cost per time step, since it has to solve the RHR relations (3.22)–(3.23).

Personal contribution: My contribution to this work was to implement the numerical code, extend Florian Müller's work on the limiter and the analytical derivations, run simulations and write most of the paper.
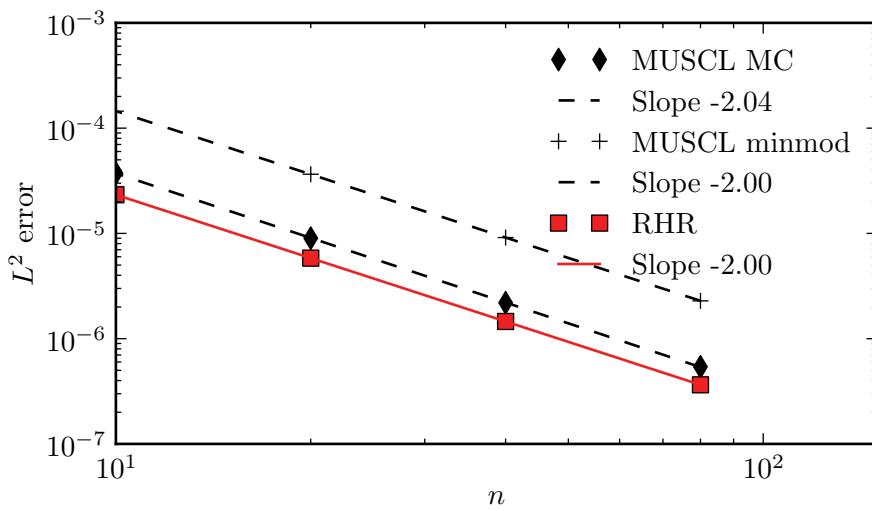
Figure 4.5.: Grid convergence of the L^2 norm of the density error for the 2D isothermal Euler equations (L5).

If I have not seen as far as others,
it is because giants were standing
on my shoulders.

Hal Abelson

5
Conclusions and outlook

The present thesis has contributed to new models for two-phase flow with relaxation terms accounting for mass, heat and volume transfer. A mass transfer model for pipeline flow based on statistical rate theory was suggested. Moreover, accurate and robust numerical methods suitable to solve such models with source terms have been considered.

A hierarchy of relaxation two-phase flow models was introduced, with relaxation in pressure, temperature and chemical potential. The basic model of the hierarchy was shown to satisfy the first and second laws of thermodynamics in paper L1, which can be said to be a crucial requirement for any physically valid model. The $p\mu$-model (described in paper L1) and the three models without pressure equilibrium, namely the T-, μ- and $T\mu$-models (described in paper L2), represented original contributions, and their possible applications are still open to investigation. Although pressure relaxation is more rapid than relaxation of temperature and chemical potential in most two-phase flow applications, one could possibly imagine situations where this is not the case, making the three latter models relevant.

All the models where shown to satisfy the subcharacteristic condition with respect to each other in papers L1 and L2, which is closely related to stability in the stiff limit where the relaxation process is infinitely rapid. This condition has proven to be an important trait of models describing

physical phenomena. For the model hierarchy, the subcharacteristic condition translated to the speed of sound being reduced for each equilibrium assumption, which was shown explicitly using sums of squares. Of all the equilibrium assumptions, pressure equilibrium was found to have the most significant effect on the speed of sound, compared to the basic model. Moreover, with equilibrium in all three relaxation processes, the two-phase speed of sound was discontinuous in the single-phase limit, which may result in numerical difficulties. It would be interesting to compare the expressions for the two-phase speeds of sound to measurements for various flow regimes, to determine which model is most realistic. The hierarchy could also possibly be extended to inhomogeneous flow, that is, with different velocities for the two phases.

The model with equilibrium in pressure and temperature (the pT-model) was investigated in more detail in paper L3, with mass transfer due to differences in chemical potential. The mass transfer term was modelled using statistical rate theory (SRT), which is based on transition probabilities from quantum mechanics and the Boltzmann definition of entropy. An SRT mass transfer term for pipeline simulations was derived, which was less dependent on empirical constants than other mass transfer models. As far as the authors are aware of, SRT has not been used for such simulations before. However, it should be noted that the SRT model has not yet been experimentally validated for pipeline flow.

Numerical simulation of a CO_2 pipeline depressurization case showed that the results of the SRT model are quite close to those of the homogeneous equilibrium model (HEM or $pT\mu$-model). This may indicate that the $pT\mu$-model, which includes mass transfer implicitly as an instantaneous process, is a good first approximation to a model with an explicit expression for mass transfer. It is also worth noting that the SRT model produced a characteristic pressure dip where the liquid evaporation started, which was not present when using a simple linear relaxation model for chemical potential. The magnitude of the dip was dependent on the initial volume fraction, a constant which governed the speed of mass transfer in the transition from single-phase to two-phase flow. Similar pressure profiles have been observed in other pipe depressurization cases (see for example Städtke [78, Chap. 9]), however, no explicit comparison has been made so far.

For the pT-model with mass transfer, a Godunov splitting (fractional step) approach was applied, which solved the homogeneous conservation law and the SRT mass transfer term separately. The mass transfer term

was solved using a first-order exponential time-differencing scheme (ASY1) made especially for relaxation models, and using the Backward Euler method. The ASY1 scheme had the advantage of being explicit in itself as long as the equilibrium value of the relaxation process is known. In the presented case, this equilibrium value had to be calculated using a Newton-Raphson iteration, described in paper L4. For coarse grids, the ASY1 scheme was slightly less accurate than the Backward Euler scheme, but they were otherwise comparable both in computational cost and accuracy. However, since the ASY1 scheme is explicit if the equilibrium value is known, it is expected that this scheme will be efficient and robust for relaxation processes where the equilibrium can be calculated cheaply.

Finally, the Rankine-Hugoniot-Riemann (RHR) solver was presented, which is designed to solve multidimensional conservation laws with source terms. A new limiter was introduced to eliminate stability problems that were reported with the original RHR solver by Jenny and Müller [40]. In paper L5, it was proven analytically that the solver is of second order for a 2D linear scalar advection equation. Second order was also demonstrated numerically for the 2D isothermal Euler equations and the 2D shallow water equations. The presented cases focused on solving the steady state accurately, but the RHR solver has previously [40] been used also for transient cases.

The cases presented in paper L5 had rather small source terms. However, the RHR solver should have the potential to handle more dominant source terms as well, such as the combustion cases considered by Jenny and Müller [40]. Another interesting case may be a shallow water "lake at rest"-case, where the source terms due to topography are especially important.

For the future, one could imagine a number of possible continuations of the work presented in this thesis:

- Compare the speeds of sound of the models in the hierarchy to measurements to determine which model is more realistic.

- Extend the hierarchy to nonhomogeneous flow, that is, with different phase velocities. The works of Martínez Ferrer et al. [54] and Morin and Flåtten [58] are relevant.

- Consider possible applications of the newly introduced models (the $p\mu$-, T-, μ- and $T\mu$-models) in the hierarchy.

- Compare the SRT model to experimental results, for example for a

depressurization case such as the Edwards case [26, 78], and estimate a proper value for the initial volume fraction.

- Apply the first-order exponential time-differencing scheme ASY1 to a relaxation model with an easy-to-compute equilibrium value. This should give a significant advantage compared to the Backward Euler scheme.

- Apply the RHR solver to a case where source terms are more dominant, such as the shallow water equations with a topography source term.

- Apply the RHR solver to relaxation models for two-phase flow.

- Use a more realistic equation of state than the stiffened gas EOS.

Bibliography

[1] D. M. Anderson, G. B. McFadden, and A. A. Wheeler. Diffuse interface methods in fluid mechanics. *Annual Review of Fluid Mechanics*, 30:139–165, 1998.

[2] P. Aursand, S. Evje, T. Flåtten, K. E. T. Giljarhus, and S. T. Munkejord. An exponential time-differencing method for monotonic relaxation systems. *Preprint*, 2010. Available at `http://www.math.ntnu.no/conservation/2011/008.pdf`.

[3] P. Aursand, M. Hammer, S. T. Munkejord, and Ø. Wilhelmsen. Pipeline transport of CO_2 mixtures: Models for transient simulation. *International Journal of Greenhouse Gas Control*, 15:174–185, 2013.

[4] M. R. Baer and J. W. Nunziato. A two-phase mixture theory for the deflagration-to-detonation transition (DDT) in reactive granular materials. *Int. J. Multiphase Flow*, 12(6):861–889, 1986.

[5] D. S. Bale, R. J. LeVeque, S. Mitran, and J. Rossmanith. A wave-propagation method for conservation laws and balance laws with spatially varying flux functions. *SIAM J. Sci. Comput.*, 24(3):955–978, 2002.

[6] M. Baudin, C. Berthon, F. Coquel, R. Masson, and Q. H. Tran. A relaxation method for two-phase flow models with hydrodynamic closure law. *Numerische Mathematik*, 99(3):411–440, January 2005.

[7] M. Baudin, F. Coquel, and Q. H. Tran. A semi-implicit relaxation scheme for modeling two-phase flow in a pipeline. *SIAM Journal of Scientific Computing*, 27:914–936, 2005.

[8] K. H. Bendiksen, D. Malnes, R. Moe, and S. Nuland. The dynamic two-fluid model OLGA: Theory and application. *SPE Production Engineering*, 6(2):171–180, 1991.

[9] A. Bermudez and M. E. Vazquez. Upwind methods for hyperbolic conservation laws with source terms. *Computers & Fluids*, 23(8):1049–1071, 1994.

[10] T. Berstad, C. Dørum, J. P. Jakobsen, H. Li, H. Lund, A. Morin, S. T. Munkejord, M. J. Mølnvik, H. O. Nordhagen, and E. Østby. CO_2 pipeline integrity: A new evaluation methodology. *Energy Procedia*, 4:3000–3007, 2011.

[11] D. Bestion. The physical closure laws in the CATHARE code. *Nuclear Engineering and Design*, 124:229–245, 1990.

[12] J. A. Boure, A. E. Bergles, and L. S. Tong. Review of two-phase flow instability. *Nuclear Engineering and Design*, 25(2):165–192, 1973.

[13] K. E. Carlson, R. A. Riemke, S. Z. Rouhani, R. W. Shumway, and W. L. Weaver. RELAP5/MOD3 code manual volume I: Code structure, system models and solution methods. *INEL Report, NUREG/CR-5535 (EGG-2596)*, 1990.

[14] G.-Q. Chen, C. D. Levermore, and T.-P. Liu. Hyperbolic conservation laws with stiff relaxation terms and entropy. *Communications on Pure and Applied Mathematics*, 47:787–830, 1994.

[15] A. Chinnayya, E. Daniel, and R. Saurel. Modelling detonation waves in heterogeneous energetic materials. *Journal of Computational Physics*, 196(2):490–538, 2004.

[16] M.-S. Chung, K.-S. Chang, and S.-J. Lee. Wave propagation in two-phase flow based on a new hyperbolic two-fluid model. *Numerical Heat Transfer, Part A*, 38:169–191, 2000.

[17] S. Clerc. Numerical simulation of the homogeneous equilibrium model for two-phase flows. *Journal of Computational Physics*, 161:354–375, 2000.

[18] J. Cortes. On the construction of upwind schemes for non-equilibrium transient two-phase flows. *Computers & Fluids*, 31:159–182, 2002.

[19] C. Coste, C. Laroche, and S. Fauve. Sound propagation in a liquid with vapor bubbles. *Europhysics Letters*, 11:343–347, 1990.

[20] S. M. Cox and P. P. Matthews. Exponential time differencing for stiff systems. *J. Comput. Phys.*, 176:430–455, 2002.

[21] T. Danielson, K. Bansal, B. Djoric, E. D. Duret, S. Johansen, and Ø. Hellan. Testing and qualification of a new multiphase flow simulator. Offshore Technology Conference, Houston, Texas, USA, 2–5 May, 2011.

[22] G. de Koeijer, J. H. Borch, M. Drescher, H. Li, Ø. Wilhelmsen, and J. Jakobsen. CO_2 transport – depressurization, heat transfer and impurities. *Energy Procedia*, 4:3008 – 3015, 2011.

[23] R. Donat and A. Martinez-Gavara. Hybrid second order schemes for scalar balance laws. *Journal of Scientific Computing*, 48(1-3):52–69, 2011.

[24] D. A. Drew. Mathematical modeling of two-phase flow. *Annual Review of Fluid Mechanics*, 15(1):261–291, 1983.

[25] D. A. Drew and S. L. Passman. *Theory of Multicomponent Fluids*. Springer-Verlag, New York, 1999.

[26] A. R. Edwards and T. P. O'Brien. Studies of phenomena connected with the depressurization of water reactors. *Journal of the British Nuclear Energy Society*, 9:125–135, 1970.

[27] S. Evje and T. Flåtten. On the wave structure of two-phase flow models. *SIAM Journal of Applied Mathematics*, 67(2):487–511, 2007.

[28] T. Flåtten, A. Morin, and S. T. Munkejord. Wave propagation in multicomponent flow models. *SIAM Journal on Applied Mathematics*, 70(8):2861–2882, 2010.

[29] T. Flåtten and S. T. Munkejord. The approximate Riemann solver of Roe applied to a drift-flux two-phase flow model. *ESAIM: Mathematical Modelling and Numerical Analysis*, 40:735–764, 2006.

[30] R. Gonzalez-Cinca, R. Folch, R. Benitez, L. Ramirez-Piscina, J. Casademunt, and A. Hernandez-Machado. Phase-field models in interfacial pattern formation out of equilibrium. In E. Korutcheva and R. Cuerno, editors, *Advances in Condensed Matter and Statistical Mechanics*, pages 203–236. Nova Science Publishers, New York, 2004.

[31] L. Gosse. A well-balanced flux-vector splitting scheme designed for hyperbolic systems conservation laws with source terms. *Computers and Mathematics with Applications*, 39:135–159, 2000.

[32] F. H. Harlow and J. E. Welch. Numerical calculation of time-dependent viscous incompressible flow of fluid with a free surface. *Phys. Fluid*, 8:2182–2189, 1965.

[33] C. W. Hirt and B. D. Nichols. Volume of fluid (VOF) method for the dynamics of free boundaries. *Journal of Computational Physics*, 39:201–225, 1981.

[34] M. Hochbruck, C. Lubich, and H. Selhofer. Exponential integrators for large systems of differential equations. *SIAM J. Sci. Comput.*, 19:1552–1574, 1998.

[35] M. E. Hubbard and P. García-Navarro. Flux difference splitting and the balancing of source terms and flux gradients. *Journal of Computational Physics*, 165:89–125, 2000.

[36] IEA. *Energy Technology Perspectives 2012 – Pathways to a Clean Energy System*. Paris, 2012.

[37] IPCC. *IPCC Special Report on Carbon Dioxide Capture and Storage*. Cambridge University Press, Cambridge, United Kingdom and New York, NY, USA., 2005. Prepared by Working Group III of the Intergovernmental Panel on Climate Change [Metz, B., O. Davidson, H. C. de Coninck, M. Loos, and L. A. Meyer (eds.)].

[38] M. Ishii. *Thermo-Fluid Dynamic Theory of Two-phase Flow*. Collection de la Direction des études et recherches d'Électricité de France. Eyrolles, Paris, 1975.

[39] M. Ishii and T. Hibiki. *Thermo-Fluid Dynamics of Two-Phase Flow*. Springer, New York, 2nd edition, 2011.

[40] P. Jenny and B. Müller. Rankine-Hugoniot-Riemann solver considering source terms and multidimensional effects. *Journal of Computational Physics*, 145:575–610, 1997.

[41] O. Jørstad. *Equations of State for Hydrocarbon Mixtures*. PhD thesis, NTH, 1997.

[42] S. Kakac and B. Bon. A review of two-phase flow dynamic instabilities in tube boiling systems. *Int. J. Heat Mass Transfer*, 51(3–4):399–433, 2008.

[43] A. K. Kapila, R. Menikoff, J. B. Bdzil, S. F. Son, and D. S. Stewart. Two-phase modeling of deflagration-to-detonation transition in granular materials: Reduced equations. *Physics of Fluids*, 13(10):3002–3024, 2001.

[44] B. L. Keyfitz, R. Sanders, and M. Sever. Lack of hyperbolicity in the two-fluid model for two-phase incompressible flow. *Discrete and continuous dynamical systems – Series B*, 3(3):541–563, 2003.

[45] S. W. Kieffer. Sound speed in liquid-gas mixtures: Water-air and water-steam. *Journal of Geophysical research*, 82(20):2895–2904, 1977.

[46] C. Kittel and H. Kroemer. *Thermal Physics*. W. H. Freeman and Company, New York, second edition, 1980.

[47] J. Leray. *Hyperbolic differential equations*. Lecture notes at The Institute for Advanced Study, Princeton, 1953.

[48] R. J. LeVeque. Balancing source terms and flux gradients in high-resolution Godunov methods: The quasi-steady wave-propagation algorithm. *J. Comput. Phys.*, 146:346–365, 1998.

[49] R. J. LeVeque. *Finite Volume Methods for Hyperbolic Problems*. Cambridge University Press, Cambridge, UK, 2002.

[50] R. J. LeVeque. A well-balanced path-integral f-wave method for hyperbolic problems with source terms. *Journal of Scientific Computing*, 48:209–226, 2011.

[51] R. J. LeVeque and D. S. Bale. Wave propagation methods for conservation laws with source terms. In *International Series of Numerical Mathematics*, volume 130. Birkhäuser, 1999.

[52] T.-P. Liu. Hyperbolic conservation laws with relaxation. *Commun. Math. Phys.*, 108:153–175, 1987.

[53] H. Lund, T. Flåtten, and S. T. Munkejord. Depressurization of carbon dioxide in pipelines – models and methods. *Energy Procedia*, 4:2984–2991, 2011.

[54] P. J. Martínez Ferrer, T. Flåtten, and S. T. Munkejord. On the effect of temperature and velocity relaxation in two-phase flow models. *ESAIM: Mathematical Modelling and Numerical Analysis*, 46:411–442, 2012.

[55] R. Menikoff. Empirical equations of state for solids. *Shock Wave Science and Technology Reference Library*, 2:143–188, 2007.

[56] R. Menikoff and B. J. Plohr. The Riemann problem for fluid flow of real materials. *Rev. Mod. Phys.*, 61(1):75–130, 1989.

[57] G. Moretti. The λ-scheme. *Computers and Fluids*, 7:191–205, 1979.

[58] A. Morin and T. Flåtten. A two-fluid four-equation model with instantaneous thermodynamical equilibrium. 2013. Preprint available at `http://www.math.ntnu.no/conservation/2013/002.pdf`. Submitted to *SIAM Journal on Applied Mathematics*.

[59] J. Murillo and P. García-Navarro. Weak solutions for partial differential equations with source terms: Application to the shallow water equations. *Journal of Computational Physics*, 229(11):4327–4368, 2010.

[60] F. Müller. Rankine-Hugoniot-Riemann solver for two-dimensional conservation laws. Master's thesis, ETH Zürich, 2010.

[61] S. Noelle, Y. Xing, and C.-W. Shu. High-order well-balanced schemes. In G. Puppo and G. Russo, editors, *Numerical Methods for Balance Laws. Quaderni di Matematica*, volume 24, pages 1–66. 2010.

[62] S. Noelle, N. Pankratz, G. Puppo, and J. R. Natvig. Well-balanced finite volume schemes of arbitrary order of accuracy for shallow water flows. *Journal of Computational Physics*, 213(2):474–499, 2006.

[63] S. Noelle, Y. Xing, and C.-W. Shu. High-order well-balanced finite volume WENO schemes for shallow water equation with moving water. *Journal of Computational Physics*, 226(1):29–58, 2007.

[64] S. Osher and R. P. Fedkiw. Level set methods. *Journal of Computational Physics*, 169:462–502, 2001.

[65] C. L. Pauchon and H. Dhulesia. TACITE: a transient tool for multiphase pipeline and well simulation. In *Proceedings – SPE Annual Technical Conference and Exhibition, Π Production Operations and Engineering, vol. 2, SPE 28545*, pages 311–326. Society of Petroleum Engineers, New Orleans, Louisiana, USA, 1994.

[66] M. Pelanti and K.-M. Shyue. A mixture-energy-consistent six-equation two-phase numerical model for fluids with interfaces, cavitation and evaporation waves. *Journal of Computational Physics*, 2013. Preprint.

[67] F. Petitpas, R. Saurel, E. Franquet, and A. Chinnayya. Modelling detonation waves in condensed energetic materials: multiphase CJ conditions and multidimensional computations. *Shock Waves*, 19(5):377–401, 2009.

[68] O. Redlich and J. N. S. Kwong. On the thermodynamics of solutions. V. An equation of state. Fugacities of gaseous solutions. *Chemical Review*, 44:233–244, 1949.

[69] J. Romate. An approximate Riemann solver for a two-phase flow model with numerically given slip relation. *Computers & Fluids*, 27(4):455–477, 1998.

[70] R. Saurel and R. Abgrall. A multiphase Godunov method for compressible multifluid and multiphase flow. *Journal of Computational Physics*, 150(2):425–467, Apr 1999.

[71] R. Saurel and R. Abgrall. A simple method for compressible multifluid flows. *SIAM J. Sci. Comput.*, 21(3):1115–1145, 1999.

[72] R. Saurel, F. Petitpas, and R. Abgrall. Modelling phase transition in metastable liquids: application to cavitating and flashing flows. *Journal of Fluid Mechanics*, 607:313–350, 2008.

[73] R. Saurel, F. Petitpas, and R. A. Berry. Simple and efficient relaxation methods for interfaces separating compressible fluids, cavitating flows and shocks in multiphase mixtures. *Journal of Computational Physics*, 228:1678–1712, 2009.

[74] R. Scardovelli and S. Zaleski. Direct numerical simulation of free-surface and interfacial flow. *Annual Review of Fluid Mechics*, 31:567–603, 1999.

[75] J. Sesterhenn. *Zur numerischen Berechnung kompressibler Strömungen bei kleinen Mach-Zahlen*. PhD thesis, ETH Zürich, 1995. Diss. ETH Nr. 11334.

[76] J. C. Slattery. Flow of viscoelastic fluids through porous media. *AIChE Journal*, 13(6):1066–1071, 1967.

[77] H. B. Stewart and B. Wendroff. Two-phase flow: Models and methods. *Journal of Computational Physics*, 56(3):363–409, 1984.

[78] H. Städtke. *Gasdynamic Aspects of Two-Phase Flow*. Wiley-VCH, Weinberg, Germany, 2006.

[79] Y. Taitel and D. Barnea. Two-phase slug flow. In *Advances in Heat Transfer*, volume 20, pages 83–132. Academic Press, San Diego, 1990.

[80] E. F. Toro. Multi-stage predictor-corrector fluxes for hyperbolic equations. Technical Report NI03037-NPA, Isaac Newton Institute for Mathematical Sciences, University of Cambridge, UK, 17th June 2003.

[81] E. F. Toro. *Riemann solvers and numerical methods for fluid dynamics*. Springer-Verlag, Berlin, 3rd edition, 2009.

[82] I. Toumi. An upwind numerical method for two-fluid two-phase flow models. *Nuclear Science and Engineering*, 123:147–168, 1996.

[83] G. Tryggvason, B. Bunner, A. Esmaeeli, D. Juric, N. Al-Rawahi, W. Tauber, J. Han, S. Nas, and Y. J. Jan. A front-tracking method for the computations of multiphase flow. *Journal of Computational Physics*, 169(2):708–759, 2001.

[84] G. Tryggvason, R. Scardovelli, and S. Zaleski. *Direct Numerical Simulations of Gas-Liquid Multiphase Flows*. Cambridge University Press, Cambridge, UK, 2011.

[85] J. O. Valderrama. The state of the cubic equations of state. *Ind. Eng. Chem. Res.*, 42:1603–1618, 2003.

[86] B. van Leer. Towards the ultimate conservative difference scheme V. A second order sequel to Godunov's method. *Journal of Computational Physics*, 32(1):101–136, July 1979.

[87] G. B. Wallis. *One-dimensional Two-phase Flow*. McGraw-Hill, New York, 1969.

[88] G. B. Whitham. *Linear and nonlinear waves*. John Wiley & Sons, New York, 1974.

[89] Y. Xing, C.-W. Shu, and S. Noelle. On the advantage of well-balanced schemes for moving-water equilibria of the shallow water equations. *Journal of Scientific Computing*, 48(1-3):339–349, 2011.

[90] W.-A. Yong. Basic aspects of hyperbolic relaxation systems. In *Advances in the Theory of Shock Waves*, volume 47 of *Progress in Nonlinear Differential Equations and Their Applications*, pages 259–305. Birkhäuser Boston, 2001.

[91] A. Zein, M. Hantke, and G. Warnecke. Modeling phase transition for compressible two-phase flows applied to metastable liquids. *Journal of Computational Physics*, 229(8):2964–2998, 2010.

[92] N. Zuber and J. A. Findlay. Average volumetric concentration in two-phase flow systems. *Journal of Heat Transfer - Transactions of the ASME*, 87:453–468, 1965.

My publications

[L1] T. Flåtten and H. Lund. Relaxation two-phase flow models and the subcharacteristic condition. *Mathematical Models and Methods in Applied Sciences*, 21(12):2379–2407, 2011.

[L2] H. Lund. A hierarchy of relaxation models for two-phase flow. *SIAM Journal of Applied Mathematics*, 72(6):1713–1741, 2012.

[L3] H. Lund and P. Aursand. Two-phase flow of CO_2 with phase transfer. *Energy Procedia*, 23:246–255, 2012.

[L4] H. Lund and P. Aursand. Splitting methods for relaxation two-phase flow models. *International Journal of Materials Engineering Innovation*, 4(2):117–131, 2013.

[L5] H. Lund, F. Müller, B. Müller, and P. Jenny. Rankine-Hugoniot-Riemann solver for steady multidimensional conservation laws with source terms. *Journal of Computational Physics*, 2013. Submitted for publication.

Doch Forschung strebt und ringt, ermüdend nie,
Nach dem Gesetz, dem Grund, Warum und Wie.

Johann Wolfgang von Goethe (1749–1832)
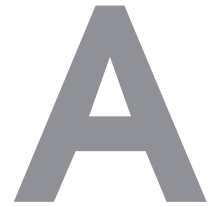
A
Research articles

Paper L1

Relaxation two-phase flow models and the subcharacteristic condition

Tore Flåtten and Halvor Lund

Is not included due to copyright

Paper L2

A hierarchy of relaxation models for two-phase flow

Halvor Lund

A HIERARCHY OF RELAXATION MODELS FOR TWO-PHASE FLOW[*]

HALVOR LUND[†]

Abstract. A hierarchy of relaxation two-phase flow models is considered, formulated as hyperbolic relaxation systems with source terms. The relaxation terms cause volume, heat, and mass transfer due to differences in pressure, temperature, and chemical potential, respectively, between the two phases. The subcharacteristic condition is a concept closely related to the stability of such relaxation systems. It states that the wave speeds of an equilibrium system never can exceed the speeds of the corresponding relaxation system. The work of Flåtten and Lund [*Math. Models Methods Appl. Sci.*, 21 (2011), pp. 2379–2407] is extended, with analytical expressions for the wave velocities in each model in the mentioned hierarchy. The subcharacteristic condition is explicitly shown to be satisfied using sums of squares, subject only to physically fundamental assumptions.

1. Introduction. Two-phase flow is found in many industrial applications, such as nuclear reactors [6], heat exchangers, petroleum production [4], and carbon dioxide capture, transport, and storage (CCS) [5]. Modeling such flow for use in simulations is a challenging task due to the complex nature of the interactions between the two phases, such as the movement and shape of the interface, and heat and mass transfer across it. In cases where the precise shape of the interface is of less importance or too computationally expensive to calculate, one may apply *averaging* (see, e.g., Ishii and Hibiki [13]) of the quantities of the two-phase fluid over a certain area or volume. These averaged models can often be formulated as hyperbolic relaxation systems with source terms accounting for the phase interactions, in the form

$$(1.1) \qquad \frac{\partial \boldsymbol{U}}{\partial t} + \boldsymbol{A}(\boldsymbol{U}) \frac{\partial \boldsymbol{U}}{\partial x} + \frac{1}{\varepsilon} \boldsymbol{R}(\boldsymbol{U}) = 0,$$

where $\boldsymbol{U} \in \mathbb{R}^n$ is the vector of unknowns, and ε is a characteristic time for the relaxation process described by $\boldsymbol{R}(\boldsymbol{U})$. The hyperbolicity requires that the $n \times n$ matrix $\boldsymbol{A}(\boldsymbol{U})$ be diagonalizable with real eigenvalues. Such relaxation systems have been analyzed by Chen, Levermore, and Liu [7], Liu [18], and Yong [30]. For a further review of the literature on such systems, see, e.g., Natalini [21].

We now assume that there exists a constant $k \times n$ matrix $\boldsymbol{P}$ associated with $\boldsymbol{R}$ which has the property that

$$(1.2) \qquad \boldsymbol{P}\boldsymbol{R}(\boldsymbol{U}) = 0.$$

[†]Department of Energy and Process Engineering, Norwegian University of Science and Technology (NTNU), NO-7491 Trondheim, Norway (halvor.lund@ntnu.no).

By multiplying (1.1) with $\boldsymbol{P}$ on the left, we get an equation system for the reduced variables $\boldsymbol{u} = \boldsymbol{P}\boldsymbol{U}$,

$$\text{(1.3)} \qquad \frac{\partial \boldsymbol{u}}{\partial t} + \boldsymbol{P}\boldsymbol{A}(\boldsymbol{U})\frac{\partial \boldsymbol{U}}{\partial x} = 0.$$

We now make the assumption that $\boldsymbol{u}$ determines an equilibrium value $\boldsymbol{U} = \mathcal{E}(\boldsymbol{u})$ such that $\boldsymbol{R}(\mathcal{E}(\boldsymbol{u})) = 0$ and

$$\text{(1.4)} \qquad \boldsymbol{P}\mathcal{E}(\boldsymbol{u}) = \boldsymbol{u}.$$

We finally assume that $\boldsymbol{u}$ is sufficiently smooth, so that we may formulate a quasi-linear *equilibrium* system as

$$\text{(1.5)} \qquad \frac{\partial \boldsymbol{u}}{\partial t} + \boldsymbol{B}(\boldsymbol{u})\frac{\partial \boldsymbol{u}}{\partial x} = 0,$$

$$\text{(1.6)} \qquad \boldsymbol{U} = \mathcal{E}(\boldsymbol{u}),$$

where $\boldsymbol{B}(\boldsymbol{u}) = \boldsymbol{P}\boldsymbol{A}(\mathcal{E}(\boldsymbol{u}))\partial_{\boldsymbol{u}}\mathcal{E}(\boldsymbol{u})$. As the relaxation time ε of the relaxation system (1.1) goes to zero, we expect the solutions to approach the solutions of the equilibrium system (1.5). This was rigorously justified by Yong [29] for quasi-linear relaxation systems satisfying a structural stability condition.

1.1. The subcharacteristic condition. The subcharacteristic condition is a concept which has proven to be closely related to the stability of relaxation systems. This was first mentioned by Whitham [28] for the linear case, and later developed for 2×2 nonlinear systems by Liu [18]. A similar condition was also discussed by Leray [17]. For more general systems, Yong [30] introduced a *relaxation criterion*, which imposes a certain stability requirement on the (linearized) relaxation system and requires that the relaxation term $\boldsymbol{R}(\boldsymbol{U})$ be nonoscillatory, and showed that for $k = n - 1$ this criterion leads to (a) convergence of the solution in the limit $\varepsilon \to 0$, and (b) the subcharacteristic condition being fulfilled.

The subcharacteristic condition has also proven to be an important trait of many physically revelant models. For this reason, the literature on relaxation systems puts a strong emphasis on this condition; see, e.g., Baudin et al. [2], Baudin, Coquel, and Tran [3], and Flåtten [11].

In the context of our relaxation system (1.1) and the corresponding equilibrium system (1.5), the subcharacteristic condition can be defined as follows.

DEFINITION 1. *Let the eigenvalues of the matrix* $\boldsymbol{A}(\boldsymbol{U})$ *of the relaxation system* (1.1) *be given by*

$$\text{(1.7)} \qquad \Lambda_1 \leq \cdots \leq \Lambda_i \leq \Lambda_{i+1} \leq \cdots \leq \Lambda_n.$$

Similarly, let the eigenvalues of the matrix $\boldsymbol{B}(\boldsymbol{u})$ *of the equilibrium system* (1.5) *be given by*

$$\text{(1.8)} \qquad \lambda_1 \leq \cdots \leq \lambda_i \leq \lambda_{i+1} \leq \cdots \leq \lambda_k.$$

Also let the equilibrium system's eigenvalues λ_i *be* interlaced *with the relaxation system's eigenvalues, in the sense that* $\lambda_i \in [\Lambda_i, \Lambda_{i+n-k}]$. *Here, the relaxation eigenvalues* Λ_i *are evaluated in an equilibrium state such that*

$$\text{(1.9)} \qquad \Lambda_i = \Lambda_i(\mathcal{E}(\boldsymbol{u})), \qquad \lambda_i = \lambda_i(\boldsymbol{u}).$$

Then the equilibrium system (1.5) *is said to satisfy the* subcharacteristic condition *with respect to the relaxation system* (1.1).

Chen, Levermore, and Liu [7] proved that the subcharacteristic condition is satisfied if there exists a convex entropy function for the relaxation system (1.1), and that this entropy is locally dissipated by the relaxation term **R**.

1.2. The model hierarchy. In a completely general (averaged) two-phase flow model, one may imagine that the two phases have separate pressures p_k, temperatures T_k, chemical potentials μ_k,[1] and velocities v_k, where k is the phase index. The system can then be moved towards equilibrium by employing *relaxation source terms*, causing volume transfer due to pressure differences, heat transfer due to temperature differences, mass transfer due to chemical potential differences, and momentum transfer due to velocity differences between the two phases.

In our paper, we consider only homogeneous flow models, i.e., models where the phase velocities are equal. Discussion of models with different velocities, typically called two-fluid models, may be found in [1, 9, 22, 31]. We are then left with three relaxation processes, namely relaxation of pressure, temperature, and chemical potential. By considering either the equilibrium (stiff) limit or the nonequilibrium (nonstiff) limit of these three processes, we get a hierarchy of models with different equilibrium assumptions.

Figure 1.1 illustrates this hierarchy, where circles symbolize models and arrows denote how the models are related through equilibrium assumptions on individual variables. Each arrow corresponds to a subcharacteristic condition for the wave speeds of the two models which the arrow connects. To the far left in this figure, we find the basic model, denoted by 0, and to the far right, we find the homogeneous equilibrium model ($pT\mu$), in which the two phases are in full equilibrium. The full hierarchy is based on the work by Flåtten and Lund [10], who developed the basis (the basic model) for the hierarchy, along with the p, pT, $p\mu$, and $pT\mu$-models, shown with dashed lines in Figure 1.1. In the present work, we complete the hierarchy with the T, μ, and $T\mu$-models, and the seven related subcharacteristic conditions, shown with solid lines in Figure 1.1.

In this paper, we will present each of the models in this hierarchy. In particular, the formulation of the hyperbolic relaxation systems and the wave velocities (and hence the speed of sound) of the models will be presented, and we will explicitly show how the subcharacteristic condition is satisfied for each equilibrium assumption. More specifically, we will show how to relate the mixture speed of sound $\tilde{a}$ of an equilibrium model $\mathcal{X}$ and the corresponding relaxation (nonequilibrium) model $\mathcal{Y}$ by writing

$$(1.10) \qquad\qquad \tilde{a}_{\mathcal{X}}^{-2} = \tilde{a}_{\mathcal{Y}}^{-2} + Z_{\mathcal{X}}^{\mathcal{Y}},$$

where $Z_{\mathcal{X}}^{\mathcal{Y}}$ is a positive term expressed using sums of squares. This is shown to be sufficient to satisfy the subcharacteristic condition of Definition 1.

Stiff relaxation terms will cause dispersion of sound waves, with a speed of sound dependent on the wave number and the relaxation parameter ε. For more discussion regarding sound wave dispersion in certain models, see, e.g., Städtke [26, Chap. 6] or Jinliang and Tingkuan [14]. We will focus our analysis on the nonstiff limit and the equilibrium limit, which are without dispersion.

---

[1]Not to be confused with dynamic viscosity.
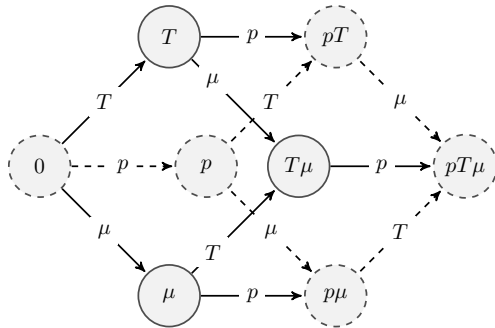
Fig. 1.1. *Model hierarchy. Each circle symbolizes a two-phase flow model assuming equilibrium in zero or more of the variables p (pressure), T (temperature), and μ (chemical potential). Arrows represent a relaxation process of one variable, pointing in the direction of equilibrium in that variable. Solid lines indicate original contributions in the present paper, dashed lines indicate results presented in* [10].

1.3. Paper outline. In the following, we will, in turn, present each of the eight different models shown in Figure 1.1 in sections 2–9. Three of the models have, to the best of the author's knowledge, not been described elsewhere, and thus represent original contributions. The models in question are the thermal equilibrium, the chemical equilibrium, and the thermal-chemical equilibrium models, described in sections 4, 5, and 8, respectively. The remaining models are those developed by Flåtten and Lund [10], which are all briefly included here for completeness. For each model, we aim towards an explicit expression of the mixture speed of sound, and prove that the subcharacteristic condition of Definition 1 is satisfied by relating speeds of sound in the different models using sums of squares.

In section 10, we show plots of the mixture speeds of sound in the models of the hierarchy as functions of gas volume fraction, for relevant cases for water and carbon dioxide. Finally, section 11 draws some conclusions and outlines possible further work.

2. Basic model. In this section, we present the basic one-dimensional two-phase flow model, in which we let the two phases have separate pressures, temperatures, and chemical potentials, while the velocity v is equal in the two phases. Heat, mass, and volume transfer between the phases are modeled using relaxation source terms. The model was proposed in this form by Flåtten and Lund [10], and forms the basis from which we can derive the other models in the hierarchy.

2.1. Mass balance. In general, we have one mass balance equation for each phase, which may be written as [10]

$$(2.1) \qquad \frac{\partial(\alpha_g \rho_g)}{\partial t} + \frac{\partial(\alpha_g \rho_g v)}{\partial x} = \mathcal{K}(\mu_\ell - \mu_g),$$

$$(2.2) \qquad \frac{\partial(\alpha_\ell \rho_\ell)}{\partial t} + \frac{\partial(\alpha_\ell \rho_\ell v)}{\partial x} = \mathcal{K}(\mu_g - \mu_\ell),$$

where we use the following notation:

$\quad$ α_k $\quad$ volume fraction of phase k,
$\quad$ ρ_k $\quad$ density of phase k,
$\quad$ v $\quad$ fluid velocity,
$\quad$ μ_k $\quad$ chemical potential of phase k,
$\quad$ $\mathcal{K} \geq 0$ $\quad$ chemical potential relaxation parameter.

Here the chemical potential relaxation source term ensures that mass flows from high to low chemical potential, if we only assume that $\mathcal{K} \geq 0$. Mass transfer modeled using such a relaxation term can be found in the works of, e.g., Saurel, Petitpas, and Abgrall [23] and Stewart and Wendroff [25]. Adding (2.1)–(2.2) yields the conservation equation for total mass,

$$(2.3) \qquad \frac{\partial \rho}{\partial t} + \frac{\partial (\rho v)}{\partial x} = 0.$$

Here, the mixture density ρ is given by

$$(2.4) \qquad \rho = \alpha_g \rho_g + \alpha_\ell \rho_\ell.$$

2.2. Volume advection. We assume that volume transfer, in Lagrangian coordinates, can only be caused by differences in pressure, which is a common assumption also found, e.g., in models by Baer and Nunziato [1] and Saurel and Abgrall [22],

$$(2.5) \qquad D_t \alpha_g = \mathcal{J}(p_g - p_\ell),$$

where we have introduced the *material derivative*, defined by

$$(2.6) \qquad D_t \equiv \frac{\partial}{\partial t} + v \frac{\partial}{\partial x},$$

and the notation

$\quad$ p_k $\quad$ pressure of phase k,
$\quad$ $\mathcal{J} \geq 0$ $\quad$ pressure relaxation parameter.

Here, we note that the pressure relaxation causes volume to be transferred *to* the phase with highest pressure; i.e., the expanding phase has the highest pressure. The only assumption made is that the relaxation parameter is nonnegative, $\mathcal{J} \geq 0$.

2.3. Momentum conservation. Since the basic model is defined as a homogeneous flow model, with equal velocity v for the two phases, the momentum conservation may be formulated as a conservation equation for the total momentum,

$$(2.7) \qquad \frac{\partial (\rho v)}{\partial t} + \frac{\partial (\rho v^2 + \alpha_g p_g + \alpha_\ell p_\ell)}{\partial x} = 0.$$

2.4. Energy equations. We assume that each relaxation process should conserve energy and that in Lagrangian coordinates, only the relaxation terms contribute to entropy changes. This allows us to derive energy equations for each phase, which may be written as [10]

$$(2.8) \quad \frac{\partial E_g}{\partial t} + \frac{\partial (v E_g)}{\partial x} + \alpha_g p_g \frac{\partial v}{\partial x} + \frac{v}{\rho} m_g \frac{\partial (\alpha_g p_g + \alpha_\ell p_\ell)}{\partial x}$$
$$= \mathcal{H}(T_\ell - T_g) + p^* \mathcal{J}(p_\ell - p_g) + \left(\mu^* + \frac{1}{2} v^2 \right) \mathcal{K}(\mu_\ell - \mu_g),$$

(2.9) $\dfrac{\partial E_\ell}{\partial t} + \dfrac{\partial(vE_\ell)}{\partial x} + \alpha_\ell p_\ell \dfrac{\partial v}{\partial x} + \dfrac{v}{\rho}m_\ell \dfrac{\partial(\alpha_{\mathrm{g}}p_{\mathrm{g}} + \alpha_\ell p_\ell)}{\partial x}$

$$= \mathcal{H}(T_{\mathrm{g}} - T_\ell) + p^* \mathcal{J}(p_{\mathrm{g}} - p_\ell) + \left(\mu^* + \frac{1}{2}v^2\right)\mathcal{K}(\mu_{\mathrm{g}} - \mu_\ell),$$

where p^* and μ^* are the pressure and chemical potential, respectively, at the gas-liquid interface. The detailed derivation can be found in [10]. For brevity, we have also introduced $m_k = \alpha_k \rho_k$, the mass per volume of phase k. The total energy in each phase, E_k, is given by

(2.10) $$E_k = \alpha_k \rho_k \left(e_k + \frac{1}{2}v^2\right).$$

The temperature relaxation parameter is denoted by $\mathcal{H} \geq 0$, and the corresponding heat source term $\mathcal{H}(T_\ell - T_{\mathrm{g}})$ causes heat to flow from the hot to the cold phase.

2.5. Entropy evolution. When deriving the wave velocities of the present model and other models in the hierarchy, it is often useful to formulate the model using entropy evolution equations instead of the energy equations (2.8)–(2.9). These can be formulated as [10]

(2.11) $\mathrm{D}_t s_{\mathrm{g}} = \left(\dfrac{\mu^* - \mu_{\mathrm{g}}}{T_{\mathrm{g}}} - s_{\mathrm{g}}\right)\dfrac{\mathcal{K}}{m_{\mathrm{g}}}(\mu_\ell - \mu_{\mathrm{g}}) + \dfrac{\mathcal{H}}{m_{\mathrm{g}}}\dfrac{T_\ell - T_{\mathrm{g}}}{T_{\mathrm{g}}} + \dfrac{p^* - p_{\mathrm{g}}}{m_{\mathrm{g}}T_{\mathrm{g}}}\mathcal{J}(p_\ell - p_{\mathrm{g}}),$

(2.12) $\mathrm{D}_t s_\ell = \left(\dfrac{\mu^* - \mu_\ell}{T_\ell} - s_\ell\right)\dfrac{\mathcal{K}}{m_\ell}(\mu_{\mathrm{g}} - \mu_\ell) + \dfrac{\mathcal{H}}{m_\ell}\dfrac{T_{\mathrm{g}} - T_\ell}{T_\ell} + \dfrac{p^* - p_\ell}{m_\ell T_\ell}\mathcal{J}(p_{\mathrm{g}} - p_\ell),$

where s_k is the entropy density of phase k. These equations may also be formulated in a balance form,

(2.13) $T_{\mathrm{g}}\left(\dfrac{\partial(m_{\mathrm{g}}s_{\mathrm{g}})}{\partial t} + \dfrac{\partial(m_{\mathrm{g}}s_{\mathrm{g}}v)}{\partial x}\right)$

$$= \mathcal{H}(T_\ell - T_{\mathrm{g}}) + (p^* - p_{\mathrm{g}})\mathcal{J}(p_\ell - p_{\mathrm{g}}) + (\mu^* - \mu_{\mathrm{g}})\mathcal{K}(\mu_\ell - \mu_{\mathrm{g}}),$$

(2.14) $T_\ell\left(\dfrac{\partial(m_\ell s_\ell)}{\partial t} + \dfrac{\partial(m_\ell s_\ell v)}{\partial x}\right)$

$$= \mathcal{H}(T_{\mathrm{g}} - T_\ell) + (p^* - p_\ell)\mathcal{J}(p_{\mathrm{g}} - p_\ell) + (\mu^* - \mu_\ell)\mathcal{K}(\mu_{\mathrm{g}} - \mu_\ell).$$

The latter equations may be derived by using the entropy equations (2.11)–(2.12), the mass balance equations (2.1)–(2.2), and the volume fraction equation (2.5).

2.6. The laws of thermodynamics. An important point made by Flåtten and Lund [10] is that this basic model satisfies the first and second laws of thermodynamics, which is a sensible requirement to have on any two-phase flow model. By adding the two energy equations (2.8)–(2.9), we get

(2.15) $$\dfrac{\partial(E_{\mathrm{g}} + E_\ell)}{\partial t} + \dfrac{\partial[(E_{\mathrm{g}} + E_\ell + \alpha_{\mathrm{g}}p_{\mathrm{g}} + \alpha_\ell p_\ell)v]}{\partial x} = 0,$$

and thus the total energy is conserved, and the model fulfills the first law. The second law, expressing that entropy should be nondecreasing, is also satisfied, only requiring that

$$\text{(2.16)} \qquad \mathcal{H} \geq 0,$$

$$\text{(2.17)} \qquad \mathcal{J} \geq 0,$$

$$\text{(2.18)} \qquad \mathcal{K} \geq 0,$$

$$\text{(2.19)} \qquad \min(p_{\mathrm{g}}, p_\ell) \leq p^* \leq \max(p_{\mathrm{g}}, p_\ell),$$

$$\text{(2.20)} \qquad \min(\mu_{\mathrm{g}}, \mu_\ell) \leq \mu^* \leq \max(\mu_{\mathrm{g}}, \mu_\ell).$$

The full proof can be found in [10].

2.7. Wave velocities. In the nonstiff limit $\mathcal{K}, \mathcal{J}, \mathcal{H} \to 0$, the wave velocities of the basic model (2.1)–(2.2), (2.5)–(2.7), (2.11)–(2.12) can be found to be [10]

$$\text{(2.21)} \qquad \boldsymbol{\lambda}_0 = \{v - \tilde{a}_0, v, v, v, v + \tilde{a}_0\},$$

where $\tilde{a}_0$ is the mixture speed of sound of the basic model, given by

$$\text{(2.22)} \qquad \tilde{a}_0 = \frac{m_{\mathrm{g}} c_{\mathrm{g}}^2 + m_\ell c_\ell^2}{\rho},$$

i.e., a mass weighted average of the single-phase speeds of sound, which, in turn (for phase k), are defined as

$$\text{(2.23)} \qquad c_k^2 = \left(\frac{\partial p_k}{\partial \rho_k} \right)_{s_k}.$$

3. Pressure relaxation. In this section, we consider the model that results when we impose volume transfer equilibrium in the basic model of section 2. In other words, we let the pressure relaxation parameter $\mathcal{J}$ go to infinity, which we expect to correspond to the assumption

$$\text{(3.1)} \qquad p_{\mathrm{g}} = p_\ell = p^* = p,$$

i.e., mechanical equilibrium between the two phases. The mechanical equilibrium model equations may be obtained by replacing the pressure relaxation term $\mathcal{J}(p_{\mathrm{g}} - p_\ell)$ using the volume fraction equation (2.5), as described in detail by Flåtten, Morin, and Munkejord [11]. The full model equations are not stated here, but the derivation may be found in [10]. This five-equation model has been studied by a number of authors [11, 15, 20, 23, 24, 26], with slightly varying formulations.

3.1. Wave velocities. The wave velocities of the mechanical equilibrium model, in the nonstiff limit where $\mathcal{H}, \mathcal{K} \to 0$, are given by [11]

$$\text{(3.2)} \qquad \boldsymbol{\lambda}_p = \{v - \tilde{a}_p, v, v, v + \tilde{a}_p\},$$

where $\tilde{a}_p$ is the mixture speed of sound, given by

$$\text{(3.3)} \qquad \tilde{a}_p^{-2} = \rho \left(\frac{\alpha_{\mathrm{g}}}{\rho_{\mathrm{g}} c_{\mathrm{g}}^2} + \frac{\alpha_\ell}{\rho_\ell c_\ell^2} \right).$$

This is a classic, well-known expression, also referred to as the *Wood speed of sound* [24] or *Wallis speed of sound* [27].

As shown by Flåtten and Lund [10], the mechanical equilibrium model satisfies the subcharacteristic condition with respect to the basic model, only requiring $\rho_k > 0$. This can be shown by writing the mixture speed of sound as

$$(3.4) \qquad \tilde{a}_p^{-2} = \tilde{a}_0^{-2} + Z_p^0,$$

where

$$(3.5) \qquad Z_p^0 = \tilde{a}_0^{-2} \frac{\alpha_\mathrm{g} \alpha_\ell}{\rho_\mathrm{g} c_\mathrm{g}^2 \rho_\ell c_\ell^2} (\rho_\mathrm{g} c_\mathrm{g}^2 - \rho_\ell c_\ell^2)^2.$$

4. Temperature relaxation. In this section, we consider the model that results when we impose heat transfer equilibrium in the basic model of section 2. In other words, we let the temperature relaxation parameter $\mathcal{H}$ go to infinity, which we expect to correspond to the assumption

$$(4.1) \qquad T_\mathrm{g} = T_\ell = T,$$

i.e., thermal equilibrium between the two phases. The model equations and wave velocities for this model have not been found elsewhere, and will thus be derived here.

When we let the temperature relaxation parameter go to infinity, $\mathcal{H} \to \infty$, the value of the temperature relaxation term $\mathcal{H}(T_\ell - T_\mathrm{g})$ is no longer defined. Thus, to derive the equations describing the current model, we find it necessary to determine an explicit expression for the temperature relaxation (or heat transfer) term.

To this end, we consider the two following thermodynamic differentials:

$$(4.2) \qquad \mathrm{d}T = \frac{\Gamma_\mathrm{g} T}{\rho_\mathrm{g} c_\mathrm{g}^2} \mathrm{d}p_\mathrm{g} + \frac{T}{c_{p,\mathrm{g}}} \mathrm{d}s_\mathrm{g} = \frac{\Gamma_\ell T}{\rho_\ell c_\ell^2} \mathrm{d}p_\ell + \frac{T}{c_{p,\ell}} \mathrm{d}s_\ell,$$

$$(4.3) \qquad \mathrm{d}p_k = c_k^2 \mathrm{d}\rho_k + \rho_k \Gamma_k T \mathrm{d}s_k,$$

where Γ_k is the *Grüneisen coefficient* and $c_{p,k}$ is the specific heat capacity at constant pressure, defined by

$$(4.4) \qquad \Gamma_k = \frac{1}{\rho_k} \left(\frac{\partial p_k}{\partial e_k} \right)_{\rho_k},$$

$$(4.5) \qquad c_{p,k} = T_k \left(\frac{\partial s_k}{\partial T_k} \right)_{p_k}.$$

By using (2.1)–(2.2), (2.5), (2.11)–(2.12), together with (4.2)–(4.3) expressed with the material derivative, we may solve for the heat transfer term, which yields

$$(4.6) \quad \mathcal{H}(T_\ell - T_\mathrm{g}) = \frac{\Gamma_\mathrm{g} - \Gamma_\ell}{\frac{\Gamma_\mathrm{g}^2}{m_\mathrm{g} c_\mathrm{g}^2} + \frac{1}{C_{p,\mathrm{g}} T} + \frac{\Gamma_\ell^2}{m_\ell c_\ell^2} + \frac{1}{C_{p,\ell} T}} \frac{\partial v}{\partial x}$$

$$- \frac{\frac{\Gamma_\mathrm{g}}{m_\mathrm{g}} + \frac{\Gamma_\ell}{m_\ell} + \left(\frac{\Gamma_\mathrm{g}^2}{m_\mathrm{g} c_\mathrm{g}^2} + \frac{1}{C_{p,\mathrm{g}} T} \right)(\mu^* - h_\mathrm{g}) + \left(\frac{\Gamma_\ell^2}{m_\ell c_\ell^2} + \frac{1}{C_{p,\ell} T} \right)(\mu^* - h_\ell)}{\frac{\Gamma_\mathrm{g}^2}{m_\mathrm{g} c_\mathrm{g}^2} + \frac{1}{C_{p,\mathrm{g}} T} + \frac{\Gamma_\ell^2}{m_\ell c_\ell^2} + \frac{1}{C_{p,\ell} T}} \mathcal{K}(\mu_\ell - \mu_\mathrm{g})$$

$$- \frac{\frac{\Gamma_\mathrm{g}}{\alpha_\mathrm{g}} + \frac{\Gamma_\ell}{\alpha_\ell} + \left(\frac{\Gamma_\mathrm{g}^2}{m_\mathrm{g} c_\mathrm{g}^2} + \frac{1}{C_{p,\mathrm{g}} T} \right)(p^* - p_\mathrm{g}) + \left(\frac{\Gamma_\ell^2}{m_\ell c_\ell^2} + \frac{1}{C_{p,\ell} T} \right)(p^* - p_\ell)}{\frac{\Gamma_\mathrm{g}^2}{m_\mathrm{g} c_\mathrm{g}^2} + \frac{1}{C_{p,\mathrm{g}} T} + \frac{\Gamma_\ell^2}{m_\ell c_\ell^2} + \frac{1}{C_{p,\ell} T}} \mathcal{J}(p_\ell - p_\mathrm{g}),$$

where

$$(4.7) \qquad C_{p,k} = \alpha_k \rho_k c_{p,k}$$

is the extensive heat capacity at constant pressure. We may now formulate the equations describing the thermal equilibrium model.

4.1. The thermal equilibrium model. The thermal equilibrium model can now be summarized using the following equations.

- Mass balance:

$$(4.8) \qquad \frac{\partial(\alpha_g \rho_g)}{\partial t} + \frac{\partial(\alpha_g \rho_g v)}{\partial x} = \mathcal{K}(\mu_\ell - \mu_g),$$

$$(4.9) \qquad \frac{\partial(\alpha_\ell \rho_\ell)}{\partial t} + \frac{\partial(\alpha_\ell \rho_\ell v)}{\partial x} = \mathcal{K}(\mu_g - \mu_\ell).$$

- Momentum conservation:

$$(4.10) \qquad \frac{\partial(\rho v)}{\partial t} + \frac{\partial(\rho v^2 + \alpha_g p_g + \alpha_\ell p_\ell)}{\partial x} = 0.$$

- Volume fraction evolution:

$$(4.11) \qquad \mathrm{D}_t \alpha_g = \mathcal{J}(p_g - p_\ell).$$

- Energy conservation:

$$(4.12) \qquad \frac{\partial E}{\partial t} + \frac{\partial[(E + p)v]}{\partial x} = 0.$$

These model equations are (2.1)–(2.2), (2.5), (2.7), and (2.15) from the basic model. Herein, E is the total energy per volume, defined by

$$(4.13) \qquad E = E_g + E_\ell \equiv \alpha_g \rho_g \left(e_g + \frac{1}{2} v^2 \right) + \alpha_\ell \rho_\ell \left(e_\ell + \frac{1}{2} v^2 \right).$$

4.2. Wave velocities. We now wish to derive the wave velocities in the nonstiff limit where the pressure and chemical potential relaxation parameters vanish, $\mathcal{J}, \mathcal{K} \to 0$. To this end, we find it useful to derive the material derivative of the effective pressure $p_{\mathrm{eff}} \equiv \alpha_g p_g + \alpha_\ell p_\ell$,

$$(4.14) \qquad \mathrm{D}_t p_{\mathrm{eff}} = \alpha_g \mathrm{D}_t p_g + \alpha_\ell \mathrm{D}_t p_\ell + (p_g - p_\ell) \mathrm{D}_t \alpha_g.$$

We insert for the pressure differentials $\mathrm{D}_t p_k$ from (4.3), and then rewrite the density differentials $\mathrm{D}_t \rho_k$ using the product rule on $\mathrm{D}_t m_k$, yielding

$$(4.15) \qquad \mathrm{D}_t p_{\mathrm{eff}} = c_g^2 \mathrm{D}_t m_g + m_g \Gamma_g T \mathrm{D}_t s_g + c_\ell^2 \mathrm{D}_t m_\ell + m_\ell \Gamma_\ell T \mathrm{D}_t s_\ell,$$

where have used that $\mathrm{D}_t \alpha_g \to 0$ since $\mathcal{J} \to 0$. The terms $\mathrm{D}_t m_k$ may be found by rewriting the mass balance equations (4.8)–(4.9). We also replace $\mathrm{D}_t s_k$ from (2.11)–(2.12) and (4.6), keeping in mind that $\mathcal{K}, \mathcal{J} \to 0$, and finally get

$$(4.16) \qquad \mathrm{D}_t p_{\mathrm{eff}} = -\rho \tilde{a}_T^2 \frac{\partial v}{\partial x},$$

where

$$(4.17) \qquad \tilde{a}_T^2 = \frac{1}{\rho} \frac{m_\ell c_\ell^2 m_{\mathrm{g}} c_{\mathrm{g}}^2 \left(\frac{\Gamma_{\mathrm{g}}}{m_{\mathrm{g}} c_{\mathrm{g}}^2} + \frac{\Gamma_\ell}{m_\ell c_\ell^2} \right)^2 + \frac{1}{T} \left(\frac{1}{C_{p,\mathrm{g}}} + \frac{1}{C_{p,\ell}} \right) (m_{\mathrm{g}} c_{\mathrm{g}}^2 + m_\ell c_\ell^2)}{\frac{1}{m_{\mathrm{g}} c_{\mathrm{g}}^2} \Gamma_{\mathrm{g}}^2 + \frac{1}{m_\ell c_\ell^2} \Gamma_\ell^2 + \frac{1}{T} \left(\frac{1}{C_{p,\mathrm{g}}} + \frac{1}{C_{p,\ell}} \right)}.$$

Using the gas mass balance equation (4.8) and total continuity equation (2.3), we find that the gas mass fraction $Y_{\mathrm{g}} \equiv \frac{m_{\mathrm{g}}}{\rho}$ satisfies

$$(4.18) \qquad \mathrm{D}_t Y_{\mathrm{g}} = \frac{\mathcal{K}}{\rho} (\mu_\ell - \mu_{\mathrm{g}}).$$

Thus, in the nonstiff limit $\mathcal{J}, \mathcal{K} \to 0$, we know from (2.5) and (4.18) that Y_{g} and α_{g} are characteristic variables with a corresponding eigenvalue v. The remaining model equations, namely the total continuity equation (2.3), momentum conservation (4.10), and pressure evolution equation (4.16), may be formulated as a quasi-linear system,

$$(4.19) \qquad \boldsymbol{u}_t + \begin{bmatrix} 0 & 1 & 0 \\ -v^2 & 2v & 1 \\ -v\tilde{a}_T^2 & \tilde{a}_T^2 & v \end{bmatrix} \boldsymbol{u}_x \equiv \boldsymbol{u}_t + \boldsymbol{A}(\boldsymbol{u})\boldsymbol{u}_x = 0,$$

where $\boldsymbol{u} = [\rho, \rho v, p_{\mathrm{eff}}]$. The eigenvalues of the matrix $\boldsymbol{A}(\boldsymbol{u})$ are given by $\{v - \tilde{a}_T, v, v + \tilde{a}_T\}$, so the eigenstructure of the full model is given by

$$(4.20) \qquad \boldsymbol{\lambda}_T = \{v - \tilde{a}_T, v, v, v + \tilde{a}_T\},$$

where the mixture speed of sound is $\tilde{a}_T$, given by (4.17).

4.2.1. The subcharacteristic condition with respect to the basic model. From (2.22) and (4.17), we find that the mixture speed of sound of the thermal equilibrium model can be written as

$$(4.21) \qquad \tilde{a}_T^{-2} = \tilde{a}_0^{-2} + Z_T^0,$$

where

$$(4.22) \qquad Z_T^0 = \frac{1}{\tilde{a}_0^2} \frac{(\Gamma_{\mathrm{g}} - \Gamma_\ell)^2}{m_\ell c_\ell^2 m_{\mathrm{g}} c_{\mathrm{g}}^2 \left(\frac{\Gamma_{\mathrm{g}}}{m_{\mathrm{g}} c_{\mathrm{g}}^2} + \frac{\Gamma_\ell}{m_\ell c_\ell^2} \right)^2 + \left(\frac{1}{C_{p,\ell} T} + \frac{1}{C_{p,\mathrm{g}} T} \right) \rho \tilde{a}_0^2}.$$

PROPOSITION 1. *The thermal equilibrium model given by (4.8)–(4.12) satisfies the subcharacteristic condition with respect to the basic model of section 2, subject only to the physically fundamental conditions*

$$\rho_k > 0,$$
$$c_{p,k} > 0,$$
$$T > 0.$$

Proof. By (2.21) and (4.20), we see that the interlacing condition in Definition 1 reduces to the requirement that

$$(4.23) \qquad \tilde{a}_0 \geq \tilde{a}_T,$$

which follows from (4.21)–(4.22) and the given conditions for ρ_k, $c_{p,k}$, and T. $\qquad \blacksquare$

5. Chemical potential relaxation. In this section, we investigate the model that arises when we impose mass transfer equilibrium in the basic model of section 2. In other words, the phase transition between liquid and gas will be infinitely fast. This is equivalent to letting the chemical potential relaxation parameter $\mathcal{K}$ go to infinity, which we expect to correspond to the assumption

$$(5.1) \qquad \mu_{\mathrm{g}} = \mu_\ell = \mu = \mu^*,$$

i.e., equal chemical potentials and chemical equilibrium. The model equations and wave velocities for this model have not been found elsewhere, and will thus be derived here.

5.1. Mass fraction evolution equations. In the limit $\mathcal{K} \to \infty$, the chemical potentials in the two phases are equal, $\mu_{\mathrm{g}} = \mu_\ell$, and hence the value of the mass relaxation term $\mathcal{K}(\mu_{\mathrm{g}} - \mu_\ell)$ is undefined. To find an expression for this quantity, we find it necessary to derive some differentials. Since the chemical potentials are equal, $\mu_{\mathrm{g}} = \mu_\ell$, so are their differentials, $\mathrm{d}\mu_{\mathrm{g}} = \mathrm{d}\mu_\ell$, which yields

$$(5.2) \qquad \frac{1}{\rho_\ell}\mathrm{d}p_\ell - s_\ell \mathrm{d}T_\ell = \frac{1}{\rho_{\mathrm{g}}}\mathrm{d}p_{\mathrm{g}} - s_{\mathrm{g}}\mathrm{d}T_{\mathrm{g}}.$$

The temperature and pressure differentials can be written as

$$(5.3) \qquad \mathrm{d}T_k = \frac{\Gamma_k T_k}{\rho_k c_k^2}\mathrm{d}p_k + \frac{T_k}{c_{p,k}}\mathrm{d}s_k,$$

$$(5.4) \qquad \mathrm{d}p_k = c_k^2 \mathrm{d}\rho_k + \rho_k \Gamma_k T_k \mathrm{d}s_k.$$

We then insert for the temperature differential (5.3) and then the pressure differential (5.4) in (5.2), which yields

$$(5.5) \qquad \frac{\xi_\ell^2}{\rho_\ell}\mathrm{d}\rho_\ell + \left(\frac{\rho_\ell}{s_\ell}(c_\ell^2 - \xi_\ell^2) - \frac{s_\ell T_\ell}{c_{p,\ell}}\right)\mathrm{d}s_\ell = \frac{\xi_{\mathrm{g}}^2}{\rho_{\mathrm{g}}}\mathrm{d}\rho_{\mathrm{g}} + \left(\frac{\rho_{\mathrm{g}}}{s_{\mathrm{g}}}(c_{\mathrm{g}}^2 - \xi_{\mathrm{g}}^2) - \frac{s_{\mathrm{g}} T_{\mathrm{g}}}{c_{p,\mathrm{g}}}\right)\mathrm{d}s_{\mathrm{g}},$$

where we have introduced the abbreviation $\xi_k^2 \equiv c_k^2 - \Gamma_k s_k T_k$. Next, we have use for the differential of the total density,

$$(5.6) \qquad \mathrm{d}\rho = \alpha_{\mathrm{g}}\mathrm{d}\rho_{\mathrm{g}} + \alpha_\ell \mathrm{d}\rho_\ell + (\rho_{\mathrm{g}} - \rho_\ell)\mathrm{d}\alpha_{\mathrm{g}},$$

and gas mass fraction differential

$$(5.7) \qquad \mathrm{d}Y_{\mathrm{g}} = -\frac{m_{\mathrm{g}}}{\rho^2}\mathrm{d}\rho + \frac{1}{\rho}(\alpha_{\mathrm{g}}\mathrm{d}\rho_{\mathrm{g}} + \rho_{\mathrm{g}}\mathrm{d}\alpha_{\mathrm{g}}).$$

By writing (5.5)–(5.7) using the material derivative, together with the equations for entropy (2.11)–(2.12), volume fraction (2.5), total continuity (2.3), and gas mass fraction (4.18), we arrive at the mass fraction evolution equation,

$$(5.8) \quad \mathrm{D}_t Y_{\mathrm{g}} = \frac{1}{\left(\frac{\xi_{\mathrm{g}}^4}{m_{\mathrm{g}} c_{\mathrm{g}}^2} + \frac{\xi_\ell^4}{m_\ell c_\ell^2} + \frac{s_\ell^2 T_\ell}{C_{p,\ell}} + \frac{s_{\mathrm{g}}^2 T_{\mathrm{g}}}{C_{p,\mathrm{g}}}\right)\rho}$$

$$\cdot\left[(\xi_{\mathrm{g}}^2 - \xi_\ell^2)\frac{\partial v}{\partial x} + \left(-\frac{\xi_\ell^2(c_\ell^2 - \xi_\ell^2)}{m_\ell c_\ell^2 s_\ell T_\ell} - \frac{\xi_{\mathrm{g}}^2(c_{\mathrm{g}}^2 - \xi_{\mathrm{g}}^2)}{m_{\mathrm{g}} c_{\mathrm{g}}^2 s_{\mathrm{g}} T_{\mathrm{g}}} + \frac{s_\ell}{C_{p,\ell}} + \frac{s_{\mathrm{g}}}{C_{p,\mathrm{g}}}\right)\mathcal{H}(T_\ell - T_{\mathrm{g}})\right.$$

$$\left. + \left(p_{\mathrm{g}}^*\left(\frac{s_{\mathrm{g}}}{C_{p,\mathrm{g}}} + \frac{\xi_{\mathrm{g}}^2(\xi_{\mathrm{g}}^2 - c_{\mathrm{g}}^2)}{m_{\mathrm{g}} c_{\mathrm{g}}^2 s_{\mathrm{g}} T_{\mathrm{g}}}\right) + p_\ell^*\left(\frac{s_\ell}{C_{p,\ell}} + \frac{\xi_\ell^2(\xi_\ell^2 - c_\ell^2)}{m_\ell c_\ell^2 s_\ell T_\ell}\right) - \frac{\xi_{\mathrm{g}}^2}{\alpha_{\mathrm{g}}} - \frac{\xi_\ell^2}{\alpha_\ell}\right)\mathcal{J}(p_\ell - p_{\mathrm{g}})\right],$$

where we have introduced an interface-bulk pressure difference $p_k^* = p^* - p_k$.

5.2. The chemical equilibrium model. The chemical equilibrium model may now be formulated using the following equations.

- Mass conservation:

$$(5.9) \qquad \frac{\partial \rho}{\partial t} + \frac{\partial(\rho v)}{\partial x} = 0.$$

- Momentum conservation:

$$(5.10) \qquad \frac{\partial(\rho v)}{\partial t} + \frac{\partial(\rho v^2 + \alpha_{\mathrm{g}} p_{\mathrm{g}} + \alpha_\ell p_\ell)}{\partial x} = 0.$$

- Volume fraction evolution:

$$(5.11) \qquad \mathrm{D}_t \alpha_{\mathrm{g}} = \mathcal{J}(p_{\mathrm{g}} - p_\ell).$$

- Energy equations:

(5.12)

$$\frac{\partial E_{\mathrm{g}}}{\partial t} + \frac{\partial(vE_{\mathrm{g}})}{\partial x} + \frac{v}{\rho} m_{\mathrm{g}} \frac{\partial p_{\mathrm{eff}}}{\partial x} - \left(\frac{(\xi_{\mathrm{g}}^2 - \xi_\ell^2)\left(\mu + \frac{1}{2}v^2\right)}{\frac{\xi_{\mathrm{g}}^4}{m_{\mathrm{g}}c_{\mathrm{g}}^2} + \frac{\xi_\ell^4}{m_\ell c_\ell^2} + \frac{s_\ell^2 T_\ell}{C_{p,\ell}} + \frac{s_{\mathrm{g}}^2 T_{\mathrm{g}}}{C_{p,\mathrm{g}}}} - \alpha_{\mathrm{g}} p_{\mathrm{g}} \right) \frac{\partial v}{\partial x}$$

$$= \left[\frac{\left(-\frac{\Gamma_\ell \xi_\ell^2}{m_\ell c_\ell^2} - \frac{\Gamma_{\mathrm{g}} \xi_{\mathrm{g}}^2}{m_{\mathrm{g}} c_{\mathrm{g}}^2} + \frac{s_\ell}{C_{p,\ell}} + \frac{s_{\mathrm{g}}}{C_{p,\mathrm{g}}} \right)\left(\mu + \frac{1}{2}v^2\right)}{\frac{\xi_{\mathrm{g}}^4}{m_{\mathrm{g}}c_{\mathrm{g}}^2} + \frac{\xi_\ell^4}{m_\ell c_\ell^2} + \frac{s_\ell^2 T_\ell}{C_{p,\ell}} + \frac{s_{\mathrm{g}}^2 T_{\mathrm{g}}}{C_{p,\mathrm{g}}}} + 1 \right] \mathcal{H}(T_\ell - T_{\mathrm{g}})$$

$$+ \left[\frac{\left(\left(-\frac{\Gamma_{\mathrm{g}} \xi_{\mathrm{g}}^2}{m_{\mathrm{g}} c_{\mathrm{g}}^2} + \frac{s_{\mathrm{g}}}{C_{p,\mathrm{g}}} \right) p_{\mathrm{g}}^* + \left(-\frac{\Gamma_\ell \xi_\ell^2}{m_\ell c_\ell^2} + \frac{s_\ell}{C_{p,\ell}} \right) p_\ell^* - \frac{\xi_{\mathrm{g}}^2}{\alpha_{\mathrm{g}}} - \frac{\xi_\ell^2}{\alpha_\ell} \right)\left(\mu + \frac{1}{2}v^2\right)}{\frac{\xi_{\mathrm{g}}^4}{m_{\mathrm{g}}c_{\mathrm{g}}^2} + \frac{\xi_\ell^4}{m_\ell c_\ell^2} + \frac{s_\ell^2 T_\ell}{C_{p,\ell}} + \frac{s_{\mathrm{g}}^2 T_{\mathrm{g}}}{C_{p,\mathrm{g}}}} + p^* \right]$$

$$\cdot \mathcal{J}(p_\ell - p_{\mathrm{g}}),$$

(5.13)

$$\frac{\partial E_\ell}{\partial t} + \frac{\partial(vE_\ell)}{\partial x} + \frac{v}{\rho} m_\ell \frac{\partial p_{\mathrm{eff}}}{\partial x} - \left(\frac{(\xi_\ell^2 - \xi_{\mathrm{g}}^2)\left(\mu + \frac{1}{2}v^2\right)}{\frac{\xi_\ell^4}{m_\ell c_\ell^2} + \frac{\xi_{\mathrm{g}}^4}{m_{\mathrm{g}} c_{\mathrm{g}}^2} + \frac{s_{\mathrm{g}}^2 T_{\mathrm{g}}}{C_{p,\mathrm{g}}} + \frac{s_\ell^2 T_\ell}{C_{p,\ell}}} - \alpha_\ell p_\ell \right) \frac{\partial v}{\partial x}$$

$$= \left[\frac{\left(-\frac{\Gamma_{\mathrm{g}} \xi_{\mathrm{g}}^2}{m_{\mathrm{g}} c_{\mathrm{g}}^2} - \frac{\Gamma_\ell \xi_\ell^2}{m_\ell c_\ell^2} + \frac{s_{\mathrm{g}}}{C_{p,\mathrm{g}}} + \frac{s_\ell}{C_{p,\ell}} \right)\left(\mu + \frac{1}{2}v^2\right)}{\frac{\xi_\ell^4}{m_\ell c_\ell^2} + \frac{\xi_{\mathrm{g}}^4}{m_{\mathrm{g}} c_{\mathrm{g}}^2} + \frac{s_{\mathrm{g}}^2 T_{\mathrm{g}}}{C_{p,\mathrm{g}}} + \frac{s_\ell^2 T_\ell}{C_{p,\ell}}} + 1 \right] \mathcal{H}(T_{\mathrm{g}} - T_\ell)$$

$$+ \left[\frac{\left(\left(-\frac{\Gamma_\ell \xi_\ell^2}{m_\ell c_\ell^2} + \frac{s_\ell}{C_{p,\ell}} \right) p_\ell^* + \left(-\frac{\Gamma_{\mathrm{g}} \xi_{\mathrm{g}}^2}{m_{\mathrm{g}} c_{\mathrm{g}}^2} + \frac{s_{\mathrm{g}}}{C_{p,\mathrm{g}}} \right) p_{\mathrm{g}}^* - \frac{\xi_\ell^2}{\alpha_\ell} - \frac{\xi_{\mathrm{g}}^2}{\alpha_{\mathrm{g}}} \right)\left(\mu + \frac{1}{2}v^2\right)}{\frac{\xi_\ell^4}{m_\ell c_\ell^2} + \frac{\xi_{\mathrm{g}}^4}{m_{\mathrm{g}} c_{\mathrm{g}}^2} + \frac{s_{\mathrm{g}}^2 T_{\mathrm{g}}}{C_{p,\mathrm{g}}} + \frac{s_\ell^2 T_\ell}{C_{p,\ell}}} + p^* \right]$$

$$\cdot \mathcal{J}(p_{\mathrm{g}} - p_\ell).$$

Herein, the continuity, momentum conservation, and volume fraction equations are those known from the basic model, (2.3), (2.5), and (2.7), while the energy equations (5.12)–(5.13) are derived by inserting for the chemical potential relaxation term $\mathcal{K}(\mu_\ell - \mu_{\mathrm{g}})$ in (2.8)–(2.9) using (5.8) and (4.18).

5.3. Wave velocities. We wish to calculate the wave velocities, and hence the mixture speed of sound, of the chemical equilibrium model (5.9)–(5.13) in the nonstiff limit where $\mathcal{H}, \mathcal{J} \to 0$. To this end, we find it useful to derive an evolution equation for the effective pressure p_{eff}.

The material derivative of the effective pressure p_{eff} is given by (4.14). In this equation, we replace $D_t p_{\text{g}}$ and $D_t p_{\ell}$ using (5.2)–(5.4) and (5.6). We then insert for $D_t s_{\text{g}}$ and $D_t s_{\ell}$ by replacing the chemical potential relaxation term in the basic model entropy equations (2.11) and (2.12) using (5.8) and (4.18). Finally, using that $D_t \alpha_{\text{g}} = 0$ due to (2.5) and the fact that $\mathcal{J}, \mathcal{H} \to 0$, gives

$$D_t p_{\text{eff}} = \tilde{a}_{\mu}^2 D_t \rho, \tag{5.14}$$

where

$$\tilde{a}_{\mu}^2 = \frac{\left(\frac{\xi_{\ell}^2}{m_{\ell} c_{\ell}^2} + \frac{\xi_{\text{g}}^2}{m_{\text{g}} c_{\text{g}}^2} \right)^2 m_{\text{g}} c_{\text{g}}^2 m_{\ell} c_{\ell}^2 + (m_{\text{g}} c_{\text{g}}^2 + m_{\ell} c_{\ell}^2) \left(\frac{s_{\ell}^2 T_{\ell}}{C_{p,\ell}} + \frac{s_{\text{g}}^2 T_{\text{g}}}{C_{p,\text{g}}} \right)}{\rho \left(\frac{\xi_{\text{g}}^4}{m_{\text{g}} c_{\text{g}}^2} + \frac{\xi_{\ell}^4}{m_{\ell} c_{\ell}^2} + \frac{s_{\ell}^2 T_{\ell}}{C_{p,\ell}} + \frac{s_{\text{g}}^2 T_{\text{g}}}{C_{p,\text{g}}} \right)}. \tag{5.15}$$

We may now write the full equation system in a quasi-linear form,

$$\boldsymbol{u}_t + \begin{bmatrix} 0 & 1 & 0 & 0 & 0 \\ -v^2 & 2v & 0 & 0 & 1 \\ vG & -G & v & 0 & 0 \\ vL & -L & 0 & v & 0 \\ -v\tilde{a}_{\mu}^2 & \tilde{a}_{\mu}^2 & 0 & 0 & v \end{bmatrix} \boldsymbol{u}_x \equiv \boldsymbol{u}_t + \boldsymbol{A}(\boldsymbol{u})\boldsymbol{u}_x = 0, \tag{5.16}$$

where $\boldsymbol{u} = [\rho, \rho v, s_{\text{g}}, s_{\ell}, p_{\text{eff}}]^{\text{T}}$ and

$$G = \frac{s_{\text{g}}(\xi_{\ell}^2 - \xi_{\text{g}}^2)}{\rho c_{\text{g}}^2 m_{\text{g}} \left(\frac{\xi_{\ell}^4}{m_{\ell} c_{\ell}^2} + \frac{\xi_{\text{g}}^4}{m_{\text{g}} c_{\text{g}}^2} + \frac{s_{\ell}^2 T_{\ell}}{C_{p,\ell}} + \frac{s_{\text{g}}^2 T_{\text{g}}}{C_{p,\text{g}}} \right)}, \tag{5.17}$$

$$L = \frac{s_{\ell}(\xi_{\text{g}}^2 - \xi_{\ell}^2)}{\rho c_{\ell}^2 m_{\ell} \left(\frac{\xi_{\text{g}}^4}{m_{\text{g}} c_{\text{g}}^2} + \frac{\xi_{\ell}^4}{m_{\ell} c_{\ell}^2} + \frac{s_{\text{g}}^2 T_{\text{g}}}{C_{p,\text{g}}} + \frac{s_{\ell}^2 T_{\ell}}{C_{p,\ell}} \right)}. \tag{5.18}$$

The equation system has been formed by the equations for mass (5.9), momentum (5.10), and pressure (5.14), along with the entropy equations, which are obtained by replacing the mass transfer term in (2.11)–(2.12) using (4.18) and (5.8). The eigenvalues of the matrix $\boldsymbol{A}$ are

$$\boldsymbol{\lambda}_{\mu} \in \{v - \tilde{a}_{\mu}, v, v, v, v + \tilde{a}_{\mu}\}, \tag{5.19}$$

and hence the mixture speed of sound of the chemical equilibrium model is $\tilde{a}_{\mu}$, given by (5.15).

5.3.1. The subcharacteristic condition with respect to the basic model. Using the expressions for the mixture speed of sound in the basic model (2.22) and the chemical equilibrium model (5.15), we can show that

$$\tilde{a}_{\mu}^{-2} = \tilde{a}_0^{-2} + Z_{\mu}^0, \tag{5.20}$$

where

$$(5.21) \qquad Z_\mu^0 = \frac{(\xi_\ell^2 - \xi_g^2)^2}{\left[\left(\frac{\xi_g^2}{m_g c_g^2} + \frac{\xi_\ell^2}{m_\ell c_\ell^2} \right)^2 c_\ell^2 c_g^2 m_g m_\ell + \left(\frac{s_\ell^2 T_\ell}{C_{p,\ell}} + \frac{s_g^2 T_g}{C_{p,g}} \right) \rho \tilde{a}_0^2 \right] \tilde{a}_0^2}.$$

PROPOSITION 2. *The chemical equilibrium model given by (5.9)–(5.13) satisfies the subcharacteristic condition with respect to the basic model of section 2, subject only to the physically fundamental conditions*

$$\rho_k > 0,$$
$$c_{p,k} > 0,$$
$$T_k > 0.$$

Proof. From the eigenstructure of the basic model (2.21) and the chemical equilibrium model (5.19), we see that the interlacing condition in Definition 1 reduces to the requirement that

$$(5.22) \qquad \tilde{a}_0 \geq \tilde{a}_\mu,$$

which follows from (5.20)–(5.21) and the given conditions for ρ_k, $c_{p,k}$, and T_k. □

6. Pressure-temperature relaxation. In this section, we investigate the model that arises when we impose volume and heat transfer equilibrium. In other words, we let the pressure and temperature relaxation parameters $\mathcal{J}, \mathcal{H}$ go to infinity. This corresponds to taking the limit

$$(6.1) \qquad \mathcal{H} \to \infty$$

in the mechanical equilibrium model of section 3, or equivalently taking the limit

$$(6.2) \qquad \mathcal{J} \to \infty$$

in the thermal equilibrium model (4.8)–(4.12), which we expect to correspond to the assumptions

$$(6.3) \qquad T_g = T_\ell = T,$$
$$(6.4) \qquad p_g = p_\ell = p^* = p,$$

i.e., equal temperatures and pressures. The model equations may be found in [10].

6.1. Wave velocities. The wave structure of the mechanical-thermal equilibrium model was investigated by Flåtten, Morin, and Munkejord [11] in the general case of n different components with n mass balance equations, in the nonstiff limit where $\mathcal{K} \to 0$. In the case of two components, $n = 2$, the wave velocities were found to be

$$(6.5) \qquad \boldsymbol{\lambda}_{pT} = \{v - \tilde{a}_{pT}, v, v, v + \tilde{a}_{pT}\},$$

where

$$(6.6) \qquad \tilde{a}_{pT}^{-2} = \rho \left(\frac{\alpha_g}{\rho_g c_g^2} + \frac{\alpha_\ell}{\rho_\ell c_\ell^2} \right) + \rho T \frac{C_{p,g} C_{p,\ell}}{C_{p,g} + C_{p,\ell}} \left(\frac{\Gamma_\ell}{\rho_\ell c_\ell^2} - \frac{\Gamma_g}{\rho_g c_g^2} \right)^2.$$

This model and its wave velocities are also described by Städtke [26, Chap. 4].

6.1.1. The subcharacteristic condition with respect to the p-model. As shown by Flåtten and Lund [10], the mechanical-thermal equilibrium model satisfies the subcharacteristic condition with respect to the mechanical equilibrium model of section 3, given only the physically fundamental requirements $\rho_k > 0$, $c_{p,k} > 0$, $T > 0$. This is easily seen from (6.6),

$$\tilde{a}_{pT}^{-2} = \tilde{a}_p^{-2} + Z_{pT}^p, \tag{6.7}$$

where

$$Z_{pT}^p = \rho T \frac{C_{p,\mathrm{g}} C_{p,\ell}}{C_{p,\mathrm{g}} + C_{p,\ell}} \left(\frac{\Gamma_\ell}{\rho_\ell c_\ell^2} - \frac{\Gamma_\mathrm{g}}{\rho_\mathrm{g} c_\mathrm{g}^2} \right)^2. \tag{6.8}$$

6.1.2. The subcharacteristic condition with respect to the T-model. From (4.17) and (6.6) we see that the mixture speed of sound in the mechanical-thermal equilibrium model may be expressed as

$$\tilde{a}_{pT}^{-2} = \tilde{a}_T^{-2} + Z_{pT}^T, \tag{6.9}$$

where

(6.10)

$$Z_{pT}^T$$
$$= \frac{\left(\left(\frac{\Gamma_\mathrm{g}}{m_\mathrm{g} c_\mathrm{g}^2} + \frac{\Gamma_\ell}{m_\ell c_\ell^2} \right) \left(\frac{\Gamma_\mathrm{g}}{\rho_\mathrm{g} c_\mathrm{g}^2} - \frac{\Gamma_\ell}{\rho_\ell c_\ell^2} \right) m_\mathrm{g} c_\mathrm{g}^2 m_\ell c_\ell^2 - \alpha_\ell \alpha_\mathrm{g} \left(\frac{1}{C_{p,\mathrm{g}} T} + \frac{1}{C_{p,\ell} T} \right) (\rho_\mathrm{g} c_\mathrm{g}^2 - \rho_\ell c_\ell^2) \right)^2 \rho}{m_\ell c_\ell^2 m_\mathrm{g} c_\mathrm{g}^2 \left(\frac{1}{C_{p,\mathrm{g}} T} + \frac{1}{C_{p,\ell} T} \right) \left(\left(\frac{\Gamma_\mathrm{g}}{m_\mathrm{g} c_\mathrm{g}^2} + \frac{\Gamma_\ell}{m_\ell c_\ell^2} \right)^2 m_\ell c_\ell^2 m_\mathrm{g} c_\mathrm{g}^2 + \left(\frac{1}{C_{p,\mathrm{g}} T} + \frac{1}{C_{p,\ell} T} \right) \rho \tilde{a}_0^2 \right)}.$$

PROPOSITION 3. *The mechanical-thermal equilibrium model satisfies the subcharacteristic condition with respect to the thermal equilibrium model of section 4, subject only to the physically fundamental conditions*

$$\rho_k > 0,$$
$$c_{p,k} > 0,$$
$$T > 0.$$

Proof. By (4.20) and (6.5), we see that the interlacing condition of Definition 1 reduces to the requirement that

$$\tilde{a}_T \geq \tilde{a}_{pT}, \tag{6.11}$$

which follows from (6.9)–(6.10) and the given conditions for ρ_k, $c_{p,k}$, and T. ∎

7. Pressure-chemical relaxation. In this section, we investigate the model that arises when we impose volume and mass transfer equilibrium. In other words, we let the pressure and chemical potential relaxation parameters $\mathcal{J}, \mathcal{K}$ go to infinity. This corresponds to taking the limit

$$\mathcal{J} \to \infty \tag{7.1}$$

in the chemical equilibrium model (5.9)–(5.13), or equivalently the limit

$$\text{(7.2)} \qquad\qquad\qquad\qquad \mathcal{K} \to \infty$$

in the mechanical equilibrium model of section 3, which we expect to correspond to the assumptions

$$\text{(7.3)} \qquad\qquad\qquad\qquad p_{\mathrm{g}} = p_\ell = p^* = p,$$
$$\text{(7.4)} \qquad\qquad\qquad\qquad \mu_{\mathrm{g}} = \mu_\ell = \mu^* = \mu,$$

i.e., equal pressures and chemical potentials. This model was first introduced in this form by Flåtten and Lund [10].

7.1. The mechanical-chemical equilibrium model. The mechanical-chemical equilibrium model can be formulated as follows:
- Mass conservation:

$$\text{(7.5)} \qquad\qquad\qquad\qquad \frac{\partial \rho}{\partial t} + \frac{\partial(\rho v)}{\partial x} = 0.$$

- Momentum conservation:

$$\text{(7.6)} \qquad\qquad\qquad \frac{\partial(\rho v)}{\partial t} + \frac{\partial(\rho v^2 + \alpha_{\mathrm{g}} p_{\mathrm{g}} + \alpha_\ell p_\ell)}{\partial x} = 0.$$

- Energy equations:

$$
\begin{aligned}
\text{(7.7)} \quad & \frac{\partial E_{\mathrm{g}}}{\partial t} + \frac{\partial}{\partial x}\left(v E_{\mathrm{g}}\right) + \frac{m_{\mathrm{g}}}{\rho} v \frac{\partial p}{\partial x} + p\alpha_{\mathrm{g}} \frac{\rho \tilde{a}_p^2}{\rho_{\mathrm{g}} c_{\mathrm{g}}^2} \frac{\partial v}{\partial x} \\
& \qquad - \frac{\rho \tilde{a}_{p\mu}^2}{P_{\mathrm{g}}} \frac{m_{\mathrm{g}} s_{\mathrm{g}} T_{\mathrm{g}} C_{p,\ell}}{s_{\mathrm{g}}^2 T_{\mathrm{g}} C_{p,\ell} + s_\ell^2 T_\ell C_{p,\mathrm{g}}} \\
& \qquad\quad \cdot \left(\mu + \frac{1}{2}v^2 + p\frac{\alpha_{\mathrm{g}}(\Gamma_\ell s_\ell T_\ell - c_\ell^2) + \alpha_\ell(\Gamma_{\mathrm{g}} s_{\mathrm{g}} T_{\mathrm{g}} - c_{\mathrm{g}}^2)}{\rho_{\mathrm{g}} \alpha_\ell c_{\mathrm{g}}^2 + \rho_\ell \alpha_{\mathrm{g}} c_\ell^2}\right) \frac{\partial v}{\partial x} \\
& \qquad = \left(1 - p\frac{\alpha_{\mathrm{g}} \Gamma_\ell + \alpha_\ell \Gamma_{\mathrm{g}}}{\rho_{\mathrm{g}} \alpha_\ell c_{\mathrm{g}}^2 + \rho_\ell \alpha_{\mathrm{g}} c_\ell^2}\right) \mathcal{H}(T_\ell - T_{\mathrm{g}}) \\
& \qquad\quad + \mathcal{H}(T_\ell - T_{\mathrm{g}})\left(\mu + \frac{1}{2}v^2 + p\frac{\alpha_{\mathrm{g}}(\Gamma_\ell s_\ell T_\ell - c_\ell^2) + \alpha_\ell(\Gamma_{\mathrm{g}} s_{\mathrm{g}} T_{\mathrm{g}} - c_{\mathrm{g}}^2)}{\rho_{\mathrm{g}} \alpha_\ell c_{\mathrm{g}}^2 + \rho_\ell \alpha_{\mathrm{g}} c_\ell^2}\right) \\
& \qquad\qquad \cdot \left(\frac{s_{\mathrm{g}} C_{p,\ell} + s_\ell C_{p,\mathrm{g}}}{s_{\mathrm{g}}^2 T_{\mathrm{g}} C_{p,\ell} + s_\ell^2 T_\ell C_{p,\mathrm{g}}}\left(\frac{\tilde{a}_{p\mu}}{\tilde{a}_p}\right)^2\right. \\
& \qquad\qquad\quad \left. - \left(\frac{\Gamma_{\mathrm{g}}}{\rho_{\mathrm{g}} c_{\mathrm{g}}^2} - \frac{\Gamma_\ell}{\rho_\ell c_\ell^2}\right) \cdot \frac{\rho \tilde{a}_{p\mu}^2}{P_{\mathrm{g}}} \frac{\rho_{\mathrm{g}} \alpha_{\mathrm{g}} s_{\mathrm{g}} T_{\mathrm{g}} C_{p,\ell}}{s_{\mathrm{g}}^2 T_{\mathrm{g}} C_{p,\ell} + s_\ell^2 T_\ell C_{p,\mathrm{g}}}\right),
\end{aligned}
$$

$$(7.8) \quad \frac{\partial E_\ell}{\partial t} + \frac{\partial}{\partial x}\left(vE_\ell\right) + \frac{m_\ell}{\rho}v\frac{\partial p}{\partial x} + p\alpha_\ell\frac{\rho\tilde{a}_p^2}{\rho_\ell c_\ell^2}\frac{\partial v}{\partial x}$$

$$- \frac{\rho\tilde{a}_{p\mu}^2}{P_\ell}\frac{m_\ell s_\ell T_\ell C_{p,\mathrm{g}}}{s_\mathrm{g}^2 T_\mathrm{g} C_{p,\ell} + s_\ell^2 T_\ell C_{p,\mathrm{g}}}$$

$$\cdot\left(\mu + \frac{1}{2}v^2 + p\frac{\alpha_\mathrm{g}(\Gamma_\ell s_\ell T_\ell - c_\ell^2) + \alpha_\ell(\Gamma_\mathrm{g} s_\mathrm{g} T_\mathrm{g} - c_\mathrm{g}^2)}{\rho_\mathrm{g}\alpha_\ell c_\mathrm{g}^2 + \rho_\ell\alpha_\mathrm{g} c_\ell^2}\right)\frac{\partial v}{\partial x}$$

$$= \left(1 - p\frac{\alpha_\mathrm{g}\Gamma_\ell + \alpha_\ell\Gamma_\mathrm{g}}{\rho_\mathrm{g}\alpha_\ell c_\mathrm{g}^2 + \rho_\ell\alpha_\mathrm{g} c_\ell^2}\right)\mathcal{H}(T_\mathrm{g} - T_\ell)$$

$$+ \mathcal{H}(T_\mathrm{g} - T_\ell)\left(\mu + \frac{1}{2}v^2 + p\frac{\alpha_\mathrm{g}(\Gamma_\ell s_\ell T_\ell - c_\ell^2) + \alpha_\ell(\Gamma_\mathrm{g} s_\mathrm{g} T_\mathrm{g} - c_\mathrm{g}^2)}{\rho_\ell\alpha_\mathrm{g} c_\mathrm{g}^2 + \rho_\ell\alpha_\mathrm{g} c_\ell^2}\right)$$

$$\cdot\left(\frac{s_\mathrm{g} C_{p,\ell} + s_\ell C_{p,\mathrm{g}}}{s_\mathrm{g}^2 T_\mathrm{g} C_{p,\ell} + s_\ell^2 T_\ell C_{p,\mathrm{g}}}\left(\frac{\tilde{a}_{p\mu}}{\tilde{a}_p}\right)^2\right)$$

$$+ \left(\frac{\Gamma_\mathrm{g}}{\rho_\mathrm{g} c_\mathrm{g}^2} - \frac{\Gamma_\ell}{\rho_\ell c_\ell^2}\right)\cdot\frac{\rho\tilde{a}_{p\mu}^2}{P_\ell}\frac{\rho_\ell\alpha_\ell s_\ell T_\ell C_{p,\mathrm{g}}}{s_\mathrm{g}^2 T_\mathrm{g} C_{p,\ell} + s_\ell^2 T_\ell C_{p,\mathrm{g}}}\right).$$

As presented in [10], the energy equations (7.7)–(7.8) unfortunately contained a sign error, which has been corrected here. We have also introduced

$$(7.9) \qquad P_\mathrm{g} \equiv \left(\frac{\partial p}{\partial s_\mathrm{g}}\right)_{s_\ell} = \frac{s_\mathrm{g} T_\mathrm{g}}{c_{p,\mathrm{g}}}\left(\frac{\xi_\mathrm{g}^2}{\rho_\mathrm{g} c_\mathrm{g}^2} - \frac{\xi_\ell^2}{\rho_\ell c_\ell^2}\right)^{-1},$$

$$(7.10) \qquad P_\ell \equiv \left(\frac{\partial p}{\partial s_\ell}\right)_{s_\mathrm{g}} = \frac{s_\ell T_\ell}{c_{p,\ell}}\left(\frac{\xi_\ell^2}{\rho_\ell c_\ell^2} - \frac{\xi_\mathrm{g}^2}{\rho_\mathrm{g} c_\mathrm{g}^2}\right)^{-1},$$

and

$$(7.11)$$

$$\tilde{a}_{p\mu}^{-2} = \tilde{a}_p^{-2} + \frac{\rho C_{p,\mathrm{g}} C_{p,\ell}}{\rho_\mathrm{g}^2\rho_\ell^2(C_{p,\ell}s_\mathrm{g}^2 T_\mathrm{g} + C_{p,\mathrm{g}}s_\ell^2 T_\ell)}\left(\rho_\mathrm{g} - \rho_\ell + \rho_\mathrm{g}\rho_\ell\left(s_\mathrm{g}\frac{T_\mathrm{g}\Gamma_\mathrm{g}}{\rho_\mathrm{g} c_\mathrm{g}^2} - s_\ell\frac{T_\ell\Gamma_\ell}{\rho_\ell c_\ell^2}\right)\right)^2.$$

7.2. Wave velocities. The wave velocities of the mechanical-chemical equilibrium model (7.5)–(7.8) were analyzed by Flåtten and Lund [10] in the nonstiff limit $\mathcal{H} \to 0$. The eigenvalues were found to be

$$(7.12) \qquad \boldsymbol{\lambda}_{p\mu} = \{v - \tilde{a}_{p\mu}, v, v, v + \tilde{a}_{p\mu}\},$$

where $\tilde{a}_{p\mu}$ is the mixture speed of sound, given by (7.11).

7.2.1. The subcharacteristic condition with respect to the p-model. From (7.11), we immediately see that the mixture speed of sound can be written as a sum of squares,

$$(7.13) \qquad \tilde{a}_{p\mu}^{-2} = \tilde{a}_p^{-2} + Z_{p\mu}^p,$$

where

$$(7.14) \quad Z_{p\mu}^p = \frac{\rho C_{p,\mathrm{g}} C_{p,\ell}}{\rho_\mathrm{g}^2\rho_\ell^2(C_{p,\ell}s_\mathrm{g}^2 T_\mathrm{g} + C_{p,\mathrm{g}}s_\ell^2 T_\ell)}\left(\rho_\mathrm{g} - \rho_\ell + \rho_\mathrm{g}\rho_\ell\left(s_\mathrm{g}\frac{T_\mathrm{g}\Gamma_\mathrm{g}}{\rho_\mathrm{g} c_\mathrm{g}^2} - s_\ell\frac{T_\ell\Gamma_\ell}{\rho_\ell c_\ell^2}\right)\right)^2.$$

From this and (3.2) and (7.12), we see that the subcharacteristic condition is satisfied, given only the physically fundamental conditions $\rho_k > 0$, $c_{p,k} > 0$, $T_k > 0$ [10].

7.2.2. The subcharacteristic condition with respect to the μ-model. Using the expressions for the mixture speed of sound in the chemical equilibrium model (5.15) and the present mechanical-chemical equilibrium model (7.11), it may be shown that the latter can be written as

$$(7.15) \qquad \tilde{a}_{p\mu}^{-2} = \tilde{a}_{\mu}^{-2} + Z_{p\mu}^{\mu},$$

where

$$(7.16)$$

$$Z_{p\mu}^{\mu} = \rho \frac{m_{\mathrm{g}} c_{\mathrm{g}}^2 m_\ell c_\ell^2 \left(\left(\frac{1}{\rho_{\mathrm{g}} c_{\mathrm{g}}^2} - \frac{1}{\rho_\ell c_\ell^2} \right) \left(\frac{s_{\mathrm{g}}^2 T_{\mathrm{g}}}{C_{p,\mathrm{g}}} + \frac{s_\ell^2 T_\ell}{C_{p,\ell}} \right) + \left(\frac{\xi_{\mathrm{g}}^2}{m_{\mathrm{g}} c_{\mathrm{g}}^2} + \frac{\xi_\ell^2}{m_\ell c_\ell^2} \right) \left(\frac{\xi_{\mathrm{g}}^2}{\rho_{\mathrm{g}} c_{\mathrm{g}}^2} - \frac{\xi_\ell^2}{\rho_\ell c_\ell^2} \right) \right)^2}{\left(\frac{s_{\mathrm{g}}^2 T_{\mathrm{g}}}{C_{p,\mathrm{g}}} + \frac{s_\ell^2 T_\ell}{C_{p,\ell}} \right) \left(\left(\frac{\xi_{\mathrm{g}}^2}{m_{\mathrm{g}} c_{\mathrm{g}}^2} + \frac{\xi_\ell^2}{m_\ell c_\ell^2} \right)^2 c_\ell^2 c_{\mathrm{g}}^2 m_{\mathrm{g}} m_\ell + \left(\frac{s_\ell^2 T_\ell}{C_{p,\ell}} + \frac{s_{\mathrm{g}}^2 T_{\mathrm{g}}}{C_{p,\mathrm{g}}} \right) \rho \tilde{a}_0^2 \right)}.$$

PROPOSITION 4. *The mechanical-chemical equilibrium model given by* (7.5)–(7.8) *satisfies the subcharacteristic condition with respect to the chemical equilibrium model of section* 5, *subject only to the physically fundamental conditions*

$$\rho_k > 0,$$
$$c_{p,k} > 0,$$
$$T_k > 0.$$

Proof. By (5.19) and (7.12), we see that the interlacing condition of Definition 1 reduces to the requirement that

$$(7.17) \qquad \tilde{a}_\mu \geq \tilde{a}_{p\mu},$$

which follows from (7.15)–(7.16) and the given conditions for ρ_k, $c_{p,k}$, and T_k. □

8. Temperature-chemical relaxation. In this section, we investigate the model that results when we assume heat and mass transfer equilibrium, in other words that the relaxation parameters $\mathcal{H}, \mathcal{K}$ go to infinity. This is equivalent to taking the limit

$$(8.1) \qquad \mathcal{H} \to \infty$$

in the thermal equilibrium model of section 4, or equivalently the limit

$$(8.2) \qquad \mathcal{K} \to \infty$$

in the chemical equilibrium model of section 5. We expect this to be equivalent to the assumptions

$$(8.3) \qquad T_{\mathrm{g}} = T_\ell = T,$$
$$(8.4) \qquad \mu_{\mathrm{g}} = \mu_\ell = \mu^* = \mu,$$

i.e., thermal and chemical equilibrium. The model equations and wave velocities for this model have not been found elsewhere, and will thus be derived here.

8.1. Entropy equations. To derive the entropy equations of the thermal-chemical equilibrium model, we start by adding the balance formulations of the entropy equations (2.13)–(2.14) to eliminate the heat transfer term, which, after expanding and rewriting derivatives, yields

$$(8.5) \quad T\left(m_g D_t s_g + m_\ell D_t s_\ell + s_g \alpha_g D_t \rho_g + s_\ell \alpha_\ell D_t \rho_\ell + (m_\ell s_\ell + m_g s_g)\frac{\partial v}{\partial x}\right)$$
$$= (p_g - p_\ell - T(s_g \rho_g - s_\ell \rho_\ell))\mathcal{J}(p_g - p_\ell),$$

where we also have let $\mathcal{K}$ go to infinity, hence eliminating the mass transfer term.

To eliminate the material derivative $D_t \rho_k$, we need to establish certain differentials. Since the chemical potentials and temperatures are equal, so are their differentials, which gives us

$$(8.6) \qquad d\mu = \frac{1}{\rho_\ell}dp_\ell - s_\ell dT = \frac{1}{\rho_g}dp_g - s_g dT,$$

$$(8.7) \qquad dT = \frac{\Gamma_g T}{\rho_g c_g^2}dp_g + \frac{T}{c_{p,g}}ds_g = \frac{\Gamma_\ell T}{\rho_\ell c_\ell^2}dp_\ell + \frac{T}{c_{p,\ell}}ds_\ell,$$

$$(8.8) \qquad dp_k = c_k^2 d\rho_k + \rho_k \Gamma_k T_k ds_k.$$

Solving these three equations for $d\rho_k$ as functions of ds_g and ds_ℓ yields

$$(8.9) \qquad d\rho_g = \rho_g \frac{\left(\frac{1}{c_{p,g}}\left(-\frac{\Gamma_\ell}{c_\ell^2}\Delta h - 1\right) - \Gamma_g T\left(\frac{\Gamma_g}{c_g^2} - \frac{\Gamma_\ell}{c_\ell^2} + \frac{\Gamma_\ell \Gamma_g}{c_g^2 c_\ell^2}\Delta h\right)\right)ds_g + \frac{1}{c_{p,\ell}}ds_\ell}{c_g^2\left(\frac{\Gamma_g}{c_g^2} - \frac{\Gamma_\ell}{c_\ell^2} + \frac{\Gamma_\ell \Gamma_g}{c_g^2 c_\ell^2}\Delta h\right)},$$

$$(8.10) \qquad d\rho_\ell = \rho_\ell \frac{\left(\frac{1}{c_{p,\ell}}\left(\frac{\Gamma_g}{c_g^2}\Delta h - 1\right) - \Gamma_\ell T\left(\frac{\Gamma_\ell}{c_\ell^2} - \frac{\Gamma_g}{c_g^2} - \frac{\Gamma_g \Gamma_\ell}{c_\ell^2 c_g^2}\Delta h\right)\right)ds_\ell + \frac{1}{c_{p,g}}ds_g}{c_\ell^2\left(\frac{\Gamma_\ell}{c_\ell^2} - \frac{\Gamma_g}{c_g^2} - \frac{\Gamma_g \Gamma_\ell}{c_\ell^2 c_g^2}\Delta h\right)},$$

where $\Delta h \equiv h_g - h_\ell$. We will also have use for the differential of the mixture density,

$$(8.11) \qquad d\rho = \alpha_g d\rho_g + \alpha_\ell d\rho_\ell + (\rho_g - \rho_\ell)d\alpha_g.$$

We may now express (8.9)–(8.11) using the material derivative, which together with (8.5) allows us to solve for the entropy equations, which turn out to be slightly complex,

$$(8.12) \quad D_t s_g = C_{p,g} \left[\left(\left(\Delta h \frac{\Gamma_g}{c_g^2} \frac{\Gamma_\ell}{c_\ell^2} + \frac{\Gamma_g}{c_g^2} - \frac{\Gamma_\ell}{c_\ell^2} \right) \left(\rho + m_g \Delta h \frac{\Gamma_\ell}{c_\ell^2} \right) C_{p,\ell} T c_g^2 c_\ell^2 \right. \right.$$

$$+ \Delta h m_\ell m_g (c_\ell^2 - c_g^2 + \Delta h \Gamma_g) \frac{\partial v}{\partial x}$$

$$+ \left(\left(\Delta h \frac{\Gamma_g}{c_g^2} \frac{\Gamma_\ell}{c_\ell^2} + \frac{\Gamma_g}{c_g^2} - \frac{\Gamma_\ell}{c_\ell^2} \right) \left((\Delta h \rho_g - \Delta p) \frac{\Gamma_\ell}{c_\ell^2} + \rho_g - \rho_\ell \right) C_{p,\ell} T c_\ell^2 c_g^2 \right.$$

$$\left. \left. + \left(\Delta h \frac{\Gamma_g}{c_g^2} - 1 \right) (\Delta h \rho_g - \Delta p) m_\ell c_g^2 - (\Delta h \rho_\ell - \Delta p) c_\ell^2 m_g \right) \mathcal{J}(p_g - p_\ell) \right]$$

$$\cdot \left[\left(\left(\Delta h \frac{\Gamma_g}{c_g^2} \frac{\Gamma_\ell}{c_\ell^2} + \frac{\Gamma_g}{c_g^2} - \frac{\Gamma_\ell}{c_\ell^2} \right)^2 c_\ell^2 c_g^2 C_{p,g} C_{p,\ell} T^2 + c_g^2 m_\ell C_{p,\ell} T + c_\ell^2 m_g C_{p,g} T + \Delta h^2 m_g m_\ell \right. \right.$$

$$\left. \left. + \left(\Delta h \frac{\Gamma_\ell}{c_\ell^2} + 1 \right)^2 c_\ell^2 m_g C_{p,\ell} T + \left(\Delta h \frac{\Gamma_g}{c_g^2} - 1 \right)^2 m_\ell C_{p,g} T c_g^2 \right) m_g \right]^{-1},$$

$$(8.13) \quad D_t s_\ell = C_{p,\ell} \left[\left(\left(-\Delta h \frac{\Gamma_\ell}{c_\ell^2} \frac{\Gamma_g}{c_g^2} + \frac{\Gamma_\ell}{c_\ell^2} - \frac{\Gamma_g}{c_g^2} \right) \left(\rho - m_\ell \Delta h \frac{\Gamma_g}{c_g^2} \right) C_{p,g} T c_\ell^2 c_g^2 \right. \right.$$

$$- \Delta h m_g m_\ell \left(c_g^2 - c_\ell^2 - \Delta h \Gamma_\ell \right) \frac{\partial v}{\partial x}$$

$$+ \left(\left(\Delta h \frac{\Gamma_\ell}{c_\ell^2} \frac{\Gamma_g}{c_g^2} - \frac{\Gamma_\ell}{c_\ell^2} + \frac{\Gamma_g}{c_g^2} \right) \left((\Delta h \rho_\ell - \Delta p) \frac{\Gamma_g}{c_g^2} - \rho_\ell + \rho_g \right) C_{p,g} T c_g^2 c_\ell^2 \right.$$

$$\left. \left. + \left(\Delta h \frac{\Gamma_\ell}{c_\ell^2} + 1 \right) (\Delta h \rho_\ell - \Delta p) m_g c_\ell^2 + (\Delta h \rho_g - \Delta p) c_g^2 m_\ell \right) \mathcal{J}(p_\ell - p_g) \right]$$

$$\cdot \left[\left(\left(\Delta h \frac{\Gamma_\ell}{c_\ell^2} \frac{\Gamma_g}{c_g^2} - \frac{\Gamma_\ell}{c_\ell^2} + \frac{\Gamma_g}{c_g^2} \right)^2 c_g^2 c_\ell^2 C_{p,\ell} C_{p,g} T^2 + c_\ell^2 m_g C_{p,g} T + c_g^2 m_\ell C_{p,\ell} T + \Delta h^2 m_\ell m_g \right. \right.$$

$$\left. \left. + \left(\Delta h \frac{\Gamma_g}{c_g^2} - 1 \right)^2 c_g^2 m_\ell C_{p,g} T + \left(\Delta h \frac{\Gamma_\ell}{c_\ell^2} + 1 \right)^2 m_g C_{p,\ell} T c_\ell^2 \right) m_\ell \right]^{-1},$$

where we have used (2.3) and (2.5) to replace $D_t \rho$ and $D_t \alpha_g$, and introduced $\Delta p \equiv p_g - p_\ell$.

8.2. The thermal-chemical equilibrium model. The thermal-chemical equilibrium model can be formulated as follows:

- Mass conservation:

$$(8.14) \qquad \qquad \frac{\partial \rho}{\partial t} + \frac{\partial (\rho v)}{\partial x} = 0.$$

- Momentum conservation:

$$(8.15) \qquad \qquad \frac{\partial (\rho v)}{\partial t} + \frac{\partial (\rho v^2 + \alpha_g p_g + \alpha_\ell p_\ell)}{\partial x} = 0.$$

- Volume advection:

$$(8.16) \qquad \mathrm{D}_t \alpha_{\mathrm{g}} = \mathcal{J}(p_{\mathrm{g}} - p_\ell).$$

- Energy conservation:

$$(8.17) \qquad \frac{\partial E}{\partial t} + \frac{\partial (v(E + p))}{\partial x} = 0.$$

An alternative formulation may be obtained by using the more obscure entropy equations (8.12)–(8.13) instead of the volume fraction (8.16) and energy equations (8.17).

8.3. Wave velocities. We now wish to calculate the wave velocities, and hence the mixture speed of sound, of the thermal-chemical equilibrium model (8.14)–(8.17) in the nonstiff limit where $\mathcal{J} \to 0$. To this end, we find it useful to derive an evolution equation for the effective pressure p_{eff}.

We express (8.8)–(8.10) using the material derivative, which together with (8.12)–(8.13), (8.16), and (4.14) yields

$$(8.18) \qquad \mathrm{D}_t p_{\mathrm{eff}} = -\rho \tilde{a}_{T\mu}^2 \frac{\partial v}{\partial x},$$

where

$$(8.19)$$
$$\tilde{a}_{T\mu}^2 = \left(\frac{\rho}{C_{p,\mathrm{g}} T} \left(1 + \Delta h \frac{\Gamma_\ell}{c_\ell^2} \frac{m_{\mathrm{g}}}{\rho} \right)^2 + \frac{\rho}{C_{p,\ell} T} \left(1 - \Delta h \frac{\Gamma_{\mathrm{g}}}{c_{\mathrm{g}}^2} \frac{m_\ell}{\rho} \right)^2 + \frac{\Delta h^2 m_{\mathrm{g}} m_\ell \tilde{a}_0^2}{C_{p,\mathrm{g}} C_{p,\ell} T^2 c_{\mathrm{g}}^2 c_\ell^2} \right)$$
$$\cdot \left[\frac{m_\ell}{c_\ell^2 C_{p,\mathrm{g}} T} + \frac{m_{\mathrm{g}}}{c_{\mathrm{g}}^2 C_{p,\ell} T} + \left(\Delta h \frac{\Gamma_{\mathrm{g}}}{c_{\mathrm{g}}^2} - 1 \right)^2 \frac{m_\ell}{c_\ell^2 C_{p,\ell} T} + \left(\Delta h \frac{\Gamma_\ell}{c_\ell^2} + 1 \right)^2 \frac{m_{\mathrm{g}}}{c_{\mathrm{g}}^2 C_{p,\mathrm{g}} T} \right.$$
$$\left. + \frac{\Delta h^2 m_\ell m_{\mathrm{g}}}{C_{p,\mathrm{g}} C_{p,\ell} T^2 c_{\mathrm{g}}^2 c_\ell^2} + \left(\Delta h \frac{\Gamma_{\mathrm{g}}}{c_{\mathrm{g}}^2} \frac{\Gamma_\ell}{c_\ell^2} + \frac{\Gamma_{\mathrm{g}}}{c_{\mathrm{g}}^2} - \frac{\Gamma_\ell}{c_\ell^2} \right)^2 \right]^{-1}.$$

From (8.16), we know that α_{g} is a characteristic variable with the corresponding eigenvalue v. The remaining equations (8.14), (8.15), and (8.18) may then be expressed as a quasi-linear equation system in the variables $\boldsymbol{u} = [\rho, \rho v, p_{\mathrm{eff}}]$,

$$(8.20) \qquad \boldsymbol{u}_t + \begin{bmatrix} 0 & 1 & 0 \\ -v^2 & 2v & 1 \\ -v\tilde{a}_{T\mu}^2 & \tilde{a}_{T\mu}^2 & v \end{bmatrix} \boldsymbol{u}_x = 0.$$

The eigenvalues of this system are $\{\tilde{a}_{T\mu}, v, v + \tilde{a}_{T\mu}\}$, and thus the eigenvalues of the full model may be summarized as

$$(8.21) \qquad \boldsymbol{\lambda}_{T\mu} = \{ v - \tilde{a}_{T\mu}, v, v, v + \tilde{a}_{T\mu} \}.$$

8.3.1. The subcharacteristic condition with respect to T-model. Using (4.17) and (8.19), it may be shown that the mixture speed of sound of the present model may be written as

$$(8.22) \qquad \tilde{a}_{T\mu}^{-2} = \tilde{a}_T^{-2} + Z_{T\mu}^T,$$

where

$$(8.23) \quad Z_{T\mu}^T = \left(\Delta h \left(\frac{\Gamma_g}{C_{p,\ell}T} + \frac{\Gamma_\ell}{C_{p,g}T} \right) + (c_\ell^2 - c_g^2) \left(\frac{1}{C_{p,\ell}T} + \frac{1}{C_{p,g}T} \right) \right.$$

$$+ \left(\frac{\Gamma_\ell}{m_\ell c_\ell^2} + \frac{\Gamma_g}{m_g c_g^2} \right) \left(\Delta h \frac{\Gamma_g \Gamma_\ell}{c_g^2 c_\ell^2} + \frac{\Gamma_g}{c_g^2} - \frac{\Gamma_\ell}{c_\ell^2} \right) c_\ell^2 c_g^2 \Bigg) m_g m_\ell$$

$$\cdot \left[\left(\left(\frac{\rho}{C_{p,\ell}T} \left(1 - \Delta h \frac{m_\ell}{\rho} \frac{\Gamma_g}{c_g^2} \right)^2 + \frac{\rho}{C_{p,g}T} \left(1 + \Delta h \frac{m_g}{\rho} \frac{\Gamma_\ell}{c_\ell^2} \right)^2 \right) c_\ell^2 c_g^2 + \Delta h^2 \frac{m_g}{C_{p,g}T} \frac{m_\ell}{C_{p,\ell}T} \tilde{a}_0^2 \right) \right.$$

$$\left. \left(\left(\frac{1}{C_{p,g}T} + \frac{1}{C_{p,\ell}T} \right) \rho \tilde{a}_0^2 + \left(\frac{\Gamma_\ell}{m_\ell c_\ell^2} + \frac{\Gamma_g}{m_g c_g^2} \right)^2 m_g m_\ell c_\ell^2 c_g^2 \right) \right]^{-1}.$$

PROPOSITION 5. *The thermal-chemical equilibrium model given by (8.14)–(8.17) satisfies the subcharacteristic condition with respect to the thermal equilibrium model of section 4, subject only to the physically fundamental conditions*

$$\rho_k > 0,$$
$$c_{p,k} > 0,$$
$$T > 0.$$

Proof. By (4.20) and (8.21), we see that the interlacing condition from Definition 1 reduces to the requirement that

$$(8.24) \qquad \tilde{a}_T \geq \tilde{a}_{T\mu},$$

which follows from (8.22)–(8.23) and the given conditions for ρ_k, $c_{p,k}$, and T. ∎

8.3.2. The subcharacteristic condition with respect to the μ-model.
From (5.15) and (8.19), we find that the mixture speed of sound in the present model may be written as

$$(8.25) \qquad \tilde{a}_{T\mu}^{-2} = \tilde{a}_\mu^{-2} + Z_{T\mu}^\mu,$$

where

$$(8.26) \quad Z_{T\mu}^\mu = \left(-(\Delta h \Gamma_g - c_g^2 + c_\ell^2) \frac{s_\ell}{C_{p,\ell}} - (\Delta h \Gamma_\ell + c_\ell^2 - c_g^2) \frac{s_g}{C_{p,g}} \right.$$

$$+ \left(\frac{\rho}{m_g m_\ell} - \frac{\Gamma_\ell s_\ell T}{m_\ell c_\ell^2} - \frac{\Gamma_g s_g T}{m_g c_g^2} \right) \left(\Delta h \frac{\Gamma_g}{c_g^2} \frac{\Gamma_\ell}{c_\ell^2} + \frac{\Gamma_g}{c_g^2} - \frac{\Gamma_\ell}{c_\ell^2} \right) c_\ell^2 c_g^2 \Bigg)$$

$$\cdot \left[\left(\frac{\Delta h^2 \tilde{a}_0^2}{C_{p,g} C_{p,\ell} T^2} + \left(\frac{1}{C_{p,g}T} \left(\frac{\rho}{m_g m_\ell} + \frac{\Gamma_\ell \Delta h}{m_\ell c_\ell^2} \right) \right)^2 \right. \right.$$

$$\left. + \frac{1}{C_{p,\ell}T} \left(\frac{\rho}{m_g m_\ell} - \frac{\Gamma_g \Delta h}{m_g c_g^2} \right)^2 \right) \frac{m_\ell c_\ell^2 m_g c_g^2}{\rho} \Bigg)$$

$$\cdot \left(\left(\frac{s_g^2 T}{C_{p,g}} + \frac{s_\ell^2 T}{C_{p,\ell}} \right) \rho \tilde{a}_0^2 + m_g m_\ell \left(\frac{\rho}{m_g m_\ell} - \frac{\Gamma_\ell s_\ell T}{m_\ell c_\ell^2} - \frac{\Gamma_g s_g T}{m_g c_g^2} \right)^2 c_\ell^2 c_g^2 \right) \right]^{-1}.$$

PROPOSITION 6. *The thermal-chemical equilibrium model given by* (8.14)–(8.17) *satisfies the subcharacteristic condition with respect to the chemical equilibrium model of section* 5, *subject only to the physically fundamental conditions*

$$\rho_k > 0,$$
$$c_{p,k} > 0,$$
$$T > 0.$$

Proof. By (5.19) and (8.21), we see that the interlacing condition of Definition 1 reduces to the requirement that

(8.27) $$\tilde{a}_\mu \geq \tilde{a}_{T\mu},$$

which follows from (8.25)–(8.26) and the given conditions for ρ_k, $c_{p,k}$, and T. $\qquad\Box$

9. Full relaxation. In this section, we investigate the model that results when we let all the relaxation parameters $\mathcal{J}, \mathcal{H}, \mathcal{K}$ in the basic model of section 2 go to infinity. We expect this to correspond to the assumptions

(9.1) $$p_{\mathrm{g}} = p_\ell = p^* = p,$$
(9.2) $$T_{\mathrm{g}} = T_\ell = T,$$
(9.3) $$\mu_{\mathrm{g}} = \mu_\ell = \mu^* = \mu.$$

In other words, the two phases are in full equilibrium. This model is also referred to as the *homogeneous equilibrium model* [26], and has been used for two-phase flow simulations by a number of authors [8, 19].

9.1. The full equilibrium model. The full equilibrium model can be formulated through conservation equations for total mass, momentum, and energy:
  - Total mass conservation:

  (9.4) $$\frac{\partial \rho}{\partial t} + \frac{\partial (\rho v)}{\partial x} = 0.$$

  - Momentum conservation:

  (9.5) $$\frac{\partial (\rho v)}{\partial t} + \frac{\partial (\rho v^2 + p)}{\partial x} = 0.$$

  - Total energy conservation:

  (9.6) $$\frac{\partial E}{\partial t} + \frac{\partial (v(E + p))}{\partial x} = 0.$$

Here, the energy equation (9.6) is obtained simply by adding the energy equations (2.8)–(2.9) of the basic model.

9.2. Wave velocities. The wave velocities of the full equilibrium model have been analyzed by, e.g., Städtke [26], Saurel, Petitpas, and Abgrall [23], and Flåtten and Lund [10]. The eigenvalues are given by

(9.7) $$\boldsymbol{\lambda}_{pT\mu} = \{v - \tilde{a}_{pT\mu}, v, v + \tilde{a}_{pT\mu}\},$$

where the mixture speed of sound is given by [23]

$$(9.8) \qquad \tilde{a}_{pT\mu}^{-2} = \tilde{a}_p^{-2} + \rho T \left[\frac{\alpha_g \rho_g}{c_{p,g}} \left(\frac{\partial s_g}{\partial p} \right)_{sat}^2 + \frac{\alpha_\ell \rho_\ell}{c_{p,\ell}} \left(\frac{\partial s_\ell}{\partial p} \right)_{sat}^2 \right],$$

where the notation $(\cdot)_{sat}$ is used for differentiation along the boiling curve. The mixture speed of sound may also be expressed through the thermodynamic derivatives used earlier (Γ_k, c_k, and $c_{p,k}$), by replacing the saturation derivative using

$$(9.9) \qquad \left(\frac{\partial s_k}{\partial p} \right)_{sat} = -\frac{\Gamma_k c_{p,k}}{\rho_k c_k^2} - \frac{c_{p,k}(\rho_g - \rho_\ell)}{\rho_g \rho_\ell (h_g - h_\ell)}.$$

9.2.1. The subcharacteristic condition with respect to the pT-model. As shown by Flåtten and Lund [10], the subcharacteristic condition with respect to the mechanical-thermal equilibrium model of section 6 is satisfied, given only $\rho_k > 0$, $c_{p,k} > 0$, and $T > 0$, which was shown by writing

$$(9.10) \qquad \tilde{a}_{pT\mu}^{-2} = \tilde{a}_{pT}^{-2} + Z_{pT\mu}^{pT},$$

where

$$(9.11) \qquad Z_{pT\mu}^{pT} = \frac{\rho T}{C_{p,g} + C_{p,\ell}} \left(\frac{\rho_g - \rho_\ell}{\rho_g \rho_\ell (h_g - h_\ell)} (C_{p,g} + C_{p,\ell}) + \frac{\Gamma_g C_{p,g}}{\rho_g c_g^2} + \frac{\Gamma_\ell C_{p,\ell}}{\rho_\ell c_\ell^2} \right)^2.$$

9.2.2. The subcharacteristic condition with respect to the $p\mu$-model. Also shown by Flåtten and Lund [10], the full equilibrium model fulfills the subcharacteristic condition with respect to the mechanical-chemical equilibrium model of section 7, given only $\rho_k > 0$, $c_{p,k} > 0$, and $T > 0$, which may be shown by writing

$$(9.12) \qquad \tilde{a}_{pT\mu}^{-2} = \tilde{a}_{p\mu}^{-2} + Z_{pT\mu}^{p\mu},$$

where

$$(9.13) \qquad Z_{pT\mu}^{p\mu} = \frac{\rho}{T(C_{p,\ell} s_g^2 + C_{p,g} s_\ell^2)} \left(\frac{(\rho_\ell - \rho_g)(C_{p,g} s_\ell + C_{p,\ell} s_g)}{\rho_g \rho_\ell (s_\ell - s_g)} \right.$$
$$\left. + T \frac{C_{p,g} C_{p,\ell} s_g s_\ell \left(\frac{\Gamma_\ell}{\rho_\ell c_\ell^2} + \frac{\Gamma_g}{\rho_g c_g^2} \right) + \frac{\Gamma_g}{\rho_g c_g^2} C_{p,g}^2 s_\ell^2 + \frac{\Gamma_\ell}{\rho_\ell c_\ell^2} C_{p,\ell}^2 s_g^2}{C_{p,g} s_\ell + C_{p,\ell} s_g} \right)^2.$$

9.2.3. The subcharacteristic condition with respect to the $T\mu$-model. By algebraic manipulations, one may show that the mixture speed of sound of the full equilibrium model is related to the one of the thermal-chemical equilibrium model as given by

$$(9.14) \qquad \tilde{a}_{pT\mu}^{-2} = \tilde{a}_{T\mu}^{-2} + Z_{pT\mu}^{T\mu},$$

where

$$(9.15) \quad Z_{pT\mu}^{T\mu} = \left(\left(C_{p,\ell}T \left(\rho_{\text{g}} - \rho_\ell + \Delta h \frac{\Gamma_\ell}{c_\ell^2} \rho_{\text{g}} \right) \left(\rho + \Delta h \frac{\Gamma_\ell}{c_\ell^2} m_{\text{g}} \right) \right.\right.$$

$$\left. - C_{p,\text{g}}T \left(\rho_\ell - \rho_{\text{g}} - \Delta h \frac{\Gamma_{\text{g}}}{c_{\text{g}}^2} \rho_\ell \right) \left(\rho - \Delta h \frac{\Gamma_{\text{g}}}{c_{\text{g}}^2} m_\ell \right) + \Delta h^2 \frac{m_{\text{g}} m_\ell}{c_{\text{g}}^2 c_\ell^2} (c_{\text{g}}^2 \rho_{\text{g}} - c_\ell^2 \rho_\ell) \right)^2 \rho \right)$$

$$\cdot \left[\left(C_{p,\text{g}}T \left(\rho - m_\ell \Delta h \frac{\Gamma_{\text{g}}}{c_{\text{g}}^2} \right)^2 + C_{p,\ell}T \left(\rho + m_{\text{g}} \Delta h \frac{\Gamma_\ell}{c_\ell^2} \right)^2 \right.\right.$$

$$\left.\left. + \frac{m_{\text{g}} m_\ell}{c_{\text{g}}^2 c_\ell^2} \Delta h^2 \rho \tilde{a}_0^2 \right) \Delta h^2 \rho_{\text{g}}^2 \rho_\ell^2 \right]^{-1} .$$

PROPOSITION 7. *The full equilibrium model given by (9.4)–(9.6) satisfies the subcharacteristic condition with respect to the thermal-chemical equilibrium model of section 8, given only the physically fundamental requirements*

$$\rho_k > 0,$$
$$c_{p,k} > 0,$$
$$T > 0.$$

Proof. From (8.21) and (9.7), we find that the interlacing condition in Definition 1 translates to the requirement that

$$(9.16) \qquad \tilde{a}_{p\mu} \geq \tilde{a}_{pT\mu},$$

which follows from (9.14)–(9.15) and the given conditions for ρ_k, $c_{p,k}$, and T. $\quad\square$

9.2.4. The discontinuity of the speed of sound. We have now considered eight different models with varying equilibrium assumptions, each with its own speed of sound. One would expect that the two-phase speed of sound reduces to the single-phase speed of sound in the limit where one phase disappears, which is indeed the case with seven of the models,

$$(9.17)$$
$$\lim_{\alpha_k \to 1} \tilde{a}_0 = \lim_{\alpha_k \to 1} \tilde{a}_p = \lim_{\alpha_k \to 1} \tilde{a}_T = \lim_{\alpha_k \to 1} \tilde{a}_\mu = \lim_{\alpha_k \to 1} \tilde{a}_{pT} = \lim_{\alpha_k \to 1} \tilde{a}_{p\mu} = \lim_{\alpha_k \to 1} \tilde{a}_{T\mu} = c_k.$$

However, for the final and present full equilibrium model, the single phase limit of the two-phase speed of sound turns out to be discontinuous,

$$(9.18) \qquad \lim_{\alpha_{\text{g}} \to 1} \tilde{a}_{pT\mu} = \left(\frac{1}{c_{\text{g}}^2} + c_{p,\text{g}}T \left(\frac{\rho_{\text{g}} - \rho_\ell}{\rho_\ell(h_{\text{g}} - h_\ell)} + \frac{\Gamma_{\text{g}}}{c_{\text{g}}^2} \right)^2 \right)^{-\frac{1}{2}} \neq c_{\text{g}},$$

$$(9.19) \qquad \lim_{\alpha_\ell \to 1} \tilde{a}_{pT\mu} = \left(\frac{1}{c_\ell^2} + c_{p,\ell}T \left(\frac{\rho_\ell - \rho_{\text{g}}}{\rho_{\text{g}}(h_\ell - h_{\text{g}})} + \frac{\Gamma_\ell}{c_\ell^2} \right)^2 \right)^{-\frac{1}{2}} \neq c_\ell.$$

This implies that when an infinitesimal amount of gas is added to a pure liquid, the mixture speed of sound will change drastically, and vice versa. The discontinuity in the single-phase limit may cause significant numerical challenges, and is not physically plausible, as pointed out by, e.g., Städtke [26, Chap. 4]. It is interesting to note that only the combination of all three relaxation processes together causes this discontinuity, while any other combination does not exhibit such a behavior.

10. Speed of sound comparison. In this section, we will present plots illustrating the mixture speed of sound for water and carbon dioxide at industrially relevant conditions, illustrating the impact of the different equilibrium assumptions on the speed of sound. Plots with the same parameters were presented in [10] for five of the models, but in this section we complete the picture by considering all eight models in the hierarchy.

Figure 10.1(a) shows the mixture speed of sound in a two-phase water-steam mixture at atmospheric pressure, $p = 10^5$ Pa. The other parameters are shown in Table 10.1. We recognize that mechanical equilibrium has the most significant impact on the speed of sound, while thermal and chemical equilibrium assumptions have a much smaller effect. In Figure 10.1(b), we take a closer look at the range 0–100 m/s. The full equilibrium model is, as expected, not continuous in the single-phase limit, clearly visible at $\alpha_g = 0$, where the two-phase speed of sound is $\tilde{a}_{pT\mu} \approx 1$ m/s, whereas the liquid speed of sound is $c_\ell = 1543.4$ m/s.
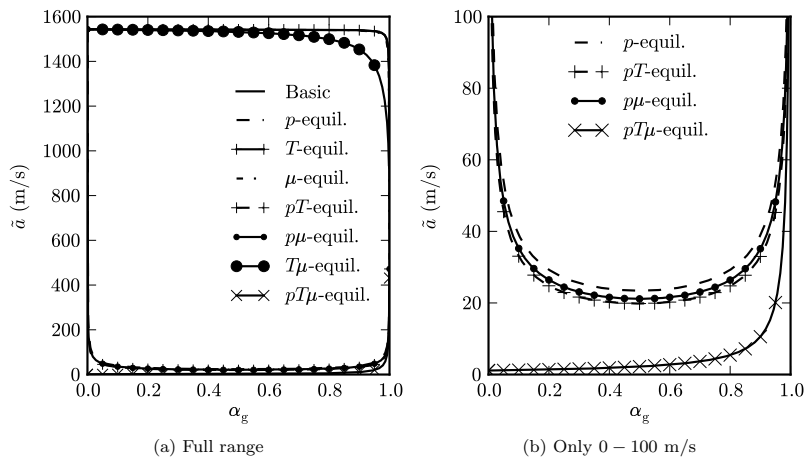
FIG. 10.1. *Mixture speed of sound in a water-steam mixture at atmospheric pressure.*

TABLE 10.1
Parameters for a water-steam mixture at atmospheric pressure.

Quantity	Symbol	Unit	Gas	Liquid
Pressure	p	MPa	0.1	0.1
Temperature	T	K	372.76	372.76
Density	ρ	kg/m^3	0.59031	958.64
Speed of sound	c	m/s	472.05	1543.4
Heat capacity	c_p	J/kg K	2075.9	4216.1
Entropy	s	m^2/s^2 K	7358.8	1302.6
Grüneisen coefficient	Γ	(dimensionless)	0.33699	0.4

The differences between the different models are perhaps even clearer in Figure 10.2, showing the speed of sound for a two-phase CO_2 mixture at $p = 50$ bar. The other parameters are listed in Table 10.2. In this figure, the subcharacteristic
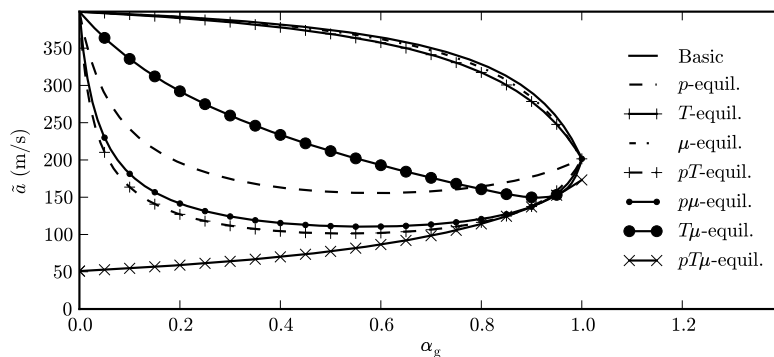
FIG. 10.2. *Mixture speed of sound in a two-phase CO_2 mixture at 50 bar.*

TABLE 10.2
Parameters for a two-phase CO_2 mixture at 50 bar.

Quantity	Symbol	Unit	Gas	Liquid
Pressure	p	MPa	5.0	5.0
Temperature	T	K	287.43	287.43
Density	ρ	kg/m^3	156.71	827.21
Speed of sound	c	m/s	201.54	398.89
Heat capacity	c_p	J/kg K	3138.0	3356.9
Entropy	s	m^2/s^2 K	1753.9	1128.8
Grüneisen coefficient	Γ	(dimensionless)	0.30949	0.63175

condition, predicting that the speed of sound is lowered for each imposed equilibrium assumption, is clearly illustrated. Once again, thermal and chemical equilibria alone have little effect on the mixture speed of sound, and only combining the three equilibrium conditions leads to a discontinuous speed of sound in the single-phase limit.

For more discussions on models and experimental values for the speed of sound in two-phase systems, a number of works exist. Henry, Grolmes, and Fauske [12] present experimental values for the speed of sound in different flow regimes in a water-steam system, while Kieffer [16] compares experimental values with certain models. Städtke [26] also discusses a variety of different models and their speeds of sound. Furthermore, Zein, Hantke, and Warnecke [31] have interesting discussions on how the speeds of the different relaxation processes typically are related.

11. Conclusion and further work. We have studied the complete hierarchy of averaged two-phase homogeneous flow models that arises by assuming equilibrium in different combinations of pressure, temperature, and chemical potential, of which the T-, μ-, and $T\mu$-equilibrium models represented original contributions. The models were formulated as hyperbolic relaxation systems with source terms accounting for heat, mass, and volume transfer between the phases. Wave velocities for each model were derived, and we showed how the subcharacteristic condition leads to the requirement that the mixture speed of sound decreases when equilibrium assumptions are imposed. This requirement was explicitly and analytically shown using sums of

squares. Furthermore, it was illustrated how the different equilibrium assumptions affect the speed of sound in relevant cases for a water-steam mixture and two-phase carbon dioxide. We have also shown how the assumption of full equilibrium leads to a discontinuous speed of sound in the single-phase limit, a phenomenon which is quite unique for this model.

In further work, the hierarchy could possibly be extended to inhomogeneous flow models, i.e., different velocities for the two phases, formulated using two momentum equations, and velocity relaxation.

REFERENCES

[1] M. R. Baer and J. W. Nunziato, *A two-phase mixture theory for the deflagration-to-detonation transition (DDT) in reactive granular materials*, Int. J. Multiphase Flow, 12 (1986), pp. 861–889.

[2] M. Baudin, C. Berthon, F. Coquel, R. Masson, and Q. H. Tran, *A relaxation method for two-phase flow models with hydrodynamic closure law*, Numer. Math., 99 (2005), pp. 411–440.

[3] M. Baudin, F. Coquel, and Q. H. Tran, *A semi-implicit relaxation scheme for modeling two-phase flow in a pipeline*, SIAM J. Sci. Comput., 27 (2005), pp. 914–936.

[4] K. H. Bendiksen, D. Malnes, R. Moe, and S. Nuland, *The dynamic two-fluid model OLGA: Theory and application*, SPE Production Engineering, 6 (1991), pp. 171–180.

[5] T. Berstad, C. Dørum, J. P. Jakobsen, S. Kragset, H. Li, H. Lund, A. Morin, S. T. Munkejord, M. J. Mølnvik, H. O. Nordhagen, and E. Østby, CO_2 *pipeline integrity: A new evaluation methodology*, Energy Procedia, 4 (2011), pp. 3000–3007.

[6] D. Bestion, *The physical closure laws in the CATHARE code*, Nuclear Engineering and Design, 124 (1990), pp. 229–245.

[7] G.-Q. Chen, C. D. Levermore, and T.-P. Liu, *Hyperbolic conservation laws with stiff relaxation terms and entropy*, Comm. Pure Appl. Math., 47 (1994), pp. 787–830.

[8] S. Clerc, *Numerical simulation of the homogeneous equilibrium model for two-phase flows*, J. Comput. Phys., 161 (2000), pp. 354–375.

[9] P. J. M. Ferrer, T. Flåtten, and S. T. Munkejord, *On the effect of temperature and velocity relaxation in two-phase flow models*, M2AN Math. Model. Numer. Anal., 46 (2012), pp. 411–442.

[10] T. Flåtten and H. Lund, *Relaxation two-phase flow models and the subcharacteristic condition*, Math. Models Methods Appl. Sci., 21 (2011), pp. 2379–2407.

[11] T. Flåtten, A. Morin, and S. T. Munkejord, *Wave propagation in multicomponent flow models*, SIAM J. Appl. Math., 70 (2010), pp. 2861–2882.

[12] R. E. Henry, M. A. Grolmes, and H. K. Fauske, *Pressure-pulse Propagation in Two-phase One- and Two-component Mixtures*, ANL, 7792, Argonne National Lab., Argonne, IL, 1971.

[13] M. Ishii and T. Hibiki, *Thermo-Fluid Dynamics of Two-Phase Flow*, 2nd ed., Springer, New York, 2011.

[14] X. Jinliang and C. Tingkuan, *Acoustic wave prediction in flowing steam-water two-phase mixture*, J. Thermal Science, 3 (1994), pp. 147–154.

[15] A. K. Kapila, R. Menikoff, J. B. Bdzil, S. F. Son, and D. S. Stewart, *Two-phase modeling of deflagration-to-detonation transition in granular materials: Reduced equations*, Physics of Fluids, 13 (2001), pp. 3002–3024.

[16] S. W. Kieffer, *Sound speed in liquid-gas mixtures: Water-air and water-steam*, J. Geophysical Research, 82 (1977), pp. 2895–2904.

[17] J. Leray, *Hyperbolic Differential Equations*, The Institute for Advanced Study, Princeton, NJ, 1953.

[18] T.-P. Liu, *Hyperbolic conservation laws with relaxation*, Comm. Math. Phys., 108 (1987), pp. 153–175.

[19] H. Lund, T. Flåtten, and S. T. Munkejord, *Depressurization of carbon dioxide in pipelines - models and methods*, Energy Procedia, 4 (2011), pp. 2984–2991.

[20] A. MURRONE AND H. GUILLARD, *A five equation model for compressible two phase flow problems*, J. Comput. Phys., 202 (2005), pp. 664–698.

[21] R. NATALINI, *Recent results on hyperbolic relaxation problems*, in Analysis of Systems of Conservation Laws, Chapman Hall/CRC Monogr. Surv. Pure Appl. Math. 99, Chapman & Hall/CRC, Boca Raton, FL, 1999, pp. 128–198.

[22] R. SAUREL AND R. ABGRALL, *A multiphase Godunov method for compressible multifluid and multiphase flow*, J. Comput. Phys., 150 (1999), pp. 425–467.

[23] R. SAUREL, F. PETITPAS, AND R. ABGRALL, *Modelling phase transition in metastable liquids: Application to cavitating and flashing flows*, J. Fluid Mech., 607 (2008), pp. 313–350.

[24] R. SAUREL, F. PETITPAS, AND R. A. BERRY, *Simple and efficient relaxation methods for interfaces separating compressible fluids, cavitating flows and shocks in multiphase mixtures*, J. Comput. Phys., 228 (2009), pp. 1678–1712.

[25] H. B. STEWART AND B. WENDROFF, *Two-phase flow: Models and methods*, J. Comput. Phys., 56 (1984), pp. 363–409.

[26] H. STÄDTKE, *Gasdynamic Aspects of Two-Phase Flow*, Wiley-VCH, Weinheim, Germany, 2006.

[27] G. B. WALLIS, *One-dimensional Two-phase Flow*, McGraw-Hill, New York, 1969.

[28] G. B. WHITHAM, *Linear and Nonlinear Waves*, John Wiley & Sons, New York, 1974.

[29] W.-A. YONG, *Singular perturbations of first-order hyperbolic systems with stiff source terms*, J. Differential Equations, 155 (1999), pp. 89–132.

[30] W.-A. YONG, *Basic aspects of hyperbolic relaxation systems*, in Advances in the Theory of Shock Waves, Progr. Nonlinear Differential Equations Appl. 47, Birkhäuser Boston, Boston, 2001, pp. 259–305.

[31] A. ZEIN, M. HANTKE, AND G. WARNECKE, *Modeling phase transition for compressible two-phase flows applied to metastable liquids*, J. Comput. Phys., 229 (2010), pp. 2964–2998.

Paper L3

Two-Phase flow of CO_2 with phase transfer

Halvor Lund and Peder Aursand

6th Trondheim CCS Conference

Two-Phase Flow of CO$_2$ with Phase Transfer

Halvor Lund[a,*], Peder Aursand[b]

[a]*Dept. of Energy and Process Engineering, Norwegian University of Science and Technology (NTNU), NO-7491 Trondheim, Norway*
[b]*SINTEF Energy Research, Sem Sælands vei 11, NO-7465 Trondheim, Norway*

Abstract

A model for two-phase pipeline flow of CO$_2$ with phase transfer is presented. Two different relaxation models for phase transfer are developed. The system of equations is solved by splitting it into a hyperbolic conservation law and a relaxation ODE, solved by a multi-stage (MUSTA) finite volume scheme and the backward Euler method, respectively. The stiffened-gas equation of state is used for calculating thermodynamic properties. Simulation results from a depressurisation case of a CO$_2$ pipe, causing phase change and cooling, are presented, showing that statistical rate theory predicts solutions close to those of an equilibrium model with instant phase transfer.

1. Introduction

Carbon dioxide capture and storage (CCS) will potentially be an important contributor to mitigating emission of CO$_2$ from stationary sources. In the BLUE map of the International Energy Agency (IEA) [1], CCS accounts for 19% of CO$_2$ emission reductions in 2050. Transport from the point of capture to a storage site is a necessary part of a CCS system and may take place using e.g. ships or pipelines. Experience with multi-phase flow in pipelines is abundant in the oil and gas industry as well as in the nuclear industry. However, knowledge on two-phase flow of CO$_2$ is available to a lesser extent.

Transport of CO$_2$ will typically take place at high pressure, at conditions at which the CO$_2$ is in its super-critical phase. However, during a pressurisation from atmospheric pressure or during a planned or possibly uncontrolled depressurisation, the fluid may enter the two-phase region with gas and liquid coexisting. Due to phase change in such a situation, the fluid will cool significantly, potentially leading to temperatures low enough to make the pipe steel brittle. This, in turn, makes the pipe vulnerable to rupture and possible severe damage. The prediction of the temperature drop during such depressurisations requires modeling of phase transfer (i.e. evaporation and condensation) between the two phases.

---

*Corresponding author
Email address:* `halvor.lund@ntnu.no` (Halvor Lund)

Our paper is organized as follows: In Section 2, we present our two-phase drift-flux flow model, which needs a phase transfer model to be fully defined. Two such models are developed in Section 3. Section 4 briefly describes the thermodynamic model (equation of state) we have used. The numerical methods used to solve the fluid-mechanical and phase transfer equations are presented in Section 5. Results from a depressurisation of a CO_2 pipeline are presented in Section 6. Finally, Section 7 concludes our work.

2. Two-phase flow model

The goal of our work is to demonstrate modeling of a phase transfer process in a pipe with two-phase flow. We therefore aim for a model which incorporates phase transfer, but otherwise is as simple as possible. Hence, we make the assumptions that the two phases

1. have equal velocities, i.e. a homogeneous flow model,
2. are in thermal equilibrium, i.e. have equal temperatures,
3. are in mechanical equilibrium, i.e. have equal pressures.

This allows us to formulate a four-equation drift-flux model consisting of two mass balance equations, and conservation equations for the total momentum and energy.

$$\frac{\partial(\alpha_g \rho_g)}{\partial t} + \frac{\partial(\alpha_g \rho_g v)}{\partial x} = \Gamma, \tag{1}$$

$$\frac{\partial(\alpha_\ell \rho_\ell)}{\partial t} + \frac{\partial(\alpha_\ell \rho_\ell v)}{\partial x} = -\Gamma, \tag{2}$$

$$\frac{\partial(\rho v)}{\partial t} + \frac{\partial(\rho v^2 + p)}{\partial x} = 0, \tag{3}$$

$$\frac{\partial E}{\partial t} + \frac{\partial[(E + p)v]}{\partial x} = 0, \tag{4}$$

where α_k is the volume fraction of phase k, ρ_k is the density of phase k, and $\rho = \alpha_g \rho_g + \alpha_\ell \rho_\ell$ is the mixture density. The fluid velocity is denoted by v and the pressure by p. The total energy per unit volume, E, is given by

$$E = E_g + E_\ell, \tag{5}$$

$$E_k = \alpha_k \rho_k (e_k + \frac{1}{2} v^2), \quad k \in \{g, \ell\}, \tag{6}$$

where e_k is the internal energy per mass of phase k. The phase transfer source term appears in the mass balance equations as Γ. This model has been analyzed by e.g. Flåtten and Lund [2] and Flåtten, Morin, and Munkejord [3] in the non-stiff limit where $\Gamma \to 0$.

The two-phase flow model presented above has the advantage of being quite simple, while still allowing for phase transfer modeling; the only simpler alternative possibly being an isentropic model. Although terms accounting for e.g. wall friction, heat transfer between the pipe and the fluid, and fluid heat conduction are omitted here, such terms may be added later if desired.

3. Phase transfer model

The phase transfer can be written (disregarding the transport terms) as

$$\frac{d(\alpha_g \rho_g)}{dt} = -\frac{d(\alpha_\ell \rho_\ell)}{dt} = \Gamma. \tag{7}$$

Physically, differences in the chemical potentials of the two phases will cause a mass flux from one phase to the other, in the direction of decreasing chemical potential. We therefore seek a phase transfer term in the form

$$\Gamma = \mathcal{K}(\mu_\ell - \mu_g), \tag{8}$$

where $\mathcal{K} > 0$ is some function of flow and thermodynamic variables. The function $\mathcal{K}$ should fulfill some important requirements:

1. $\mathcal{K} = 0$ if $m_g = 0$ and $\mu_g > \mu_\ell$
2. $\mathcal{K} = 0$ if $m_\ell = 0$ and $\mu_g < \mu_\ell$

These requirements avoids phase transfer *from* a non-existing phase.

In the limit where $\mathcal{K} \to \infty$, we arrive at an equilibrium model in which phase transfer is instantaneous, i.e. the phases always have equal chemical potential. In this limit, the model (1)–(4) may be written as the classical Euler equations of gas dynamics [2],

$$\frac{\partial \rho}{\partial t} + \frac{\partial(\rho v)}{\partial x} = 0, \qquad \frac{\partial(\rho v)}{\partial t} + \frac{\partial(\rho v^2 + p)}{\partial x} = 0, \qquad \frac{\partial E}{\partial t} + \frac{\partial[(E + p)v]}{\partial x} = 0. \tag{9}$$

This model is also known as the homogeneous equilibrium model, which was investigated for use in carbon dioxide pipeline depressurisation simulations in Ref. [4].

3.1. Simple model

As an initial approach, we suggest the simplest model possible which fulfills the two requirements stated earlier,

$$\mathcal{K} = \begin{cases} \mathcal{K}_0 m_g & \text{if } \mu_g > \mu_\ell, \\ \mathcal{K}_0 m_\ell & \text{if } \mu_g < \mu_\ell, \\ 0 & \text{otherwise,} \end{cases} \tag{10}$$

where $\mathcal{K}_0 > 0$ is an adjustable parameter whose magnitude determines the rate of the phase transfer. The value of $\mathcal{K}_0$ in this model is unknown, which makes it more of a qualitative model. We would like to compare it with a quantitative model, in which the magnitude of $\mathcal{K}$ is more precise. To this end, we develop an expression based on statistical rate theory in the following section.

3.2. Statistical rate theory

In the literature, modeling of mass fluxes across interfaces is described using a variety of different approaches. Of the most common are kinetic theory and irreversible (non-equilibrium) thermodynamics. Recently, statistical rate theory (SRT) has been proposed by Ward and Fang [5] as an alternative approach to model liquid evaporation. One of the reasons of the introduction of SRT was that kinetic theory predicted unreasonable temperature profiles near the interface [6], so-called anomalous temperature profiles. Further discussion on this matter can be found in the works of Koffman, Plesset, and Lees [7] and Rahimi and Ward [8]. The SRT model predicts more reasonable temperature profiles, in better accordance with experimental results. Another significant advantage of SRT when modeling evaporation and condensation, compared to kinetic theory or irreversible thermodynamics, is that it is free of any fitting parameters.

Statistical rate theory is a rather new approach to modeling of evaporation and condensation, based on transition probabilities from quantum mechanics and the Boltzmann definition of entropy. It assumes that the interfacial transport processes are the result of single molecular events and calculates the probabilities using first-order perturbation analysis of the Schrödinger equation. The theory was first introduced by Ward [9] in 1977, and was later laid out more fundamentally in the early 1980s by Ward, Findlay, and Rizk [10]. It has since been applied to as diverse transport processes as crystal growth [11], solution/solid adsorption [12, 13], gas/solid adsorption [14, 15], temperature programmed desorption [16], ion permeation across lipid membranes [17], chemical reactions [18], and evaporation and condensation [5, 19, 20].

We will now derive an expression for the evaporation and condensation mass flux, based on the SRT model, closely following the derivations in Refs. [5, 10]. As noted previously, the SRT approach is based on the probability of single molecular events. Let λ_j denote a "current" molecular distribution, and λ_k denote a distribution in which one molecule has been transferred from the liquid phase to the vapor. From perturbation analysis, the probability of a transition from distribution λ_j to λ_k is [10]

$$\tau(\lambda_j \to \lambda_k) = K(\lambda_j \to \lambda_k)\frac{\Omega(\lambda_k)}{\Omega(\lambda_j)}, \tag{11}$$

where $\Omega(\lambda)$ is the number of microscopic states with molecular distribution λ. The constant K will be determined later in the derivation. Using the Boltzmann definition of entropy, the probability (11) reads

$$\tau(\lambda_j \to \lambda_k) = K(\lambda_j \to \lambda_k) \exp \left[\frac{S(\lambda_k) - S(\lambda_j)}{k_B} \right], \tag{12}$$

where $S(\lambda)$ is the total entropy of the molecular distribution λ. Similarly, let λ_i denote a distribution in which one molecule has been transferred from the vapor phase to the liquid. The probability for this transition, $\tau(\lambda_j \to \lambda_i)$, is then given by Eq. (12) with k replaced by i. The change in entropy from one state to the other is given by the sum over all phases. The change of entropy can then be expressed as

$$S(\lambda_k) - S(\lambda_j) = \sum_{i=g,\ell} (S_i(\lambda_k) - S_i(\lambda_j)) = \sum_{i=g,\ell} \Delta S_i, \tag{13}$$

where $\Delta S_i \equiv S_i(\lambda_k) - S_i(\lambda_j)$ is the change in entropy of phase i. From the Gibbs-Duhem relation and the fundamental relation $U = TS - pV + gN$, we have [10]

$$T_i \Delta S_i = \Delta U_i + p_i \Delta V_i - g_i \Delta N_i, \tag{14}$$

where g_i is the chemical potential per molecule, U_i is the total internal energy, T_i is the temperature and N_i the number of molecules in phase i. Solving for ΔS_i and inserting into the sum in Eq. (13) yields

$$S(\lambda_k) - S(\lambda_j) = \frac{\Delta U_g + p_g \Delta V_g - g_g \Delta N_g}{T_g} + \frac{\Delta U_\ell + p_\ell \Delta V_\ell - g_\ell \Delta N_\ell}{T_\ell}. \tag{15}$$

We recall that the transition from distribution λ_j to λ_k corresponds to one molecule making the transition from the liquid to the gas phase, which means that $\Delta N_\ell = -1$ and $\Delta N_g = 1$. We can also utilize that the phases have equal pressures and temperatures (by definition in our model), which yields

$$S(\lambda_k) - S(\lambda_j) = \frac{1}{T} (\Delta U_g + \Delta U_\ell + p(\Delta V_g + \Delta V_\ell) + g_\ell - g_g). \tag{16}$$

Since we are considering an isolated system, the total energy and total volume are conserved, thus we have

$$S(\lambda_k) - S(\lambda_j) = \frac{1}{T} (g_\ell - g_g). \tag{17}$$

The chemical potential per mass, μ_k, can easily be calculated by dividing g_k by the molecule mass. We may now insert the entropy expressions in the expression for the transition probability (12), yielding

$$\tau(\lambda_j \to \lambda_k) = K_{\ell \to g} \exp \left[\frac{1}{k_B T} (g_\ell - g_g) \right] \tag{18}$$

for the transport from liquid to gas, where we write $K_{\ell \to g} \equiv K(\lambda_j \to \lambda_k)$ to make the direction liquid-to-gas clearer. Similarly, for transport from gas to liquid we get

$$\tau(\lambda_j \to \lambda_i) = K_{g \to \ell} \exp \left[\frac{1}{k_B T} (g_g - g_\ell) \right]. \tag{19}$$

The number of molecules transferred from liquid to gas in a time Δt is

$$\Delta N_{\ell \to g} = \tau(\lambda_j \to \lambda_k) \Delta t, \tag{20}$$

provided that Δt is small enough not to change τ. The flux (number of transitions per time per area) is then

$$j_{\ell \to g} = \frac{\Delta N_{\ell \to g}}{\Delta t} = K_{\ell \to g} \exp \left[\frac{1}{k_B T} (g_\ell - g_g) \right]. \tag{21}$$

An equivalent expression applies to the transition from gas to liquid. This is equivalent to the expression which Ward and Fang [5] arrive at, if one assumes equal temperatures.

The net flux from liquid to gas can then be written as the difference between the fluxes in each direction, yielding the net flux

$$j = j_{\ell \to g} - j_{g \to \ell} = K_{\ell \to g} \exp\left[\frac{1}{k_B T}(g_\ell - g_g)\right] - K_{g \to \ell} \exp\left[\frac{1}{k_B T}(g_g - g_\ell)\right] \tag{22}$$

In an equilibrium condition, with $g_g = g_\ell$, the two fluxes have to cancel each other, giving a net flux of zero. This means that $K_{\ell \to g} = K_{g \to \ell} = K_e$. To calculate the value of this constant, we turn to classical kinetic theory and assume that in equilibrium all molecules that collide with the liquid-vapor interface are transferred to the other phase. The collision rate of gas molecules can be predicted using the Maxwell-Boltzmann velocity distribution, and may be expressed as

$$K_e = \rho_g \sqrt{\frac{k_B T}{2\pi m^3}}, \tag{23}$$

where m is the molecular mass. This is a well-known result for ideal gases, but as Kapoor and Elliott [19] point out, it is equally valid for a non-ideal gas. Furthermore, we assume that we always are close to equilibrium, so that we always have $K_e = K_{\ell \to g} = K_{g \to \ell}$. We may now write the mass flux, obtained by multiplying the net flux (22) by the molecular mass m, as

$$J = \rho_g \sqrt{\frac{kT}{2\pi m}}\left(\exp\left[\frac{g_\ell - g_g}{k_B T}\right] - \exp\left[\frac{g_g - g_\ell}{k_B T}\right]\right). \tag{24}$$

This expression is, as we can see, free of any fitting parameters.

Having a flux, we only need an expression for the interfacial area to arrive at an expression for the transferred mass Γ. First, we express the total gas mass M_g in a pipe section of length ΔL as

$$M_g = \rho_g A_g \Delta L = \alpha_g \rho_g A \Delta L, \tag{25}$$

where A_g is the area of the pipe cross section occupied by gas. The time derivative of this quantity is caused by the flux across the interface,

$$\frac{dM_g}{dt} = J A_{int} = J W_{int} \Delta L \tag{26}$$

where A_{int} is the interfacial area in the pipe section, and W_{int} is the width of the interface across the pipe cross-section. By differentiating Eq. (25) with respect to time and using Eq. (7), we get

$$\frac{dM_g}{dt} = \frac{d(\alpha_g \rho_g)}{dt} A \Delta L = \Gamma A \Delta L. \tag{27}$$

The two last equations yield

$$\Gamma = \frac{4 J W_{int}}{\pi D^2}, \tag{28}$$

where we have used that the cross-sectional area of a circular pipe with diameter D is $A = \pi D^2/4$.

When it comes to approximating the interface width W_{int}, a number of considerations have to be made. We wish it to be zero when no mass is left in the *source* phase, but greater than zero when there is no mass in the *receiving* phase. The latter is necessary to allow a start-up of the condensation or evaporation process, even without presence of the phase which receives mass . We may then suggest

$$W_{int} = \begin{cases} 4D(\alpha_g + \delta)\alpha_\ell & \text{if } g_g < g_\ell, \\ 4D\alpha_g(\alpha_\ell + \delta) & \text{if } g_\ell < g_g, \\ 0 & \text{otherwise,} \end{cases} \tag{29}$$

where $\delta \ll 1$ is a tunable *initial volume fraction*, to avoid zero interfacial area when one phase disappears. This factor will only govern the start-up phase of evaporation or condensation, when the volume fraction α_k of the receiving phase is on the order of δ. W_{int} may be looked upon as an approximation of the interfacial width in stratified flow, with $W_{int}(\alpha_g = 0.5) = D + O(\delta)$. Almost all other flow regimes will have a larger interface width.

Inserting the expressions for J and W_{int} from Eqs. (24) and (29) into Eq. (28) yields

$$\Gamma = \begin{cases} \frac{16\rho_g(\alpha_g+\delta)\alpha_\ell}{\pi D} \sqrt{\frac{k_B T}{2\pi m}} \left(\exp\left[\frac{m(\mu_\ell-\mu_g)}{k_B T} \right] - \exp\left[\frac{m(\mu_g-\mu_\ell)}{k_B T} \right] \right) & \text{if } \mu_g < \mu_\ell, \\ \frac{16\rho_g\alpha_g(\alpha_\ell+\delta)}{\pi D} \sqrt{\frac{k_B T}{2\pi m}} \left(\exp\left[\frac{m(\mu_\ell-\mu_g)}{k_B T} \right] - \exp\left[\frac{m(\mu_g-\mu_\ell)}{k_B T} \right] \right) & \text{if } \mu_\ell \le \mu_g, \end{cases} \quad (30)$$

where we have used that $g_k = m\mu_k$ and μ_k is the chemical potential per mass for phase k. Bond [21] notes that the exponents in (30) are small enough to allow a linearizing of the exponential terms. Expanding (30) in powers of $\Delta\mu = \mu_\ell - \mu_g$ then yields

$$\Gamma = \begin{cases} \frac{32\rho_g(\alpha_g+\delta)\alpha_\ell}{\pi D} \sqrt{\frac{m}{2\pi k_B T}}(\mu_\ell - \mu_g) & \text{if } \mu_g < \mu_\ell, \\ \frac{32\rho_g\alpha_g(\alpha_\ell+\delta)}{\pi D} \sqrt{\frac{m}{2\pi k_B T}}(\mu_\ell - \mu_g) & \text{if } \mu_\ell \le \mu_g. \end{cases} \quad (31)$$

In this form, the phase transfer process may be viewed as a relaxation of the difference in chemical potential, $\Delta\mu \equiv \mu_\ell - \mu_g$. Other authors, e.g. Saurel et al. [22] and Stewart and Wendroff [23], have discussed phase transfer models in this form, however without giving an explicit expression for the rate constant, which we have managed to obtain here. The two-phase flow models presented by Bestion [24], Chung et al. [25], Cortes [26], and Toumi [27] also include mass transfer models in different forms, but Toumi [27] points out that his model is not chosen for its physical validity, but rather for its simplicity. We would like to point out the advantage of our model having both a physical basis and an explicit mathematical expression.

4. Equation of state

We choose to use the *stiffened gas* equation of state (EOS), advocated by e.g. Menikoff [28, 29], as our thermodynamic model. The stiffened-gas EOS can be seen as a local linearisation of a more general EOS, and is mathematically similar to the ideal gas EOS, but with stiffening terms to allow for finite density at zero pressure. It has the important advantage of being significantly simpler than most other EOSes, while still being relatively accurate in the vicinity of a chosen reference point.

The pressure, internal energy and chemical potential (for a single phase) are given by

$$p(\rho, T) = \rho(\gamma - 1)c_v T - p_\infty, \quad (32)$$

$$e(\rho, T) = c_v T + \frac{p_\infty}{\rho} + e_*, \quad (33)$$

$$\mu(\rho, T) = \gamma c_v T + e_* - c_v T \ln\left(\frac{T}{T_0} \left(\frac{\rho_0}{\rho} \right)^{\gamma-1} \right) - s_0 T, \quad (34)$$

where the ratio of specific heats is denoted by γ, the specific heat capacity at constant volume by c_v, and the zero point of energy by e_*. The reference temperature, density and entropy are denoted by T_0, ρ_0 and s_0, respectively. Finally, the parameter p_∞ has the effect of "stiffening" the phase, increasing the sound velocity. All these parameters are specific for each phase, which can be fitted using experimental data for a given fluid. Although the stiffened gas equation of state is one of the simplest EOSes available, it is nevertheless complex enough to allow modeling and simulation of a phase transfer process and even analytical expressions for most thermodynamic relations. As the main goal of this work is to demonstrate modeling of phase transfer, the limited range of validity of the stiffened gas EOS is not an important issue. If increased accuracy was required, one could replace the stiffened gas with a more complex EOS.

To write the flux function of the fluid mechanical equations (1)–(4) in terms of the conserved variables, i.e. the mass of each phase, the momentum and the total energy, all per unit volume, we need to express the pressure and temperature as functions of these variables. This may be accomplished using the procedure described by Flåtten, Morin, and Munkejord [30].

5. Numerical method

In order to numerically solve the two-phase flow model (1)–(4), we use a fractional-step method [31, Ch. 17]. In vector notation, the model can be written as

$$\frac{\partial \boldsymbol{q}}{\partial t} + \frac{\partial \boldsymbol{f}(\boldsymbol{q})}{\partial x} = \boldsymbol{s}(\boldsymbol{q}), \tag{35}$$

where $\boldsymbol{q} = [\alpha_g \rho_g, \alpha_\ell \rho_\ell, \rho v, E]^T$ is the vector of conserved variables, $\boldsymbol{f}$ is the flux function and $\boldsymbol{s}$ is the phase transfer source term.

We let Δt be the time step length and denote the numerical solution at $t^n = t_0 + n \Delta t$ by $\boldsymbol{q}^n$. In a simple first-order fractional-step method, often referred to as Godunov splitting, the numerical solution $\boldsymbol{q}^n$ is advanced in time using two steps:

1. Solve the hyperbolic conservation law

$$\frac{\partial \boldsymbol{q}}{\partial t} + \frac{\partial \boldsymbol{f}(\boldsymbol{q})}{\partial x} = 0 \tag{36}$$

    in one time step yielding an intermediate solution $\boldsymbol{q}^*$.
2. Then solve the initial value problem

$$\frac{\partial \boldsymbol{q}}{\partial t} = \boldsymbol{s}(\boldsymbol{q}), \quad t \in [0, \Delta t], \quad \boldsymbol{q}(t = 0) = \boldsymbol{q}^*, \tag{37}$$

    yielding the solution $\boldsymbol{q}^{n+1}$.

The above scheme is first-order accurate in time as long as the numerical schemes used in each sub-step are at least first-order accurate.

One benefit of using a fractional-step method is that the composite problem is divided into sub-problems that are more easily solved by standard methods. The methods used in the sub-problems (36) and (37) are discussed below.

5.1. Hyperbolic part

The hyperbolic part of the fractional-step method (36) can be solved using a finite volume scheme, in which one divides the computational domain into control volumes. These numerical schemes ensures that the physically conserved variables are also conserved numerically. A finite volume scheme for Eq. (36) is obtained by integrating over a control volume, which yields

$$\frac{\mathrm{d} \boldsymbol{Q}_i}{\mathrm{d} t} = -\frac{1}{\Delta x}(\boldsymbol{F}_{i+1/2} - \boldsymbol{F}_{i-1/2}), \tag{38}$$

where $\boldsymbol{Q}_i$ is the average of $\boldsymbol{q}$ in control volume i, and $\boldsymbol{F}_{i+1/2}$ is the numerical flux between control volume i and $i + 1$. Eq. (38) is an ODE which can be solved using e.g. the forward Euler or higher-order Runge-Kutta time-stepping methods. At each cell interface, there is a discontinuity in $\boldsymbol{Q}$ at each time step t^n, and finding the solution for later times ($t > t^n$) is commonly referred to as a Riemann problem.

The multi-stage (MUSTA) approach was first suggested by Toro [32], Titarev and Toro [33], and is based on solving the Riemann problem using a first-order centred scheme on a *local* grid at each cell interface. The solution from the local grid is then used to find the flux in the *global* grid. An advantage with the MUSTA scheme, compared to other Riemann solvers, is that it is relatively simple. We will use the MUSTA 2–2 scheme investigated by Munkejord, Evje, and Flåtten [34] for solving the phase transfer model (1)–(4) and the equilibrium model (9).

To achieve a higher-order method, one can employ the monotone upwind-centred scheme for conservation laws (MUSCL) (see e.g. van Leer [35], Osher [36]), which is based on making a piecewise linear reconstruction using the data $\{\boldsymbol{Q}_i\}$. The allowable slope in each cell is determined by a *slope-limiter* function, of which there are many possible choices. We choose the minmod limiter, which was demonstrated as a good choice by Munkejord, Evje, and Flåtten [34].

5.2. Relaxation ODE

The initial value problem (37) can in principle be solved by a large number of schemes for solving ODEs. In this work we use the first-order backward Euler scheme, given by

$$q^{n+1} = q^* + s(q^{n+1}) \Delta t. \tag{39}$$

The implicit scheme ensures a stable and robust numerical solution, even for stiff problems. The nonlinear equation system (39) was solved using the Newton-Raphson method.

6. Simulation results

In this section, we will present results from simulation of a depressurisation of a pipe of length $L = 80$ m with pure CO_2. As the initial condition at time $t = 0$ s, we have liquid at $p_{0,L} = 60$ bar in the left ($x < 50$ m) part of the pipe, and gas at $p_{0,L} = 10$ bar in the right ($x > 50$ m) part. The temperature is $T_0 = 273$ K ≈ 0 °C, and the fluid is stationary ($v_0 = 0$ m/s). The temperature and pressure at each end is kept constant throughout the simulation. The stiffened gas parameters used are presented in Table 1.

Table 1: Stiffened gas parameters

Phase	γ (dimensionless)	p_∞ (Pa)	c_v (J/kg K)	e_* (J/kg)	s_0 (J/kg K)	ρ_0 (kg/m^3)	T_0 (K)
Gas	1.06	$8.86 \cdot 10^5$	$2.41 \cdot 10^3$	$-3.01 \cdot 10^5$	$1.78 \cdot 10^3$	135	283.13
Liquid	1.23	$1.32 \cdot 10^8$	$2.44 \cdot 10^3$	$-6.23 \cdot 10^5$	$1.09 \cdot 10^3$	861	283.13
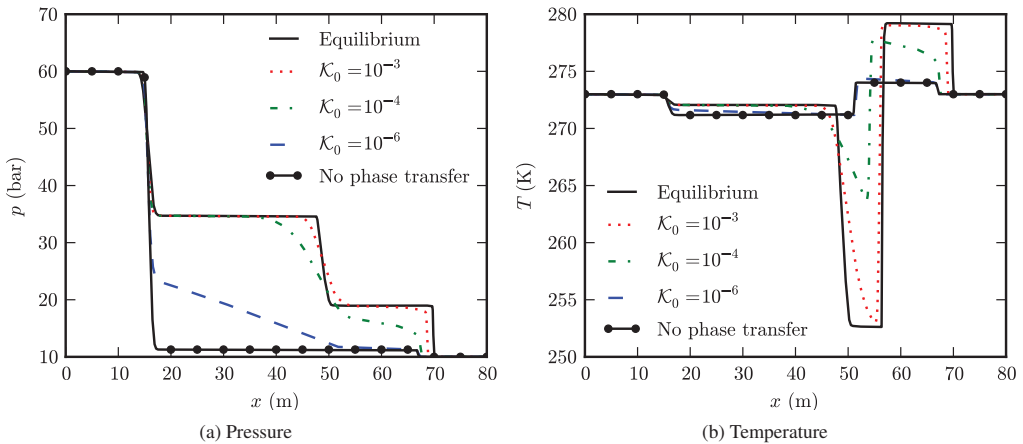
Fig. 1: Simple model, time $t = 0.08$ s. 4000 (solid lines) or 2000 (dotted/dashed lines) cells. CFL number = 0.5.

As time progresses, a rarefaction (decompression) wave will propagate leftward from $x = 50$ m, and a shock wave will propagate to the right. Figure 1 shows the results at time $t = 0.08$ s using the simple model (10), together with those of the equilibrium model (9). As expected, the value of the rate constant $\mathcal{K}_0$ is crucial to the behaviour of the system. Compared to the equilibrium model, the phase transfer model smoothens the solution, approaching the model without phase transfer as $\mathcal{K}_0 \to 0$. Having no information about the physically correct value of $\mathcal{K}_0$, this model offers little in predicting the behaviour of the actual physical system.

In Figure 2, the results at time $t = 0.08$ s for the SRT model are shown. The results are quite similar when changing the initial volume fraction δ, and are quite close to those of the equilibrium model. We note a
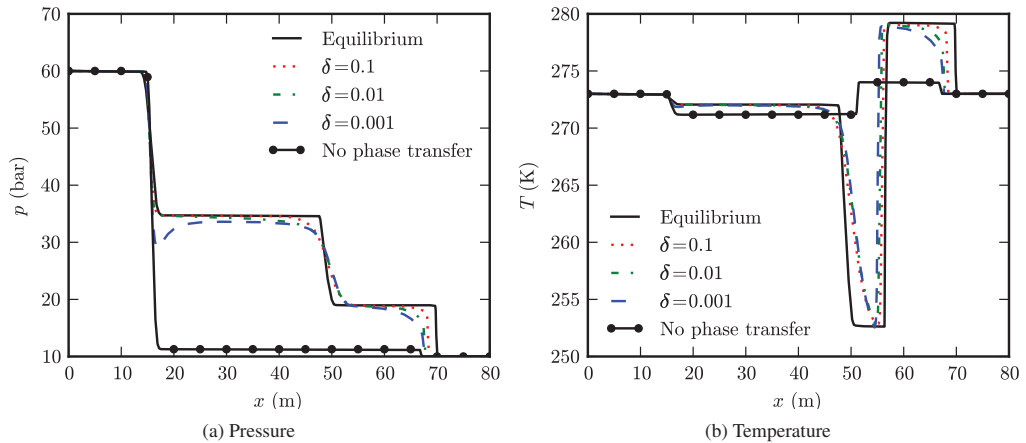
Fig. 2: SRT model, time $t = 0.08$ s. 4000 (solid lines) or 2000 (dotted/dashed lines) cells. CFL number = 0.5.

small dip in the solution for $\delta = 0.001$ at $x \approx 18$ m, which is where the border between the one-phase liquid region and the two-phase region is located. This can explain the dip, since a small initial volume fraction δ will cause a slower start-up of the evaporation. Further to the right ($x > 25$ m) into the two-phase region, we see that the dependence on δ is less pronounced, since we are past the start-up phase in this region.

As with the simple model (10), the discontinuities are smoothened quite a bit compared to the equilibrium model. We remind the reader that the interfacial area used is a lower approximation of what the actual area is. With a larger area, the phase transfer would be more rapid, and the results even closer to the equilibrium model. Hence, our results indicate that pressure and temperature during a depressurisation would be quite close to those of an equilibrium model. However, our model with phase transfer modeled using SRT avoids potential problems caused by discontinuous speed of sound in the equilibrium model, and is also able to capture the dynamics of the phase transfer process in situations where this is crucial.

7. Conclusion

We have presented two phase transfer models: a simple model and a model developed based on statistical rate theory (SRT) capable of describing evaporation and condensation of CO_2. These were combined with a two-phase drift-flux flow model to yield a framework for simulating flow in a pipeline with a two-phase CO_2 mixture. We have presented simulation results for a depressurisation of a pipeline, where the SRT model was used to predict phase transfer in a two-phase mixture flow, and which showed qualitatively very similar behaviour to the equilibrium model. Future comparison with experiments with either water or carbon dioxide will be interesting to validate the model.

Acknowledgement

References

[1] OECD/IEA, Energy Technology Perspectives 2010, 2010.
[2] T. Flåtten, H. Lund, Relaxation Two-Phase Flow Models and the Subcharacteristic Condition, Mathematical Models and Methods in Applied Sciences 21 (12) (2011) 1–29.

[3] T. Flåtten, A. Morin, S. T. Munkejord, Wave propagation in multicomponent flow models, SIAM Journal on Applied Mathematics 70 (8) (2010) 2861–2882.

[4] H. Lund, T. Flåtten, S. T. Munkejord, Depressurization of Carbon Dioxide in Pipelines - Models and Methods, Energy Procedia 4 (2011) 2984–2991.

[5] C. A. Ward, G. Fang, Expression for predicting liquid evaporation flux: Statistical rate theory approach, Phys. Rev. E 59 (1) (1999) 429–440, doi:10.1103/PhysRevE.59.429.

[6] Y.-P. Pao, Application of Kinetic Theory to the Problem of Evaporation and Condensation, Physics of Fluids 14 (2) (1971) 306–312, doi:10.1063/1.1693429, URL http://link.aip.org/link/?PFL/14/306/1.

[7] L. D. Koffman, M. S. Plesset, L. Lees, Theory of evaporation and condensation, Physics of Fluids 27 (4) (1984) 876–880, doi:10.1063/1.864716, URL http://link.aip.org/link/?PFL/27/876/1.

[8] P. Rahimi, C. A. Ward, Kinetics of Evaporation: Statistical Rate Theory Approach, Int. J. of Thermodynamics 8 (2005) 1–14.

[9] C. A. Ward, The rate of gas absorption at a liquid interface, The Journal of Chemical Physics 67 (1) (1977) 229–235, doi:10.1063/1.434547, URL http://link.aip.org/link/?JCP/67/229/1.

[10] C. A. Ward, R. D. Findlay, M. Rizk, Statistical rate theory of interfacial transport. I. Theoretical development, The Journal of Chemical Physics 76 (11) (1982) 5599–5605, doi:10.1063/1.442865, URL http://link.aip.org/link/?JCP/76/5599/1.

[11] M. Dejmek, C. A. Ward, A statistical rate theory study of interface concentration during crystal growth or dissolution, The Journal of Chemical Physics 108 (20) (1998) 8698–8704, doi:10.1063/1.476298, URL http://link.aip.org/link/?JCP/108/8698/1.

[12] S. Azizian, H. Bashiri, H. Iloukhani, Statistical Rate Theory Approach to Kinetics of Competitive Adsorption at the Solid/Solution Interface, Journal of Physical Chemistry C 112 (27) (2008) 10251–10255, doi:10.1021/jp802278e, URL http://pubs.acs.org/doi/abs/10.1021/jp802278e.

[13] W. Rudzinski, W. Plazinski, Kinetics of solute adsorption at solid/solution interfaces: A theoretical development of the empirical pseudo-first and pseudo-second order kinetic rate equations, based on applying the statistical rate theory of interfacial transport, Journal of Physical Chemistry B 110 (33) (2006) 16514–16525, ISSN 1520-6106, doi:10.1021/jp061779n.

[14] J. A. W. Elliott, C. A. Ward, Statistical rate theory description of beam-dosing adsorption kinetics, Journal of Chemical Physics 106 (13) (1997) 5667–5676, ISSN 0021-9606.

[15] R. D. Findlay, C. A. Ward, Statistical Rate Theory of Interfacial Transport. IV. Predicted Rate of Dissociative Adsorption, Journal of Chemical Physics 76 (11) (1982) 5624–5631, ISSN 0021-9606.

[16] J. A. W. Elliott, C. A. Ward, Temperature programmed desorption: A statistical rate theory approach, The Journal of Chemical Physics 106 (13) (1997) 5677–5684, doi:10.1063/1.473588, URL http://link.aip.org/link/?JCP/106/5677/1.

[17] F. Bordi, C. Cametti, A. Motta, Ion Permeation Across Model Lipid Membranes: A Kinetic Approach, The Journal of Physical Chemistry B 104 (22) (2000) 5318–5323, doi:10.1021/jp000005i, URL http://pubs.acs.org/doi/abs/10.1021/jp000005i.

[18] L. B. Harding, A. I. Maergoiz, J. Troe, V. G. Ushakov, Statistical rate theory for the HO + O ⇔ HO$_2$ ⇔ H + O$_2$ reaction system: SACM/CT calculations between 0 and 5000 K, Journal of Chemical Physics 113 (24) (2000) 11019–11034, ISSN 0021-9606.

[19] A. Kapoor, J. A. W. Elliott, Nonideal Statistical Rate Theory Formulation To Predict Evaporation Rates from Equations of State, Journal of Physical Chemistry B 112 (47) (2008) 15005–15013, ISSN 1520-6106, doi:10.1021/jp804982g.

[20] C. A. Ward, D. Stanga, Interfacial conditions during evaporation or condensation of water., Phys Rev E 64 (2001) 051509, ISSN 1539-3755.

[21] M. Bond, Non-Equilibrium Evaporation and Condensation, Master's thesis, University of Victoria, 2004.

[22] R. Saurel, F. Petitpas, R. Abgrall, Modelling phase transition in metastable liquids: application to cavitating and flashing flows, Journal of Fluid Mechanics 607 (2008) 313–350.

[23] H. B. Stewart, B. Wendroff, Two-phase flow: Models and methods, Journal of Computational Physics 56 (1984) 363–409.

[24] D. Bestion, The physical closure laws in the CATHARE code, Nuclear Engineering and Design 124 (1990) 229–245.

[25] M.-S. Chung, K.-S. Chang, S.-J. Lee, Wave propagation in two-phase flow based on a new hyperbolic two-fluid model, Numerical Heat Transfer, Part A 38 (2000) 169–191.

[26] J. Cortes, On the construction of upwind schemes for non-equilibrium transient two-phase flows, Computers & Fluids 31 (2002) 159–182.

[27] I. Toumi, An upwind numerical method for two-fluid two-phase flow models, Nuclear Science and Engineering 123 (1996) 147–168.

[28] R. Menikoff, B. J. Plohr, The Riemann problem for fluid flow of real materials, Rev. Mod. Phys. 61 (1989) 75–130.

[29] R. Menikoff, Empirical equations of state for Solids, Shock Wave Science and Technology Reference Library 2 (2007) 143–188.

[30] T. Flåtten, A. Morin, S. T. Munkejord, On the solution of equilibrium problems for systems of stiffened gases, SIAM Journal on Applied Mathematics 71 (1) (2011) 41–67.

[31] R. J. LeVeque, Finite Volume Methods for Hyperbolic Problems, Cambridge University Press, 2002.

[32] E. F. Toro, Multi-stage predictor-corrector fluxes for hyperbolic equations, Technical Report NI03037-NPA, Isaac Newton Institute for Mathematical Sciences, University of Cambridge, UK, 2003.

[33] V. A. Titarev, E. F. Toro, MUSTA schemes for multi-dimensional hyperbolic systems: analysis and improvements, International Journal for Numerical Methods in Fluids 49 (2005) 117–147.

[34] S. T. Munkejord, S. Evje, T. Flåtten, The multi-stage centred-scheme approach applied to a drift-flux two-phase flow model, International Journal for Numerical Methods in Fluids 52 (6) (2006) 679–705.

[35] B. van Leer, Towards the ultimate conservative difference scheme V. A second order sequel to Godunov's method, Journal of Computational Physics 32 (1) (1979) 101–136.

[36] S. Osher, Convergence of generalized MUSCL schemes, SIAM Journal on Numerical Analysis 22 (5) (1985) 947–961.

Paper L4

Splitting methods for relaxation two-phase flow models

Halvor Lund and Peder Aursand

Splitting methods for relaxation two-phase flow models

H. Lund*

Department of Energy and Process Engineering,
Norwegian University of Science and Technology (NTNU),
NO-7491 Trondheim, Norway
E-mail: halvor.lund@ntnu.no
*Corresponding author

P. Aursand

SINTEF Energy Research,
Sem Sælands vei 11,
NO-7465 Trondheim, Norway
E-mail: peder.aursand@sintef.no

Abstract: A model for two-phase pipeline flow is presented, with evaporation and condensation modelled using a relaxation source term based on statistical rate theory. The model is solved numerically using a Godunov splitting scheme, making it possible to solve the hyperbolic fluid-mechanic equation system and the relaxation term separately. The hyperbolic equation system is solved using the multi-stage (MUSTA) finite volume scheme. The stiff relaxation term is solved using two approaches: one based on the Backward Euler method, and one using a time-asymptotic scheme. The results from these two methods are presented and compared for a CO_2 pipeline depressurisation case.

Keywords: hyperbolic conservation laws; relaxation; splitting methods; phase transfer; exponential integrator; two-phase flow; statistical rate theory.

Biographical notes: H. Lund achieved his Master of Science degree in Physics from the Norwegian University of Science and Technology (NTNU) in Trondheim, Norway in 2009. Since 2010, he has been employed as a PhD candidate at NTNU, working with fluid-mechanical and thermodynamical modelling and numerics for two-phase flow of CO_2 in pipelines.

P. Aursand achieved his Master of Science degree in Physics from the Norwegian University of Science and Technology (NTNU) in Trondheim, Norway in 2011. Since 2012, he has been employed as a PhD candidate in Applied Mathematics at NTNU, working with non-linear wave equations.

1   Introduction

Two-phase flow is present in many industrial situations, such as heat exchangers, oil and gas production, CO_2 transport and storage, and in the nuclear industry. Modelling of such flows is known to be a challenging task, much due to the possibly complex behaviour of the interface in different flow regimes, and interaction between the phases occurring at this interface, for example heat or mass transfer or interface friction.

If the precise shape of the interface is of little interest or too computationally expensive to calculate, one can apply *averaging* of the physical quantities over a certain area or volume. This typically leads to systems of hyperbolic balance laws for mass, momentum and energy. Transfer of heat, mass and momentum between the two phases can then be modelled in the form of source terms in these balance equations. This paper will focus on the modelling and numerical solution of a mass transfer term which models evaporation and condensation between the liquid and gas phase. Evaporation of liquid in a pipeline will cause potentially large temperature drops, rendering the pipe steel brittle and vulnerable to rupture, and is therefore crucial to predict. Relaxation source terms for mass may be stiff, i.e., the time scales associated with the relaxation process might be significantly shorter than those of the hyperbolic flux term in the fluid-dynamical model. A stiff source term requires careful numerical treatment to avoid instabilities. One method to accomplish this, is to use a fractional-step (or splitting) method, which divides the problem into two parts: The hyperbolic (homogeneous) conservation equations and the source term. These two parts can then be solved separately using methods well suited for each part.

The paper is organised as follows: The first section presents the models needed to describe the fluid-mechanical behaviour as well as the mass transfer. Then the numerical methods for solving these models are described, where the splitting procedure is outlined, followed by methods for solving the hyperbolic fluid-mechanical conservation laws and the mass transfer source term separately. Numerical results for a CO_2 pipeline depressurisation case are presented, and the results for two different numerical methods are compared. Finally, the work is summarised and possible further work is outlined.

2   Models

To construct a model for two-phase flow with phase transfer, one needs a fluid-mechanical model, a model to describe the phase transfer, and a thermo-dynamic model or equation of state (EOS). In the following, each of these models will be presented.

2.1 Fluid-mechanical model

Fluid-mechanical models for two-phase flow are often averaged over a certain area or volume to reduce the computational cost and remove the need to explicitly model the location of the gas-liquid interface. Such averaged models are typically formulated as hyperbolic equation systems for mass, momentum and energy. In order to focus on the effect of the numerical solution of the phase transfer model, it is desirable to use a fluid-mechanical model which is as simple as possible. In this paper, a four-equation homogeneous flow model is chosen, with one mass balance (continuity) equation for each phase, together with equations for conservation of total momentum and energy,

$$\frac{\partial(\alpha_\mathrm{g}\rho_\mathrm{g})}{\partial t} + \frac{\partial(\alpha_\mathrm{g}\rho_\mathrm{g}v)}{\partial x} = \Gamma, \tag{1}$$

$$\frac{\partial(\alpha_\ell\rho_\ell)}{\partial t} + \frac{\partial(\alpha_\ell\rho_\ell v)}{\partial x} = -\Gamma, \tag{2}$$

$$\frac{\partial(\rho v)}{\partial t} + \frac{\partial(\rho v^2 + p)}{\partial x} = 0, \tag{3}$$

$$\frac{\partial E}{\partial t} + \frac{\partial[(E + p)v]}{\partial x} = 0, \tag{4}$$

where α_k is the volume fraction and ρ_k is the density of phase k, where k is g (gas) or ℓ (liquid). The mixture density is $\rho = \alpha_\mathrm{g}\rho_\mathrm{g} + \alpha_\ell\rho_\ell$, and the mixture energy is $E = \alpha_\mathrm{g}\rho_\mathrm{g}e_\mathrm{g} + \alpha_\ell\rho_\ell e_\ell + \frac{1}{2}\rho v^2$, where e_k is the internal energy of phase k. This model could be argued to be the simplest possible pipe flow model which still incorporates a phase-transfer term. Flåtten et al. (2010) (among others) have analysed this model in the frozen-phase limit $\Gamma = 0$. To close the model, it is assumed that the two phases have equal pressures p, temperatures T and velocities v. The phase transfer appears as a source term, Γ, in the mass balance equations (1) and (2).

2.2 Phase transfer model

Modelling phase transfer between gas and liquid can be done using a variety of different approaches, and there does not seem to exist a universally correct one. Among the most common are kinetic theory, non-equilibrium (irreversible) thermodynamics and statistical rate theory (SRT). The latter is a rather newly suggested approach based on statistical mechanics, and was first introduced by Ward et al. (1982) and later applied to modelling of liquid evaporation (Ward and Fang, 1999). One of the main reasons for the development of SRT was to be able to explain the anomalous temperature profiles found close to an evaporation interface (Pao, 1971). SRT assumes that interfacial transport processes, on a microscopical level, are caused by single molecular events. The probability of each event is calculated using a first-order perturbation analysis of the Schrödinger equation, together with the Boltzmann definition of entropy. Since its introduction by by Ward et al. (1982), SRT has been used to model a number of different transport processes, including crystal growth (Dejmek and Ward, 1998), solution/solid adsorption (Azizian et al., 2008; Rudzinski and Plazinski, 2006), gas/solid adsorption (Elliott and Ward, 1997a; Findlay and Ward, 1982), temperature programmed desorption (Elliott and Ward, 1997b), ion permeation across lipid membranes (Bordi et al., 2000), chemical reactions (Harding et al., 2000), and evaporation and condensation (Ward and Fang, 1999; Kapoor and Elliott, 2008; Ward and Stanga, 2001).

Lund and Aursand (2012) developed an explicit expression for the phase transfer source term Γ in equations (1) and (2) based on SRT, following an approach similar to that of Ward et al. (1982) and Ward and Fang (1999). They found an interfacial flux per area expressed as

$$J = \rho_{\mathrm{g}} \sqrt{\frac{k_{\mathrm{B}}T}{2\pi m}} \left(\exp\left[\frac{m(\mu_\ell - \mu_{\mathrm{g}})}{k_{\mathrm{B}}T} \right] - \exp\left[\frac{m(\mu_{\mathrm{g}} - \mu_\ell)}{k_{\mathrm{B}}T} \right] \right), \tag{5}$$

where m is the molecular mass and k_{B} the Boltzmann constant. The chemical potential per mass of phase k is denoted μ_k. This flux has the important property that it reduces to zero when the chemical potentials are equal, as expected. An advantage with the SRT approach, is that it is able to yield an explicit expression without any parameters that need tuning, as seen in equation (5). Other methods are often dependent on parameters which need to be empirically determined.

One also needs to approximate the interfacial area across which the flux J flows. Since the fluid-mechanical model is an averaged model, one has little information about the precise shape of the interface. Hence it is assumed that the flow is stratified-like, and that the interfacial area can be approximated by (Lund and Aursand, 2012)

$$A_{\mathrm{int}} = \begin{cases} 4DL(\alpha_{\mathrm{g}} + \delta)\alpha_\ell & \text{if } \mu_{\mathrm{g}} < \mu_\ell, \\ 4DL\alpha_{\mathrm{g}}(\alpha_\ell + \delta) & \text{if } \mu_{\mathrm{g}} \geq \mu_\ell, \end{cases} \tag{6}$$

where D is the diameter of the pipe and L is the length of the interface in x-direction. The term δ is a tunable *initial volume fraction* which ensures that the evaporation or condensation can start even when the mass-receiving phase has zero volume fraction. To ensure that this term only has a small effect, it should be kept smaller than typical volume fraction values, so $\delta \ll 1$.

With the given flux (5) and interfacial area (6), one finds the following expression for the phase transfer source term in equations (1) and (2) (Lund and Aursand, 2012):

$$\Gamma = \begin{cases} \frac{32\rho_{\mathrm{g}}(\alpha_{\mathrm{g}} + \delta)\alpha_\ell}{\pi D} \sqrt{\frac{m}{2\pi k_{\mathrm{B}}T}}(\mu_\ell - \mu_{\mathrm{g}}) & \text{if } \mu_{\mathrm{g}} < \mu_\ell, \\ \frac{32\rho_{\mathrm{g}}\alpha_{\mathrm{g}}(\alpha_\ell + \delta)}{\pi D} \sqrt{\frac{m}{2\pi k_{\mathrm{B}}T}}(\mu_\ell - \mu_{\mathrm{g}}) & \text{if } \mu_\ell \leq \mu_{\mathrm{g}}, \end{cases} \tag{7}$$

where the exponentials have been expanded to first order in $\mu_{\mathrm{g}} - \mu_\ell$. This model has the advantage of having an explicit mathematical expression, as well as being based on well-established physics principles such as statistical mechanics. Models in a similar form, with the phase transfer rate proportional to the difference in chemical potential, have also been used by a number of other authors, including Saurel et al. (2008) and Stewart and Wendroff (1984).

2.3   Equation of state

In this paper, the stiffened gas EOS (see, e.g., Menikoff and Plohr, 1989) is used, which has the advantage of allowing analytical expressions for most thermodynamic relations, while still being sophisticated enough to give reasonable results for a certain range of pressures and temperatures. It can essentially be seen as an ideal gas with a

stiffening term, p_∞, which allows a non-zero density at zero pressure, making it suitable to model liquids as well as gases. The pressure, internal energy and chemical potential in a stiffened gas are given by

$$p(\rho, T) = \rho(\gamma - 1)c_v T - p_\infty, \tag{8}$$

$$e(\rho, T) = c_v T + \frac{p_\infty}{\rho} + e_*, \tag{9}$$

$$\mu(\rho, T) = \gamma c_v T + e_* - c_v T \ln\left(\frac{T}{T_0}\left(\frac{\rho_0}{\rho}\right)^{\gamma-1}\right) - s_0 T, \tag{10}$$

where γ is the ratio of specific heats, c_v is the heat capacity at constant volume and e_* is the zero point of energy. The reference temperature, density and entropy are denoted T_0, ρ_0 and s_0, respectively. Each phase has its own set of parameters, which can be fitted to experimental values.

3 Numerics

The fluid-mechanical equation system (1) to (4) can be compactly formulated as

$$\frac{\partial \boldsymbol{q}}{\partial t} + \frac{\partial \boldsymbol{f}(\boldsymbol{q})}{\partial x} = \boldsymbol{s}(\boldsymbol{q}), \tag{11}$$

where $\boldsymbol{q} = [\alpha_g \rho_g, \alpha_\ell \rho_\ell, \rho v, E]$, $\boldsymbol{f}(\boldsymbol{q})$ is the flux function and $\boldsymbol{s}(\boldsymbol{q})$ is the source term. There typically exist well-developed methods for solving homogeneous equation systems, i.e., with $\boldsymbol{s} = 0$. However, if the source term is stiff, problems relating to stability may arise. Therefore, equation (11) will be solved using a first-order fractional-step method known as Godunov splitting [LeVeque, (2002), Ch. 17]. This advances the solution $\boldsymbol{q}^n$ from time t_n to time $t_{n+1} = t_n + \Delta t$ using two steps:

1 Solve the hyperbolic homogeneous conservation law given by

$$\frac{\partial \boldsymbol{q}}{\partial t} + \frac{\partial \boldsymbol{f}(\boldsymbol{q})}{\partial x} = 0, \qquad t \in [t_n, t_{n+1}], \qquad \boldsymbol{q}(t_n) = \boldsymbol{q}^n, \tag{12}$$

yielding an intermediate solution $\boldsymbol{q}^*$.

2 Solve the ordinary differential equation given by

$$\frac{\mathrm{d}\boldsymbol{q}}{\mathrm{d}t} = \boldsymbol{s}(\boldsymbol{q}), \qquad t \in [t_n, t_{n+1}], \qquad \boldsymbol{q}(t_n) = \boldsymbol{q}^*, \tag{13}$$

giving the solution at time t_{n+1}.

This method will be first-order accurate in time as long as each of the two steps are at least first-order accurate in time. With such a fractional-step (splitting) scheme, one can employ efficient, accurate and stable numerical methods in each step, constructed specifically for each part of the problem.

Higher-order accurate fractional-step methods can be derived, an example being the second order Strang (1968) splitting. Schemes of even higher order exist, but are often subject to stability issues. Moreover, as shown by Jin (1995), higher order splitting schemes can reduce to first-order accuracy in the stiff limit.

In this work first-order splitting will be considered, and in the following methods for solving equations (12) and (13) will be described.

3.1 Hyperbolic conservation law

As fluid-mechanical models typically are formulated as conservation laws, as is the case with equation (12), they are often solved using finite volume methods, which ensure that the physically conserved variables are also conserved numerically. By integrating equation (12) over a control volume i, one gets

$$\frac{\mathrm{d}Q_i}{\mathrm{d}t} = -\frac{1}{\Delta x}(F_{i+1/2} - F_{i-1/2}),\tag{14}$$

where Δx is the control volume size, Q_i is the average of the conserved variable q over control volume i, while $F_{i+1/2}$ is the numerical flux between control volumes i and $i+1$, which should approximate the exact flux at the interface,

$$F_{i+1/2} \approx f(q(x_{i+1/2}, t)).\tag{15}$$

As expected from a conserving scheme, the quantity Q_i is only changed due to fluxes in and out of the control volume. The challenge now lies in approximating the fluxes $\{F_{i+1/2}\}$ at the control volume interfaces, knowing only the control volume averages $\{Q_i\}$. This can be visualised as a discontinuity in Q at each interface at time t_n, and solving for later times is known as solving a Riemann problem.

There exists a number of different finite volume schemes to calculate the numerical fluxes in equation (14), and one can, in general, divide these into two groups: upwind schemes and centred schemes. Upwind schemes have the advantage that they take into account how waves propagate in the original equation system, so that each cell is only affected by information in the cells from where the waves are coming, hence the term *upwind*. One of the most well-known schemes of this type is Roe's (1981) approximate Riemann solver. The centred schemes, on the other hand, have no concept of waves and treat information in both directions equally, hence the term *centred*.

Although the upwind schemes typically perform better for, e.g., discontinuities, a centred scheme will be used in this paper, which has the advantage of being robust and easy to derive. The multi-stage (MUSTA) centred scheme was first proposed by Toro (2003), and is based on solving the Riemann problem at each interface by introducing a local grid and local time stepping. This method can be divided into the following three steps, which are also illustrated in Figure 1.

1   at each cell interface, define a local grid with $2N$ cells

2   do M time steps in each local grid, using a first-order centred FORCE flux

3   use the fluxes from the local grids as fluxes in the original grid.

To calculate the fluxes in the local grid, a first-order centred scheme known as FORCE will be used. This flux is given by (Toro, 1999)

$$F_{j+1/2}^{\mathrm{FORCE}} = \frac{1}{2}(F_{j+1/2}^{\mathrm{LF}} + F_{j+1/2}^{\mathrm{Ri}}),\tag{16}$$

where $F_{j+1/2}^{\mathrm{LF}}$ is the Lax-Friedrichs flux

$$F_{j+1/2}^{\mathrm{LF}} = \frac{1}{2}(f(Q_j) + f(Q_{j+1})) - \frac{\Delta x}{2\Delta t_{\mathrm{loc}}}(Q_{j+1} - Q_j),\tag{17}$$

and $\boldsymbol{F}^{\mathrm{Ri}}_{j+1/2}$ is the Richtmyer flux. It is computed by first defining an intermediate state

$$\boldsymbol{Q}^{\mathrm{Ri}}_{j+1/2} = \frac{1}{2}(\boldsymbol{Q}_j + \boldsymbol{Q}_{j+1}) - \frac{\Delta t_{\mathrm{loc}}}{2\Delta x}(\boldsymbol{f}(\boldsymbol{Q}_{j+1}) - \boldsymbol{f}(\boldsymbol{Q}_j)), \qquad (18)$$

and then setting the flux to

$$\boldsymbol{F}^{\mathrm{Ri}}_{j+1/2} = \boldsymbol{f}(\boldsymbol{Q}^{\mathrm{Ri}}_{j+1/2}). \qquad (19)$$

With the FORCE flux (16), one can then perform time steps on the local grid using a finite volume scheme in a form equivalent to equation (14). The time step used in the local grid is calculated using a *local* CFL criterion, given by

$$\Delta t_{\mathrm{loc}} = \frac{C_{\mathrm{loc}}\Delta x}{\max_{1\leq j\leq 2N}\left(\max_{1\leq p\leq d}|\lambda^p_j|\right)},$$

where $C_{\mathrm{loc}} \in (0,1)$ is the local CFL number. λ^p_j is the pth eigenvalue of the Jacobian $\partial_{\boldsymbol{q}}\boldsymbol{f}(\boldsymbol{q})$ at grid point j. The denominator is simply the largest absolute eigenvalue in the local grid.

Figure 1 Illustration of the steps in the MUSTA method for *one* interface, between control volumes i and $i+1$
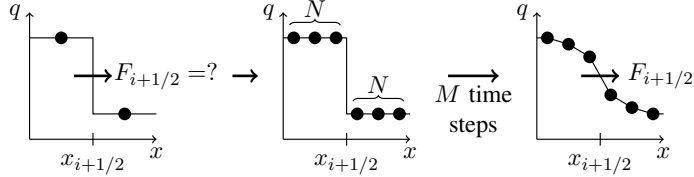
Before each time step, extrapolation boundary conditions are applied, $\boldsymbol{Q}^m_0 = \boldsymbol{Q}^m_1$ and $\boldsymbol{Q}^m_{2N+1} = \boldsymbol{Q}^m_{2N}$, where the superscript m denotes the mth time step. After the Mth time step, one has found the flux to use in the global grid, namely $\boldsymbol{F}^M_{N+1/2}$. Summarised, the local time steps at each control volume interface are performed as follows (Titarev and Toro, 2005):

1 compute fluxes using equation (16)

2 if $m = M$, then return flux $\boldsymbol{F}^M_{N+1/2}$ to be used in global grid

3 apply extrapolation boundary conditions: $\boldsymbol{Q}^m_0 = \boldsymbol{Q}^m_1$ and $\boldsymbol{Q}^m_{2N+1} = \boldsymbol{Q}^m_{2N}$

4 update solution forward in time using a local finite volume scheme similar to equation (14), with the FORCE flux (16), for $j \in \{1, 2, ..., 2N\}$

5 increase m by one and repeat from step 1.

In the numerical simulations presented in the numerical results section, a MUSTA 2-2 method ($M = N = 2$) will be used, with four local grid cells and two local time steps, similar to the one described by Munkejord et al. (2006).

3.2   Relaxation ODE

The second part of the splitting scheme concerns the relaxation term, formulated as the ODE

$$\frac{\mathrm{d}\boldsymbol{q}}{\mathrm{d}t} = \boldsymbol{s}(\boldsymbol{q}), \qquad t \in [0, \Delta t], \qquad \boldsymbol{q}(t = 0) = \boldsymbol{q}^*. \tag{20}$$

When the time scales of the relaxation process (20) become significantly smaller than the time scales of the hyperbolic conservation law (12), one is dealing with a stiff relaxation system. For efficiency and simplicity, it is often of interest to resolve the solution at time scales comparable with those of the conservation law. However, doing so in a robust manner requires an ODE solver for equation (20) with good stability properties. In particular, there is a risk of *overshooting* the equilibrium point $\boldsymbol{q}^{\mathrm{eq}}$ defined by

$$\boldsymbol{s}(\boldsymbol{q}^{\mathrm{eq}}) = 0, \tag{21}$$

in the ODE step of the fractional-step method, due to large time steps Δt.

3.2.1   Backward Euler

For first-order accuracy, an obvious choice for solving the system (20) is the implicit Backward Euler scheme, given by

$$\boldsymbol{q}^{n+1} = \boldsymbol{q}^* + \boldsymbol{s}(\boldsymbol{q}^{n+1}). \tag{22}$$

An ODE is referred to as *component-wise monotonic* if it fulfils

$$s_i(q_i) \left(q_i^{\mathrm{eq}} - q_i \right) > 0 \quad \forall q_i \neq q_i^{\mathrm{eq}}. \tag{23}$$

The relaxation ODE under consideration in this work is of this type, and it is easy to verify that for such ODEs the backward Euler scheme will be stable in the sense that the solution to (22) will not overshoot an equilibrium point (Aursand et al., 2010). However, it should be emphasised that obtaining this solution requires solving a non-linear system of equation (22) by an iterative scheme such as the Newton-Raphson method. Instabilities can still occur if the non-linear solver fails to correctly solve this system.

3.2.2 Asymptotic integration

A popular approach towards solving stiff systems in the form (20) has been the use of exponential integrators (Hochbruck et al., 1998; Cox and Matthews, 2002). The basic idea is that one gets rid of stability restrictions on the time step by approximating the stiff component of the solution as an exponential function. Recently, exponential methods tailored for relaxation systems have been proposed (Aursand et al., 2010). The first order method, referred to as ASY1, is given by

$$q_i^{n+1} = q_i^* + (q_i^{\text{eq}} - q_i^*)\left[1 - \exp\left(-\frac{\Delta t}{\tau_i}\right)\right], \tag{24}$$

where q^{eq} is the equilibrium state and

$$\tau_i = \frac{q_i^{\text{eq}} - q_i^*}{s_i(q^*)}. \tag{25}$$

The scheme (24) and (25) is unconditionally stable by construction – the numerical solution will decay exponentially to the equilibrium solution. However, the scheme requires a priori knowledge of the equilibrium state. The trade-off when using the ASY1 scheme as opposed to the Backward Euler scheme, is solving an equilibrium problem instead of an implicit numerical discretisation. Depending on the system, calculating the equilibrium state q^{eq} corresponding to an initial state q can be either trivial or very cumbersome. In the following, it will be discussed how to calculate the equilibrium state for the system (1) to (4).

When mass is moved from one phase to the other, total mass and energy are always conserved, as seen from equation (4), and by adding equations (1) and (2). Thus, to calculate the equilibrium state for the mass transfer process, one needs to find the pressure p and temperature T as functions of the mixture density ρ and internal energy $E_{\text{int}} = \alpha_{\text{g}}\rho_{\text{g}}e_{\text{g}} + \alpha_{\ell}\rho_{\ell}e_{\ell}$, such that $\mu_{\text{g}} = \mu_{\ell}$. This corresponds to finding the boiling point for the given mixture density and internal energy.

In order to accomplish this, two nested Newton-Raphson algorithms were used. The algorithm may be briefly summarised as follows:

1 Guess a pressure p.

2 Find boiling point T_{boil} by solving $f_1(T_{\text{boil}}) = \mu_{\text{g}}(p, T_{\text{boil}}) - \mu_{\ell}(p, T_{\text{boil}}) = 0$ using the Newton-Raphson method,

$$T_{\text{boil}}^{n+1} = T_{\text{boil}}^n - \frac{f_1(T_{\text{boil}})}{f_1'(T_{\text{boil}})}. \tag{26}$$

For stiffened gas, the relevant expressions are then found from Eqs. (8) and (10),

$$\mu_k(p, T) = \gamma_k c_{v,k} T + e_{*,k} - c_{v,k} T \ln\left(\frac{T}{T_{0,k}}\left(\frac{\rho_{0,k}(\gamma_k - 1)c_{v,k}T}{p + p_{\infty,k}}\right)^{\gamma_k - 1}\right) \tag{27}$$
$$- s_{0,k}T,$$

$$\left(\frac{\partial\mu_k}{\partial T}\right)_p = \frac{\mu_k - e_{*,k}}{T} - \gamma_k c_{v,k}, \tag{28}$$

where the subscript k denotes a quantity of phase k.

3   Solve

$$f_2(p) = \rho_{\mathrm{g}}(\rho - \rho_\ell)e_{\mathrm{g}} + \rho_\ell(\rho_{\mathrm{g}} - \rho)e_\ell - (\rho_{\mathrm{g}} - \rho_\ell)E_{\mathrm{int}} = 0$$

for pressure p using a Newton-Raphson method, evaluated at $T = T_{\mathrm{boil}}$. The method requires the derivative of f_2, which for stiffened gas is given by

$$\begin{aligned}
\frac{\partial f_2}{\partial p} =\ & \left((\rho - \rho_\ell)e_{\mathrm{g}} + \rho_\ell e_\ell + \frac{p}{\rho_{\mathrm{g}}}(\rho - \rho_\ell) - E\right)\left(-\frac{\rho_{\mathrm{g}}}{T}\frac{\rho_\ell - \rho_{\mathrm{g}}}{\rho_{\mathrm{g}}\rho_\ell(s_{\mathrm{g}} - s_\ell)} + \frac{1}{c_{v,\mathrm{g}}T(\gamma_{\mathrm{g}} - 1)}\right) \\
& - \left((\rho - \rho_{\mathrm{g}})e_\ell + \rho_{\mathrm{g}}e_{\mathrm{g}} + \frac{p}{\rho_\ell}(\rho - \rho_{\mathrm{g}}) - E\right) \\
& \quad \left(-\frac{\rho_\ell}{T}\frac{\rho_\ell - \rho_{\mathrm{g}}}{\rho_{\mathrm{g}}\rho_\ell(s_{\mathrm{g}} - s_\ell)} + \frac{1}{c_{v,\ell}T(\gamma_\ell - 1)}\right) \\
& + \rho_{\mathrm{g}}(\rho - \rho_\ell)\left(\gamma c_{v,\mathrm{g}}\frac{\rho_\ell - \rho_{\mathrm{g}}}{\rho_{\mathrm{g}}\rho_\ell(s_{\mathrm{g}} - s_\ell)}\right) \\
& - \rho_\ell(\rho - \rho_{\mathrm{g}})\left(\gamma c_{v,\ell}\frac{\rho_\ell - \rho_{\mathrm{g}}}{\rho_{\mathrm{g}}\rho_\ell(s_{\mathrm{g}} - s_\ell)}\right) + (\rho_{\mathrm{g}} - \rho_\ell),
\end{aligned} \tag{29}$$

where $s_k = \frac{1}{T}(e + \frac{p}{\rho} - \mu)$ is the entropy of phase k.

4   Go to step 2 until $\mu_{\mathrm{g}} - \mu_\ell$ is less than some chosen error limit.

For the present model, both the Backward Euler and ASY1 schemes require solving an iterative problem in each computational step. The relative stability and efficiency of these two schemes thus hinge on the stability and efficiency obtainable in their respective iterative schemes.

4   Numerical results

This section will present results for depressurisation of a pipe with pure CO_2. The pipe has a length of $L = 100$ m, but for the sake of clearer plots, only the part $x \in [0, 80]$ will be shown. It is initially filled with liquid CO_2 at a pressure of $p = 60$ bar in the left part ($x \leq 50$ m) and gas at 10 bar in the right part ($x > 50$ m). The parameters used for the stiffened gas EOS are shown in Table 1. The CFL number used was $C = 0.5$, while the initial volume fraction was $\delta = 0.01$. This case was also used by Lund and Aursand (2012), but in the present paper more focus is put on the results of different numerical methods.

Table 1 Stiffened gas parameters used in the simulation

Phase	γ (–)	p_∞ (Pa)	c_v (J/kg K)	e_* (J/kg)	s_0 (J/kg K)	ρ_0 (kg/m³)	T_0 (K)
Gas	1.06	$8.86 \cdot 10^5$	$2.41 \cdot 10^3$	$-3.01 \cdot 10^5$	$1.78 \cdot 10^3$	135	283.13
Liquid	1.23	$1.32 \cdot 10^8$	$2.44 \cdot 10^3$	$-6.23 \cdot 10^5$	$1.09 \cdot 10^3$	861	283.13

As time progresses, pressure waves will propagate to the left and right through the liquid and gas, respectively. Between these two pressure fronts, phase transfer in the form of evaporation and condensation will take place. Figure 2 shows the pressure after time $t = 0.08$ s, comparing the solutions using the ASY1 method and the Backward Euler method to a reference solution. The reference solution was obtained using a second order method and a very fine grid. In this reference solution, to the left of the front at $x \approx 16$ m, there is pure liquid, while there is pure gas to the right of $x \approx 55$ m.

Figure 2 Pressure at time $t = 0.08$ s
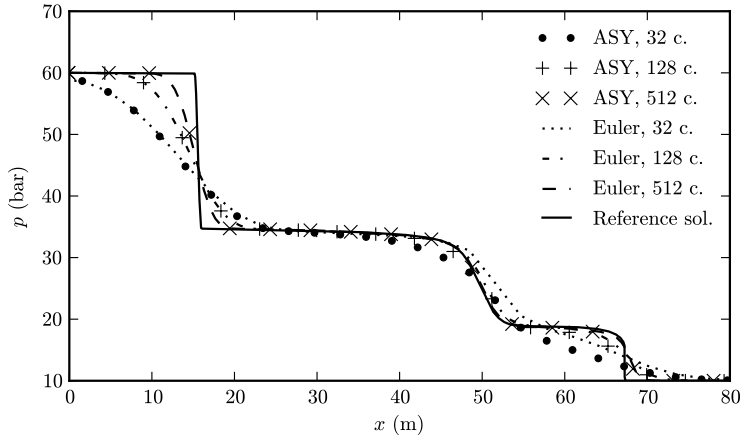
From Figure 2, one can see that the two methods have very similar results with equal grid size. In the right part of the plot, we see that ASY1 is slightly more diffusive than the Backward Euler method with 32 grid cells. This difference between the two methods is perhaps even clearer in Figure 3, which shows the temperature for the same case. The temperature dip around $x \approx 55$ m is seen to be much clearer with the Backward Euler method than the ASY1 method, especially with the coarsest grids.

Figure 3 Temperature at time $t = 0.08$ s
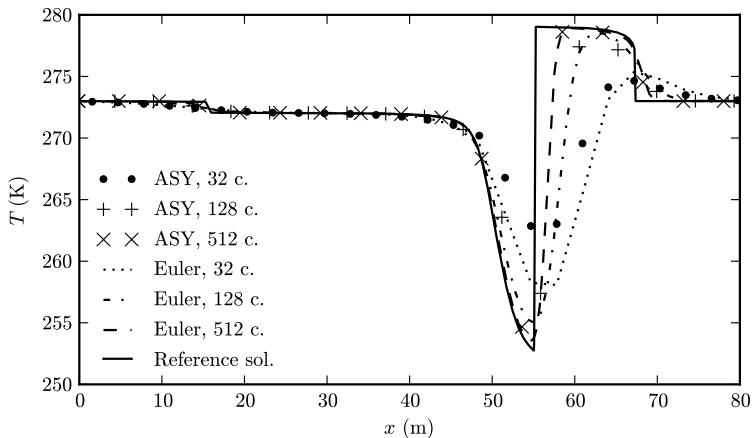
Finally, Figure 4 shows the volume fraction at the same time. One can notice that the dip in temperature seen in Figure 3 coincides with the abrupt change in volume fraction. To the left of this point, temperature drops due to evaporation of the liquid. Since the central MUSTA scheme was used, one can not expect such discontinuities to be properly resolved on coarse grids. A Roe solver is often more suitable for cases where discontinuities are dominant. Morin et al. (2009) has developed a Roe scheme for an equation system in the form presented in equations (1) to (4), in the homogeneous case where $\Gamma = 0$.

Figure 4   Gas volume fraction at time $t = 0.08$ s
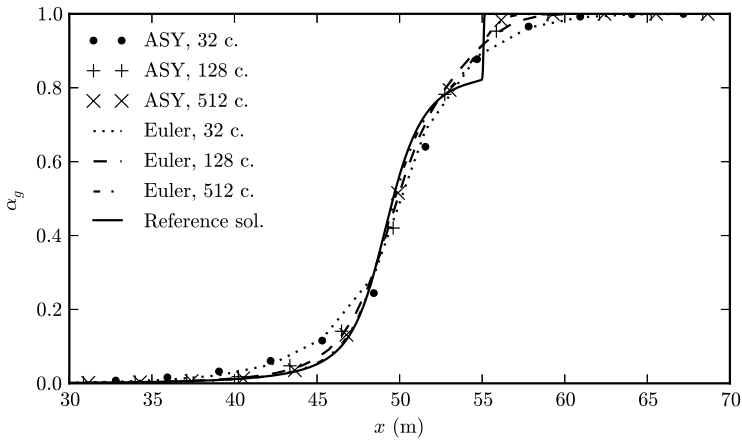
Note: The graph only shows a part of the domain, $x \in [30, 70]$.

Table 2 shows the computational time spent for a range of different grid sizes, to give an impression of how the computational cost for the two methods are related. As seen in this table, the time spent is rather similar for the same grid size, although the ASY1 scheme seems to have slightly better performance. It can be noted that the computational cost for the ASY1 method comes from calculating the equilibrium state, while the cost in the Backward Euler method is due to a Newton-Raphson iteration in the numeric scheme (22) itself. The cost for these two approaches may vary with different formulations of the source term than the one we have presented here, as it in some cases is possible to calculate the equilibrium state relatively cheap, in which case the ASY1 scheme would be expected to outperform the Backward Euler scheme.

In the present case, the equation $\mu_g = \mu_\ell$ must be solved to find the equilibrium state, which has to be done numerically due to logarithms in the expression for μ, see equation (27). Say, for example, that the relaxation process in question was instead a heat transfer process, where the equilibrium state is given by $T_g = T_\ell$. This equation could, at least for the stiffened gas EOS, be solved exactly without the use of a numerical scheme, thus decreasing the computational cost of the ASY1 scheme. Therefore one can expect the ASY1 scheme to have advantages over the Backward

Euler method for other cases than the one presented here. However, for the present case, there does not seem to be any reasons to prefer one in front of the other, since the methods produce similar results at similar computational cost.

Table 2 Computational time (in seconds) on a single Intel Core2 at 2.8 GHz for a range of different grid sizes

Grid size	ASY1	Euler
512	6.23	7.15
1,024	24.45	27.78
2,048	99.26	110.71
4,096	389.56	442.50

A final point worth making, is that the presented method is able to handle regions with volume fractions α_k of exactly zero. For other numerical methods found in the literature, it is often necessary to have non-zero volume fractions to avoid numerical instabilities (Munkejord et al., 2009; Chang and Liou, 2007). Chang and Liou (2007) report that numerical errors may be amplified when one phase disappears, leading to instabilities. The present approach has not shown to exhibit any issues related to a vanishing volume fraction.

5 Conclusions

A two-phase flow model has been presented, with phase transfer modelled using a relaxation term based on SRT. This model was solved using a first-order Godunov splitting scheme, making it possible to solve the hyperbolic equation system and the phase transfer model separately. The homogeneous hyperbolic equation system was solved using a central MUSTA scheme. Results for two different approaches to solving the phase transfer numerically were presented, one based on the Backward Euler method and one on the time-asymptotic ASY1 scheme. The ASY1 scheme has the advantage of being explicit if only the equilibrium state is known. However, with the particular model considered here, calculating the equilibrium state is done iteratively, which gives the ASY1 method similar performance to the Backward Euler method when it comes to accuracy and computational cost. In future work, one could apply the scheme to cases with an easier to compute equilibrium value, as well as investigate whether a second-order splitting scheme is beneficial when solving models similar to the one presented here.

References

Aursand, P., Evje, S., Flåtten, T., Giljarhus, K.E.T. and Munkejord, S.T. (2010) 'An exponential time-differencing method for monotonic relaxation systems', preprint [online] http://www.math.ntnu.no/conservation/2011/008.pdf (accessed 01/28/2013).

Azizian, S., Bashiri, H. and Iloukhani, H. (2008) 'Statistical rate theory approach to kinetics of competitive adsorption at the solid/solution interface', *Journal of Physical Chemistry C*, Vol. 112, No. 27, pp.10251–10255 [online] http://pubs.acs.org/doi/abs/10.1021/jp802278e.

Bordi, F., Cametti, C. and Motta, A. (2000) 'Ion permeation across model lipid membranes: a kinetic approach', *The Journal of Physical Chemistry B*, Vol. 104, No. 22, pp.5318–532 [online] http://pubs.acs.org/doi/abs/10.1021/jp000005i.

Chang, C-H. and Liou, M-S. (2007) 'A robust and accurate approach to computing compressible multiphase flow: Stratified flow model and AUSM+-up scheme', *Journal of Computational Physics*, Vol. 225, No. 1, pp.840–873.

Cox, S.M. and Matthews, P.P. (2002) 'Exponential time differencing for stiff systems', *J. Comput. Phys.*, Vol. 176, No. 2, pp.430–455.

Dejmek, M. and Ward, C.A. (1998) 'A statistical rate theory study of interface concentration during crystal growth or dissolution', *The Journal of Chemical Physics*, Vol. 108, No. 20, pp.8698–8704 [online] http://link.aip.org/link/?JCP/108/8698/1.

Elliott, J.A.W. and Ward, C.A. (1997a) 'Statistical rate theory description of beam-dosing adsorption kinetics', *Journal of Chemical Physics*, April 1, Vol. 106, No. 13, pp.5667–5676.

Elliott, J.A.W. and Ward, C.A. (1997b) 'Temperature programmed desorption: a statistical rate theory approach', *The Journal of Chemical Physics*, Vol. 106, No. 13, pp.5677–5684 [online] http://link.aip.org/link/?JCP/106/5677/1.

Findlay, R.D. and Ward, C.A. (1982) 'Statistical rate theory of interfacial transport. IV. Predicted rate of dissociative adsorption', *Journal of Chemical Physics*, Vol. 76, No. 11, pp.5624–5631.

Flåtten, T., Morin, A. and Munkejord, S.T. (2010) 'Wave propagation in multicomponent flow models', *SIAM Journal on Applied Mathematics*, September, Vol. 70, No. 8, pp.2861–2882.

Harding, L.B., Maergoiz, A.I., Troe, J. and Ushakov, V.G. (2000) 'Statistical rate theory for the $HO + O \Leftrightarrow HO_2 \Leftrightarrow H + O_2$ reaction system: SACM/CT calculations between 0 and 5000 K', *Journal of Chemical Physics*, December 22, Vol. 113, No. 24, pp.11019–11034.

Hochbruck, M., Lubich, C. and Selhofer, H. (1998) 'Exponential integrators for large systems of differential equations', *SIAM J. Sci. Comput.*, Vol. 19, No. 5, pp.1552–1574.

Jin, S. (1995) 'Runge-Kutta methods for hyperbolic systems with stiff relaxation terms', *J. Comput. Phys.*, Vol. 122, No. 1, pp.51–67.

Kapoor, A. and Elliott, J.A.W. (2008) 'Nonideal statistical rate theory formulation to predict evaporation rates from equations of state', *Journal of Physical Chemistry B*, November 27, Vol. 112, No. 47, pp.15005–15013.

LeVeque, R.J. (2002) *Finite Volume Methods for Hyperbolic Problems*, Cambridge University Press, New York.

Lund, H. and Aursand, P. (2012) 'Two-phase flow of CO_2 with phase transfer', *Energy Procedia*, Vol. 23, pp.246–255.

Menikoff, R. and Plohr, B.J. (1989) 'The Riemann problem for fluid flow of real materials', *Rev. Mod. Phys.*, Vol. 61, No. 1, pp.75–130.

Morin, A., Aursand, P.K., Flåtten, T. and Munkejord, S.T. (2009) 'Numerical resolution of CO_2 transport dynamics', in *Siam Conference on Mathematics for Industry: Challenges and Frontiers (mi09)*, October 9–10, San Francisco, CA, USA.

Munkejord, S.T., Evje, S. and Flåtten, T. (2006) 'The multi-stage centred-scheme approach applied to a drift-flux two-phase flow model', *International Journal for Numerical Methods in Fluids*, October, Vol. 52, No. 6, pp.679–705.

Munkejord, S.T., Evje, S. and Flåtten, T. (2009) 'A MUSTA scheme for a nonconservative two-fluid model', *SIAM J. Sci. Comput.*, Vol. 31, No. 4, pp.2587–2622.

Pao, Y-P. (1971) 'Application of kinetic theory to the problem of evaporation and condensation', *Physics of Fluids*, Vol. 14, No. 2, pp.306–312.

Roe, P.L. (1981) 'Approximate Riemann solvers, parameter vectors, and difference schemes', *Journal of Computational Physics*, Vol. 43, No. 2, pp.357–372.

Rudzinski, W. and Plazinski, W. (2006) 'Kinetics of solute adsorption at solid/solution interfaces: a theoretical development of the empirical pseudo-first and pseudo-second order kinetic rate equations, based on applying the statistical rate theory of interfacial transport', *Journal of Physical Chemistry B*, August 24, Vol. 110, No. 33, pp.16514–16525.

Saurel, R., Petitpas, F. and Abgrall, R. (2008) 'Modelling phase transition in metastable liquids: application to cavitating and flashing flows', *Journal of Fluid Mechanics*, Vol. 607, pp.313–350.

Stewart, H.B. and Wendroff, B. (1984) 'Two-phase flow: models and methods', *Journal of Computational Physics*, Vol. 56, No. 3, pp.363–409.

Strang, G. (1968) 'On the construction and comparison of difference schemes', *SIAM J. Numer. Anal.*, Vol. 5, No. 3, pp.506–517.

Titarev, V.A. and Toro, E.F. (2005) 'MUSTA schemes for multi-dimensional hyperbolic systems: analysis and improvements', *International Journal for Numerical Methods in Fluids*, Vol. 49, No. 2, pp.117–147.

Toro, E.F. (1999) *Riemann Solvers and Numerical Methods for Fluid Dynamics*, 2nd ed., Springer-Verlag, Berlin (ISBN 3-540-65966-8).

Toro, E.F. (2003) 'Multi-stage predictor-corrector fluxes for hyperbolic equations', Technical Report No. NI03037-NPA, June 17, Isaac Newton Institute for Mathematical Sciences, University of Cambridge, UK.

Ward, C.A. and Fang, G. (1999) 'Expression for predicting liquid evaporation flux: statistical rate theory approach', *Phys. Rev. E*, Vol. 59, No. 1, pp.429–440.

Ward, C.A. and Stanga, D. (2001) 'Interfacial conditions during evaporation or condensation of water', *Phys. Rev. E*, Vol. 64, No. 5, Pt. 1, p.051509.

Ward, C.A., Findlay, R.D. and Rizk, M. (1982) 'Statistical rate theory of interfacial transport. I. Theoretical development', *The Journal of Chemical Physics*, Vol. 76, No. 11, pp.5599–5605.

Paper L5

Rankine-Hugoniot-Riemann solver for steady multidimensional conservation laws with source terms

Halvor Lund, Florian Müller, Bernhard Müller and Patrick Jenny

Rankine-Hugoniot-Riemann solver for steady multidimensional conservation laws with source terms

Halvor Lund[a,b,*], Florian Müller[a], Bernhard Müller[b], Patrick Jenny[a]

[a]*Institute of Fluid Dynamics, ETH Zürich, Sonneggstrasse 3, 8092 Zürich, Switzerland*
[b]*Dept. of Energy and Process Engineering, Norwegian University of Science and Technology (NTNU), NO-7491 Trondheim, Norway*

Abstract

The *Rankine-Hugoniot-Riemann* (RHR) solver has been designed to solve steady multidimensional conservation laws with source terms. The solver uses a novel way of incorporating cross fluxes as source terms. The combined source term from the cross fluxes and normal source terms is imposed in the middle of a cell, causing a jump in the solution according to the Rankine-Hugoniot condition. The resulting Riemann problems at the cell faces are then solved by a conventional Riemann solver.

We prove that the solver is of second order for rectangular grids and confirm this by its application to the 2D scalar advection equation, the 2D isothermal Euler equations and the 2D shallow water equations. For these cases, the error of the RHR solver is comparable to or smaller than that of a standard Riemann solver with a MUSCL scheme.

Keywords: finite volume methods, partial differential equations, conservation laws, Rankine-Hugoniot condition, source terms
2010 MSC: 76M12, 65N08, 35L65

1. Introduction

Our goal has been to develop a numerical method to solve systems of multidimensional hyperbolic partial differential equations (PDEs) with source terms, with an emphasis on calculating steady states accurately. Such systems of equations can describe a number of physical phenomena, e.g. combustion [1], multiphase flow with phase interaction in the form of mass or heat transfer [2, 3], water/vapor flow in nuclear reactors [4], cavitation [5], shallow water flow over variable topography [6, 7], and fluid flow in a gravity field [8], to mention a few. In many cases, one can express the equations as balance laws consisting of

---

*Corresponding author. Phone +47 73593803, fax +47 73593580.
Email addresses: `halvor.lund@ntnu.no` (Halvor Lund), `florian.mueller@sam.math.ethz.ch` (Florian Müller), `bernhard.muller@ntnu.no` (Bernhard Müller), `jenny@ifd.mavt.ethz.ch` (Patrick Jenny)

a conservation law together with a source term, i.e. as

$$\frac{\partial \boldsymbol{u}}{\partial t} + \boldsymbol{\nabla} \cdot \mathcal{F}(\boldsymbol{u}) = \boldsymbol{q}(\boldsymbol{u}, \boldsymbol{x}), \tag{1}$$

where $\boldsymbol{u}$ denotes the vector of conserved variables, $\mathcal{F}(\boldsymbol{u})$ the flux tensor and $\boldsymbol{q}(\boldsymbol{u}, \boldsymbol{x})$ the source term. The procedure of solving such equations numerically in multiple dimensions involves a number of challenges compared to solving a one-dimensional homogeneous ($\boldsymbol{q} = 0$) conservation law. First, the multidimensionality introduces new effects, which may be difficult to capture accurately by just using standard one-dimensional methods based on approximate Riemann solvers. Second, a stiff source term with a magnitude similar to the flux gradients may require a whole new approach, since approximate Riemann solvers for the numerical flux assume small or vanishing source terms.

One common approach to solving equations of the form (1) is to use a *fractional-step* or *operator-splitting* method, which is based on solving the conservation law $\boldsymbol{u}_t + \boldsymbol{\nabla} \cdot \mathcal{F}(\boldsymbol{u}) = 0$ and the ODE $\boldsymbol{u}_t = \boldsymbol{q}(\boldsymbol{u}, \boldsymbol{x})$ alternately to approximate the solution of the full problem (1). The advantage of such a splitting approach is that the operators can be approximated using well-proven methods developed for homogeneous conservation laws and for ODEs, respectively. However, as e.g. LeVeque [9, Chap. 17] points out, such splitting encounters difficulties, especially when the flux gradients and the source terms nearly or completely balance each other. This drawback of operator splitting has given rise to the development of *well-balanced* schemes, whose main aim is to well approximate the balance of the flux surface integral and the source volume integral in steady state. Well-balanced schemes have been discussed by a number of authors, including Bale et al. [7], Bermudez and Vazquez [10], Donat and Martinez-Gavara [11], Gosse [4], Hubbard and García-Navarro [12], and LeVeque [6, 13]. Murillo and García-Navarro [14] solve the shallow water equations with source terms by adding an extra wave associated with the source term in their approximate Riemann solver. Noelle and co-workers [15–18] have written a number of papers on well-balanced methods, with an emphasis on the application to the shallow water equations and steady states with moving flow.

LeVeque [6] proposed a method which incorporates the source term as a singular source in the centre of each grid cell, so that the flux difference exactly equals the source term integral approximation. This in turn leads to altered Riemann problems at the cell boundaries, which can be solved using a standard approximate Riemann solver with first or higher order reconstruction. Jenny and Müller [1] used a similar idea, but rather placed the source term at the cell boundary. Their work also introduced the concept for 2D problems of treating the flux gradients in the y direction as source terms when solving the Riemann problems in the x direction, and vice versa. This solver was coined the *Rankine-Hugoniot-Riemann* (RHR) solver, since a Rankine-Hugoniot condition is combined with a Riemann solver to calculate the new Riemann problem with source term at the cell boundary.

In this paper we build on the idea by Jenny and Müller [1] of treating cross fluxes as source terms, combined with placing the source term in the cell centre, as proposed by LeVeque [6]. This allows us to develop a numerical scheme with accurate treatment of multidimensional effects as well as source terms. Some stability problems reported by

Jenny and Müller [1] for two-dimensional cases are eliminated here by introducing a novel limiter.

Our paper is organized as follows. In Section 2, we explain the Rankine-Hugoniot-Riemann solver for one and two dimensions. The method can easily be extended to three-dimensional problems. We then introduce a limiting procedure to preserve TVD-like properties and to eliminate instabilities. In Section 3 we present an analysis of the solver properties and show that it is of second spatial order for rectangular grids. Numerical investigations are presented in Section 4, where we apply the RHR solver to steady states for a 2D scalar advection equation, the 2D isothermal Euler equations and the 2D shallow water equations. The numerical error is compared to that of a second-order MUSCL scheme. Finally, in Section 5 we draw some conclusions and outline further work.

2. Rankine-Hugoniot-Riemann solver

We are interested in solving a system of two-dimensional conservation laws with source terms, formulated in the steady case as

$$\frac{\partial \boldsymbol{f}(\boldsymbol{u})}{\partial x} + \frac{\partial \boldsymbol{g}(\boldsymbol{u})}{\partial y} = \boldsymbol{q}(\boldsymbol{u}, \boldsymbol{x}), \tag{2}$$

where $\boldsymbol{u}$ denotes the vector of conserved variables, $\boldsymbol{f}$ and $\boldsymbol{g}$ the flux vectors in x- and y-direction, respectively, and $\boldsymbol{q}$ the source term vector. In [1], the RHR solver was applied to a 1D premixed laminar flame and a 2D laminar Bunsen flame, where the source term not only depends on the conserved variables $\boldsymbol{u}$, but also on $\nabla \boldsymbol{u}$. The homogeneous system is assumed to be hyperbolic, i.e. the matrix $n_x \boldsymbol{f}'(\boldsymbol{q}) + n_y \boldsymbol{g}'(\boldsymbol{q})$ is diagonalizable with real eigenvalues for all $(n_x, n_y) \in \mathbb{R}$. We will build on LeVeque's idea of implementing the source term as a singular source in the cell centre [6]. For simplicity and clarity, we shall first explain the RHR solver in one dimension. Then we continue with two dimensions, where the concept of cross fluxes as source terms is employed as suggested by Jenny and Müller [1].

2.1. One-dimensional solver

The Rankine-Hugoniot-Riemann (RHR) solver was first proposed by Jenny and Müller [1], while a similar method was presented by LeVeque [6]. They can both be applied to solve a one-dimensional conservation law with a source term, in the steady case written as

$$\frac{\partial \boldsymbol{f}(\boldsymbol{u})}{\partial x} = \boldsymbol{q}(\boldsymbol{u}, x). \tag{3}$$

The two methods have the similarity that they incorporate the source term by placing it as a singular term at either the cell face or the cell centre, and then using the Rankine-Hugoniot condition to calculate the jump in the solution due to this singular source.

In this work we use the source term treatment by LeVeque [6], who distributed the source term as a singular term to the cell centre. The strength of the source term in cell i

integrated over the whole cell is approximated by $\Delta x \boldsymbol{q}_i$. Therefore the Rankine-Hugoniot condition reads

$$\boldsymbol{f}(\boldsymbol{u}_{i,\mathrm{E}}) - \boldsymbol{f}(\boldsymbol{u}_{i,\mathrm{W}}) = \Delta x \boldsymbol{q}_i, \tag{4}$$

where $\boldsymbol{u}_{i,\mathrm{W}}$ and $\boldsymbol{u}_{i,\mathrm{E}}$ are the values in the western and eastern cell parts, respectively, cf. Fig. 1. To keep the method conservative, we also require that the average of the conservative variable in the cell is kept constant, i.e. that

$$\frac{1}{2}(\boldsymbol{u}_{i,\mathrm{E}} + \boldsymbol{u}_{i,\mathrm{W}}) = \boldsymbol{u}_i. \tag{5}$$

The reconstruction of $\boldsymbol{u}$ is illustrated in Figure 1. The new half-states are then used to solve the Riemann problems at each cell interface, e.g. the Riemann problem at the face $I_{i+1/2}$ is given by $\boldsymbol{u}_{i,\mathrm{E}}$ and $\boldsymbol{u}_{i+1,\mathrm{W}}$ as the left and right states, respectively.
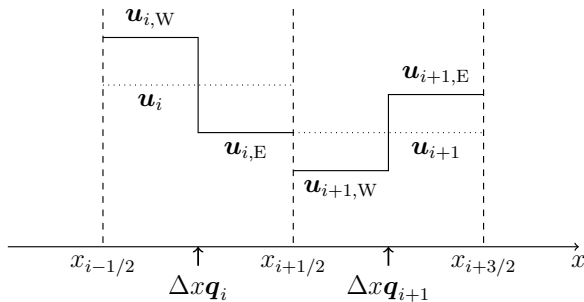
Figure 1: RHR solver in one dimension. The locations of the singular source terms are illustrated, as well as the cell averaged states (dotted lines) and the reconstruction (solid lines) of $\boldsymbol{u}$.

LeVeque [6] demonstrated that this approach is well-balanced, with an emphasis on the shallow water equations. Bale et al. [7] and LeVeque [19] argue that source term singularities placed at the cell faces instead of in the cell centres are more robust and simpler to implement. However, according to our experience, the method with cell centred singularities introduced in the present section has proven both fruitful and relatively easy to implement, since one can use a standard Riemann solver at the cell interfaces.

2.2. Multidimensional solver

We will now extend the ideas presented in Section 2.1 to multidimensional problems, formulated for steady states. For simplicity, we will derive a solver for two dimensions, but it is straightforward to extend the method to three dimensions. In two dimensions, a system of conservation laws with source terms can be formulated as written in Eq. (2). Moving the last left-hand-side term to the right-hand-side yields

$$\frac{\partial \boldsymbol{f}(\boldsymbol{u})}{\partial x} = -\frac{\partial \boldsymbol{g}(\boldsymbol{u})}{\partial y} + \boldsymbol{q}(\boldsymbol{u}, \boldsymbol{x}). \tag{6}$$

From this equation one can readily see that the y-directed flux term may be seen as a source term when solving the system in the x-direction, and vice versa. This idea of treating the cross flux as a source term was first introduced by Jenny and Müller [1], who placed the source terms at the cell faces. We will, however, continue to develop the idea of the cell centred source term described in Section 2.1, but incorporating both the source term $\boldsymbol{q}$ *and* the cross-flux term $-\partial \boldsymbol{g}(\boldsymbol{u})/\partial y$.
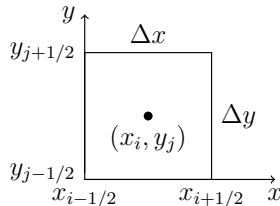
Figure 2: Sketch of cell $\mathcal{C}_{i,j}$

To find a finite volume formulation, we integrate Eq. (6) over a rectangular control volume $\mathcal{C}_{i,j}$ defined by the opposite corners $(x_{i-1/2}, y_{j-1/2})$ and $(x_{i+1/2}, y_{j+1/2}) = (x_{i-1/2} + \Delta x, y_{j-1/2} + \Delta y)$, cf. Fig. 2, which yields

$$\frac{1}{\Delta x}(\boldsymbol{f}_{i+1/2,j} - \boldsymbol{f}_{i-1/2,j}) = -\frac{1}{\Delta y}(\boldsymbol{g}_{i,j+1/2} - \boldsymbol{g}_{i,j-1/2}) + \boldsymbol{q}_{i,j}, \tag{7}$$

where $\boldsymbol{u}_{i,j}$ and $\boldsymbol{q}_{i,j}$ are the averages of $\boldsymbol{u}$ and $\boldsymbol{q}$, respectively, over control volume $\mathcal{C}_{i,j}$. The approximate averaged fluxes at the western and southern faces are given by

$$\boldsymbol{f}_{i-1/2,j} \approx \frac{1}{\Delta y} \int_{y_{j-1/2}}^{y_{j+1/2}} \boldsymbol{f}(\boldsymbol{u}(x_{i-1/2}, y)) \, \mathrm{d}y, \tag{8}$$

$$\boldsymbol{g}_{i,j-1/2} \approx \frac{1}{\Delta x} \int_{x_{i-1/2}}^{x_{i+1/2}} \boldsymbol{g}(\boldsymbol{u}(x, y_{j-1/2})) \, \mathrm{d}x. \tag{9}$$

The approximation of $-\partial \boldsymbol{g}(\boldsymbol{u})/\partial y$ on the right hand side of Eq. (7) quickly reveals that this term may be treated as a source term, similar to $\boldsymbol{q}_{i,j}$, when calculating the $\boldsymbol{f}$-fluxes in the x-direction, and vice versa. We place this source term as a singular source in the centre of the cell, in a similar fashion as explained in Section 2.1. Conservativity in control volume $\mathcal{C}_{i,j}$ and the Rankine-Hugoniot conditions can then be expressed as

$$\frac{1}{2}(\boldsymbol{u}_{i,j,\mathrm{W}} + \boldsymbol{u}_{i,j,\mathrm{E}}) = \boldsymbol{u}_{i,j}, \tag{10}$$

$$\frac{1}{2}(\boldsymbol{u}_{i,j,\mathrm{S}} + \boldsymbol{u}_{i,j,\mathrm{N}}) = \boldsymbol{u}_{i,j}, \tag{11}$$

$$\frac{1}{\Delta x}(\boldsymbol{f}(\boldsymbol{u}_{i,j,\mathrm{E}}) - \boldsymbol{f}(\boldsymbol{u}_{i,j,\mathrm{W}})) = \boldsymbol{q}_{x,i,j} \equiv \frac{\Delta \boldsymbol{g}_{i,j}}{\Delta y} + \boldsymbol{q}_{i,j}, \tag{12}$$

$$\frac{1}{\Delta y}(\boldsymbol{g}(\boldsymbol{u}_{i,j,\mathrm{N}}) - \boldsymbol{g}(\boldsymbol{u}_{i,j,\mathrm{S}})) = \boldsymbol{q}_{y,i,j} \equiv \frac{\Delta \boldsymbol{f}_{i,j}}{\Delta x} + \boldsymbol{q}_{i,j}. \tag{13}$$

5

where the subscripts N/S/E/W denote the northern/southern/eastern/western parts of the cell. The flux differences are $\Delta \boldsymbol{f}_{i,j} = \boldsymbol{f}_{i-1/2,j} - \boldsymbol{f}_{i+1/2,j}$ and $\Delta \boldsymbol{g}_{i,j} = \boldsymbol{g}_{i,j-1/2} - \boldsymbol{g}_{i,j+1/2}$. We have also introduced $\boldsymbol{q}_{x,i,j}$ and $\boldsymbol{q}_{y,i,j}$ to denote the total source term in the x and y directions, respectively. The relations (10) and (12) defining $\boldsymbol{u}_{i,j,\mathrm{W}}$ and $\boldsymbol{u}_{i,j,\mathrm{E}}$ are sketched in Fig. 3. The states $\boldsymbol{u}_{i,j,\mathrm{E}}$ and $\boldsymbol{u}_{i+1,j,\mathrm{W}}$ then define the Riemann problem at the face $I_{i+1/2,j}$, which in turn can be used to calculate the flux $\boldsymbol{f}_{i+1/2,j}$ using a Riemann solver.

Since the fluxes depend on the adjacent states to be determined, the flux differences $\Delta \boldsymbol{g}_{i,j}$ in Eq. (12) and $\Delta \boldsymbol{f}_{i,j}$ in Eq. (13) are approximated by their known values at the previous time step when doing timestepping to reach the steady state, cf. Section 4.1. Thus, $\boldsymbol{q}_{x,i,j}$ in Eq. (12) and $\boldsymbol{q}_{y,i,j}$ in Eq. (13) are assumed to be known. In general, the conditions (10)–(13) may need to be solved numerically for $\boldsymbol{u}_{i,j,\mathrm{W}}$, $\boldsymbol{u}_{i,j,\mathrm{E}}$, $\boldsymbol{u}_{i,j,\mathrm{S}}$ and $\boldsymbol{u}_{i,j,\mathrm{N}}$, using e.g. Newton's method. However, for the 2D scalar linear advection equation, the 2D isothermal Euler equations and the 2D shallow water equations presented later in this work, we are able to solve the conditions (10)–(13) analytically.

(a) Condition (10)   (b) Condition (12)
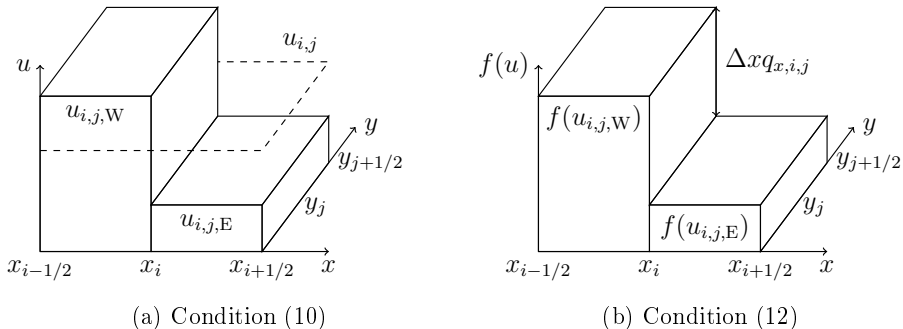
Figure 3: Sketch of the conditions (10) and (12) to define $\boldsymbol{u}_{i,j,\mathrm{W}}$ and $\boldsymbol{u}_{i,j,\mathrm{E}}$.

2.3. Limiting

The RHR solver presented by Jenny and Müller [1] was reported to have some stability problems when applied to two-dimensional balance laws. They handled these instabilities by introducing artificial numerical diffusion, which is rather arbitrary. In this paper we rather follow the ideas of Müller [20] and introduce a limiting of the western/eastern/southern/northern half-states.

The variables we limit may either be the conserved variables or the primitive variables. For the isothermal Euler equations and the shallow water equations, we limit the primitive variables, i.e. the velocity components as well as the density and the water height, respectively. The limited state $\boldsymbol{u}_{i,j,\mathrm{E}}^{\mathrm{L}}$ is calculated as follows:

$$(\boldsymbol{u}_{i,j,E}^{\mathrm{L}})_k = \min \left[\max \left[(\boldsymbol{u}_{i,j,E})_k - (\boldsymbol{u}_{i,j})_k, -|\delta_k| \right], |\delta_k| \right] + (\boldsymbol{u}_{i,j})_k \qquad (14)$$

where $\delta_k = \mathrm{minmod}((\boldsymbol{u}_{i+1,j})_k - (\boldsymbol{u}_{i,j})_k, (\boldsymbol{u}_{i,j})_k - (\boldsymbol{u}_{i-1,j})_k)$. Here $(\cdot)_k$ denotes the k-th limited variable (i.e. the k-th component of the vector of the conserved or primitive variables), and

6

$\boldsymbol{u}_{i,j,\mathrm{E}}$ is the unlimited eastern state. The limited western state $\boldsymbol{u}_{i,j,\mathrm{W}}^{\mathrm{L}}$ is then given by Eq. (10), so that the cell average is conserved. The limiter ensures that both $(\boldsymbol{u}_{i,j,\mathrm{E}}^{\mathrm{L}})_k$ and $(\boldsymbol{u}_{i,j,\mathrm{W}}^{\mathrm{L}})_k$ lie between $(\boldsymbol{u}_{i-1,j})_k$ and $(\boldsymbol{u}_{i+1,j})_k$, as long as $(\boldsymbol{u}_{i,j})_k$ also does so. The result would be completely equivalent if we limited the western state first, and then calculated the eastern state from this. An analogous requirement applies to the north state $\boldsymbol{u}_{i,j,\mathrm{N}}$.

Figure 4 illustrates this limiting procedure. Fig. 4a shows an example of a possible result of solving the RHR relations (10)–(13). In this case, the state $\boldsymbol{u}_{i,\mathrm{W}}$ is out of bounds, since it is larger than both $\boldsymbol{u}_{i-1}$ and $\boldsymbol{u}_{i+1}$. The limiter is then applied, which results in the limited states $\boldsymbol{u}_{i,\mathrm{W}}^{\mathrm{L}} = \boldsymbol{u}_{i-1}$, and $\boldsymbol{u}_{i,\mathrm{E}}^{\mathrm{L}} = 2\boldsymbol{u}_i - \boldsymbol{u}_{i,\mathrm{W}}^{\mathrm{L}}$ (which follows from Eq. (10)), illustrated in Fig. 4b. A similar case is shown in Figs. 4c–4d, where $\boldsymbol{u}_{i,\mathrm{E}}$ is out of bounds, and hence the limiter reduces this to $\boldsymbol{u}_{i,\mathrm{E}}^{\mathrm{L}} = \boldsymbol{u}_{i-1}$.
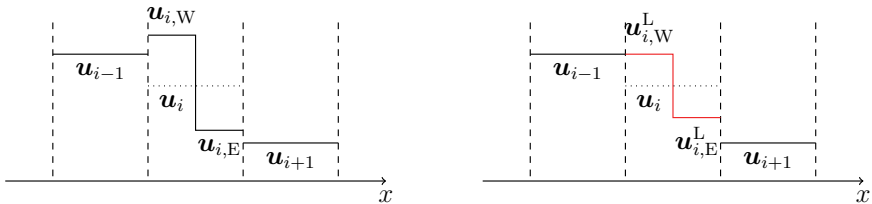
(a) Before limiting. $\boldsymbol{u}_{i,\mathrm{W}}$ lies outside the interval $[\boldsymbol{u}_{i+1}, \boldsymbol{u}_{i-1}]$ and needs to be limited.

(b) After limiting. $\boldsymbol{u}_{i,\mathrm{W}}$ is reduced, and $\boldsymbol{u}_{i,\mathrm{E}}$ is increased accordingly to conserve $\boldsymbol{u}_i$, as stated in Eq. (10).
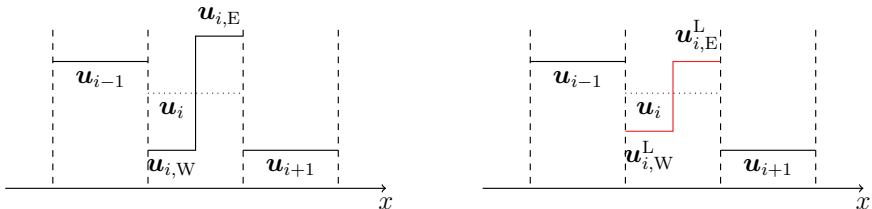
(c) Before limiting. $\boldsymbol{u}_{i,\mathrm{E}}$ lies outside the interval $[\boldsymbol{u}_{i+1}, \boldsymbol{u}_{i-1}]$ and needs to be limited.

(d) After limiting. $\boldsymbol{u}_{i,\mathrm{E}}$ is reduced, and $\boldsymbol{u}_{i,\mathrm{W}}$ is increased accordingly to conserve $\boldsymbol{u}_i$, as stated in Eq. (10).

Figure 4: Illustration of the limiting procedure for the RHR solver for two different cases.

In Figure 5a the instabilities without limiting are illustrated for the 2D steady scalar linear advection equation, i.e.

$$a\frac{\partial u}{\partial x} + b\frac{\partial u}{\partial y} = 0, \tag{15}$$

with constant velocity $\boldsymbol{v} = (a,b)^{\top} = (1, 0.5)^{\top}$ on a 20×20 grid with $\Delta x = \Delta y = 1.8$. At
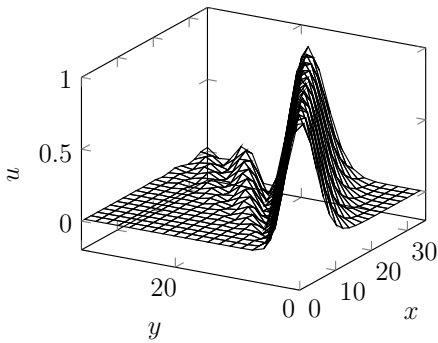
(a) Without limiting. Spurious oscillations emerge as the scalar u is advected through the domain.
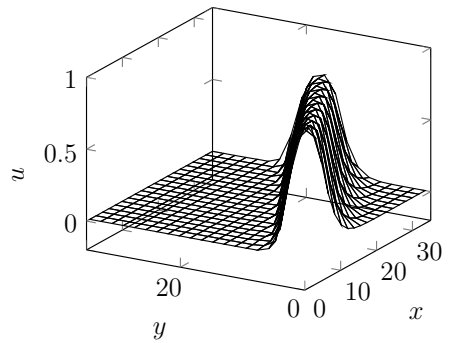
(b) With limiting.
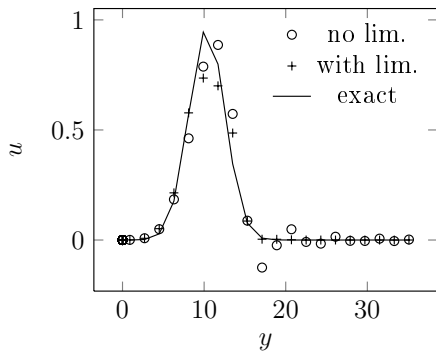
(c) Cross-section at $x = 20.7$.
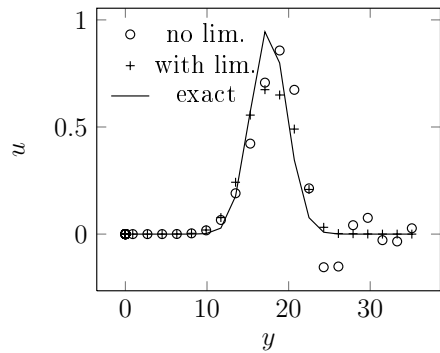
(d) Cross-section at $x = 35.1$.

Figure 5: Advection of a scalar Gauss profile (16) with velocity $(a, b)^\top = (1, 0.5)^\top$, with (with lim.) and without limiting (no lim.), on a 20×20 grid with $\Delta x = \Delta y = 1.8$.

the boundaries $x = 0$ and $y = 0$ the scalar u is set according to a Gauss profile given by

$$u(x, y) = \exp\left(-\frac{(y - \frac{b}{a} \cdot x)^2}{3^2}\right).$$ (16)

The steady state solution exhibits spurious oscillations propagating downstream on the left side of the advected crest.

After applying the limiting to the 2D steady scalar linear advection equation, the spurious oscillations are eliminated, cf. Fig. 5b. Figures 5c and 5d show two cross-sections of the numerical solutions depicted in Figures 5a and 5b, as well as the exact solution. We recognize that the limiter causes the oscillations to vanish, but also leads to slightly more diffusive solutions, e.g. the peak values are smaller than without limiting.

In the setting of the 2D unsteady linear advection equation, i.e.

$$\frac{\partial u}{\partial t} + a\frac{\partial u}{\partial x} + b\frac{\partial u}{\partial y} = 0,$$ (17)

the RHR solver combined with the proposed limiter complies with the minimum/maximum principle. Here, the minimum/maximum principle states that for a pure initial value problem with initial conditions $u_0(x, y)$ specified for $-\infty < x, y < \infty$ we have $\min(u_0) \leq u \leq \max(u_0)$ for all times t. We first observe that for a locally maximal state $u_{i,j}$, the limiter does not allow the corresponding half-states $u_{i,j,\mathrm{N}}$, $u_{i,j,\mathrm{S}}$, $u_{i,j,\mathrm{E}}$ and $u_{i,j,\mathrm{W}}$ to be different from $u_{i,j}$. Moreover, the limiter ensures that the adjacent half-states of the neighboring cells do not outreach $u_{i,j}$. Since Riemann problems between the half-states at the cell interfaces reduce to simple upwinding, we see that the locally maximal state $u_{i,j}$ cannot increase as time evolves. Certainly, new local maxima can emerge but due to the previous argument, these new maxima can no longer increase after their creation. Therefore, the upper bound provided by the initial global maximum is not violated. Along similar lines, the minimum principle is met. It is emphasized that time integration must be sufficiently accurate for this reasoning to hold.

3. Analysis of the RHR solver for the 2D steady scalar linear advection equation

In this section, in order to highlight some important properties of the RHR solver without limiter, we present an analysis of the solver for the 2D steady scalar linear advection equation with a linear source term, i.e.

$$a\frac{\partial u}{\partial x} + b\frac{\partial u}{\partial y} = cu + d,$$ (18)

where $\boldsymbol{v} = (a, b)^{\top}$ is the (constant) velocity vector and c and d are additional constants. For this equation, the flux functions are simply given by $f(u) = au$ and $g(u) = bu$. We

9

assume without loss of generality that the two velocities are positive, i.e. $a, b > 0$. In this case, the numerical fluxes at the faces are simply chosen as the upwind fluxes, i.e.

$$f_{i+1/2,j} = au_{i,j,E}, \text{ and} \tag{19}$$

$$g_{i,j+1/2} = bu_{i,j,N}. \tag{20}$$

With the given flux functions and numerical fluxes, the conservativity and Rankine-Hugoniot conditions from Eqs. (10)–(13) read

$$\frac{1}{2}(u_{i,j,W} + u_{i,j,E}) = u_{i,j}, \tag{21}$$

$$\frac{1}{2}(u_{i,j,S} + u_{i,j,N}) = u_{i,j}, \tag{22}$$

$$\frac{a}{\Delta x}(u_{i,j,E} - u_{i,j,W}) = \frac{b}{\Delta y}(u_{i,j-1,N} - u_{i,j,N}) + cu_{i,j} + d, \tag{23}$$

$$\frac{b}{\Delta y}(u_{i,j,N} - u_{i,j,S}) = \frac{a}{\Delta x}(u_{i-1,j,E} - u_{i,j,E}) + cu_{i,j} + d, \tag{24}$$

whereas the finite volume scheme (7) in the steady case reads

$$\frac{a}{\Delta x}(u_{i-1,j,E} - u_{i,j,E}) + \frac{b}{\Delta y}(u_{i,j-1,N} - u_{i,j,N}) + cu_{i,j} + d = 0. \tag{25}$$

We now wish to show how the stencil for the solution in cell (i, j), $u_{i,j}$, depends on the solution in the neighbouring cells. To this end, we solve Eq. (21) for $u_{i,j,W}$ and Eq. (22) for $u_{i,j,S}$ and substitute the results into Eqs. (23) and (24), respectively, which yields

$$\frac{2a}{\Delta x}(u_{i,j,E} - u_{i,j}) = \frac{b}{\Delta y}(u_{i,j-1,N} - u_{i,j,N}) + cu_{i,j} + d, \tag{26}$$

$$\frac{2b}{\Delta y}(u_{i,j,N} - u_{i,j}) = \frac{a}{\Delta x}(u_{i-1,j,E} - u_{i,j,E}) + cu_{i,j} + d. \tag{27}$$

Using Eq. (25), we replace the right-hand side of Eqs. (26)–(27), which leads to

$$\frac{a}{\Delta x}(u_{i,j,E} + u_{i-1,j,E} - 2u_{i,j}) = 0, \tag{28}$$

$$\frac{b}{\Delta y}(u_{i,j,N} + u_{i,j-1,N} - 2u_{i,j}) = 0. \tag{29}$$

Finally, we solve Eq. (28) for $u_{i-1,j,E}$ and Eq. (29) for $u_{i,j-1,N}$ and substitute the results into Eq. (25), which yields

$$\frac{a}{\Delta x}(u_{i,j} - u_{i,j,E}) + \frac{b}{\Delta y}(u_{i,j} - u_{i,j,N}) + \frac{c}{2}u_{i,j} + \frac{d}{2} = 0. \tag{30}$$

We now add the following equations to retrieve a stencil for $u_{i,j}$: Eqs. (28), (29) and (30), Eq. (28) with shifted indices $(i, j) \to (i, j-1)$, Eq. (29) with shifted indices $(i, j) \to (i-1, j)$,

Eq. (30) with shifted indices $(i,j) \rightarrow (i-1,j)$, Eq. (30) with shifted indices $(i,j) \rightarrow (i,j-1)$, Eq. (30) with shifted indices $(i,j) \rightarrow (i-1,j-1)$. After solving the resulting expression for $u_{i,j}$, we get

$$u_{i,j} = \frac{c\Delta x \Delta y + 2a\Delta y - 2b\Delta x}{2a\Delta y + 2b\Delta x - c\Delta x \Delta y} u_{i-1,j} + \frac{c\Delta x \Delta y - 2a\Delta y + 2b\Delta x}{2a\Delta y + 2b\Delta x - c\Delta x \Delta y} u_{i,j-1}$$
$$+ \frac{c\Delta x \Delta y + 2a\Delta y + 2b\Delta x}{2a\Delta y + 2b\Delta x - c\Delta x \Delta y} u_{i-1,j-1} + \frac{4d\Delta x \Delta y}{2a\Delta y + 2b\Delta x - c\Delta x \Delta y}. \tag{31}$$

The stencil may be viewed as an operator which maps the solution to the south, west and south-west to the location (i,j); note for example that for $\frac{\Delta x}{\Delta y} = \frac{a}{b}$ and $c = d = 0$, the stencil reduces to

$$u_{i,j} = u_{i-1,j-1}, \tag{32}$$

i.e. the RHR solver propagates the solution *exactly* diagonal to the grid. Figure 6 shows the numerical results for a case with advection of a Gauss profile given by Eq. (16) on a 10×10 grid with $\Delta x = 1.8$ and $\Delta y = 3.6$ and $2a = b$; as expected the numerical solution is exact. Although this example of advection with constant velocity is rather trivial, the result illustrates the capability of the RHR solver to capture fluxes in oblique direction with respect to the grid orientation.
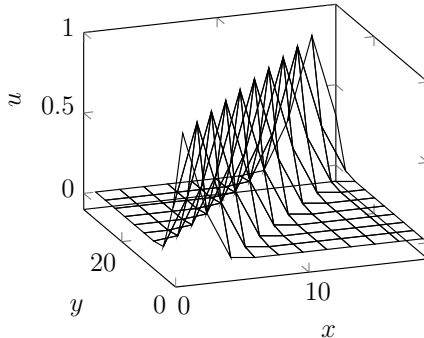
Figure 6: Advection of a scalar Gauss profile (16) with $2a = b$ and $\Delta x = 1.8$ and $\Delta y = 3.6$ on a 10×10 grid, which is solved exactly by the RHR solver (without limiter).

3.1. Error analysis

In this section, we wish to analyse the spatial order of accuracy of the RHR solver (without limiter) for the 2D steady advection equation with source term (18). We estimate the local error by the difference between the numerical solution $u_{i,j}$ and the exact solution

$\tilde{u}_{i,j}$, i.e.

$$E_{\text{local}} = \frac{c\Delta x\Delta y - 2a\Delta y - 2b\Delta x}{2a\Delta y + 2b\Delta x - c\Delta x\Delta y}\tilde{u}_{i,j} + \frac{c\Delta x\Delta y + 2a\Delta y - 2b\Delta x}{2a\Delta y + 2b\Delta x - c\Delta x\Delta y}\tilde{u}_{i-1,j}$$
$$+ \frac{c\Delta x\Delta y - 2a\Delta y + 2b\Delta x}{2a\Delta y + 2b\Delta x - c\Delta x\Delta y}\tilde{u}_{i,j-1} + \frac{c\Delta x\Delta y + 2a\Delta y + 2b\Delta x}{2a\Delta y + 2b\Delta x - c\Delta x\Delta y}\tilde{u}_{i-1,j-1}$$
$$+ \frac{4d\Delta x\Delta y}{2a\Delta y + 2b\Delta x - c\Delta x\Delta y}, \tag{33}$$

where we have used the stencil (31) to express $u_{i,j}$ as a function of the exact solution in the neighbouring cells. We now assume that the solution $\tilde{u}$ is sufficiently smooth such that $\tilde{u}_{i-1,j}$, $\tilde{u}_{i,j-1}$ and $\tilde{u}_{i-1,j-1}$ in Eq. (33) can be expressed as a Taylor series around (i,j). Since $\tilde{u}$ is an exact solution of Eq. (18), we find that the y derivative is given by

$$\frac{\partial \tilde{u}}{\partial y} = -\frac{a}{b}\frac{\partial \tilde{u}}{\partial x} + \frac{c}{b}\tilde{u} + \frac{d}{b}. \tag{34}$$

We utilize this to replace all y derivatives stemming from the Taylor series insertion into Eq. (33). This causes the zeroth, first and second order terms to cancel, leaving

$$E_{\text{local}} = \frac{\Delta x\Delta y}{3b^2\left(2a\Delta y + 2b\Delta x - c\Delta x\Delta y\right)}\left(- a^3\Delta y^2\frac{\partial^3 \tilde{u}}{\partial x^3}\Big|_{i,j} + ab^2\Delta x^2\frac{\partial^3 \tilde{u}}{\partial x^3}\Big|_{i,j} + 3a^2c\Delta y^2\frac{\partial^2 \tilde{u}}{\partial x^2}\Big|_{i,j}\right.$$
$$\left.- 3ac^2\Delta y^2\frac{\partial \tilde{u}}{\partial x}\Big|_{i,j} + c^3\Delta y^2\tilde{u}_{i,j} + c^2d\Delta y^2\right) + \text{higher order terms.} \tag{35}$$

If we assume that the ratio $\Delta x/\Delta y$ is fixed, we find

$$E_{\text{local}} = \mathcal{O}(\Delta x^3), \tag{36}$$

i.e. the local spatial error of the RHR solver is of third order. To find the global error, we realize that in order to advect the solution from the boundary to a certain cell, the stencil (31) is applied a certain number of times proportional to $1/\Delta x$. Therefore the global error is of second order,

$$E_{\text{global}} = \mathcal{O}(\Delta x^2). \tag{37}$$

We would like to point out the fact that the scheme achieves second order with a compact stencil that is only dependent on the solution value and the fluxes in the nearest neighbouring cells. This is in contrast to e.g. a MUSCL scheme, which requires two cells in all directions to achieve second order.

In this paper we mainly focus on showing the spatial properties of the RHR solver for the steady case, thus we do not investigate the temporal properties in detail. The time integration procedure is outlined in the following section.

4. Numerical investigation

In this section, we numerically investigate how the RHR solver behaves for steady states for a two-dimensional advection equation, the two-dimensional isothermal Euler equations and the two-dimensional shallow water equations. We start by describing in a general way how the time-stepping is performed, which we need to arrive at the steady states.

4.1. Time integration/solution algorithm

In general, we wish to solve a multidimensional system of conservation laws with source terms. For simplicity, we consider the two-dimensional case, i.e.

$$\frac{\partial \boldsymbol{u}}{\partial t} + \frac{\partial \boldsymbol{f}(\boldsymbol{u})}{\partial x} + \frac{\partial \boldsymbol{g}(\boldsymbol{u})}{\partial y} = \boldsymbol{q}(\boldsymbol{u}, \boldsymbol{x}). \tag{38}$$

For this system of balance laws, the finite volume scheme (7) can (in the unsteady case) be rearranged as

$$\frac{\partial \boldsymbol{u}_{i,j}}{\partial t} = \frac{1}{\Delta x}(\boldsymbol{f}_{i-1/2,j} - \boldsymbol{f}_{i+1/2,j}) + \frac{1}{\Delta y}(\boldsymbol{g}_{i,j-1/2} - \boldsymbol{g}_{i,j+1/2}) + \boldsymbol{q}_{i,j}. \tag{39}$$

From the RHR relations in Eqs. (10)–(13), we see that the system of ordinary differential equations (ODEs) for $\boldsymbol{u}_{i,j,\mathrm{E}}$ and $\boldsymbol{u}_{i,j,\mathrm{W}}$ is highly coupled between cells, since the interface fluxes $\boldsymbol{f}_{i\pm 1/2,j}$ and $\boldsymbol{g}_{i,j\pm 1/2}$ (in general) depend on the states in neighbouring cells on both sides. This presents a challenge when implementing a time integration scheme. Hence we choose to calculate the total source terms $\boldsymbol{q}_{x,i,j}$ and $\boldsymbol{q}_{y,i,j}$ based on the *previous* time step when solving the RHR relations for the next time step.

We then propose to move the solution forward in time using the following algorithm.

1. Calculate the total source terms based on the fluxes from the previous time step:

$$\boldsymbol{q}_{x,i,j}^n = \frac{\boldsymbol{g}_{i,j-1/2}^{n-1/2} - \boldsymbol{g}_{i,j+1/2}^{n-1/2}}{\Delta y} + \boldsymbol{q}_{i,j}^n, \qquad \boldsymbol{q}_{y,i,j}^n = \frac{\boldsymbol{f}_{i-1/2,j}^{n-1/2} - \boldsymbol{f}_{i+1/2,j}^{n-1/2}}{\Delta x} + \boldsymbol{q}_{i,j}^n \tag{40}$$

   For the first time step, the fluxes at time step $n-1/2$ are unknown, but are assumed to be zero.

2. Compute the half-states $\boldsymbol{u}_{i,j,\mathrm{S}}^n$, $\boldsymbol{u}_{i,j,\mathrm{N}}^n$, $\boldsymbol{u}_{i,j,\mathrm{W}}^n$ and $\boldsymbol{u}_{i,j,\mathrm{E}}^n$ using Eqs. (10)–(13) based on $\boldsymbol{u}_{i,j}^n$ and the total source terms $\boldsymbol{q}_{x,i,j}^n$ and $\boldsymbol{q}_{y,i,j}^n$ given by (40).

3. Calculate the limited states $(\boldsymbol{u}_{i,j,\mathrm{N}}^{\mathrm{L}})^n$ and $(\boldsymbol{u}_{i,j,\mathrm{E}}^{\mathrm{L}})^n$ according to Eq. (14). The limited states $(\boldsymbol{u}_{i,j,\mathrm{S}}^{\mathrm{L}})^n$ and $(\boldsymbol{u}_{i,j,\mathrm{W}}^{\mathrm{L}})^n$ are then given by Eqs. (10) and (11), respectively.

4. Solve the Riemann problems defined by the limited values $(\boldsymbol{u}_{i-1,j,\mathrm{E}}^{\mathrm{L}})^n$ and $(\boldsymbol{u}_{i,j,\mathrm{W}}^{\mathrm{L}})^n$, $(\boldsymbol{u}_{i,j,\mathrm{E}}^{\mathrm{L}})^n$ and $(\boldsymbol{u}_{i+1,j,\mathrm{W}}^{\mathrm{L}})^n$, $(\boldsymbol{u}_{i,j-1,\mathrm{N}}^{\mathrm{L}})^n$ and $(\boldsymbol{u}_{i,j,\mathrm{S}}^{\mathrm{L}})^n$, $(\boldsymbol{u}_{i,j,\mathrm{N}}^{\mathrm{L}})^n$ and $(\boldsymbol{u}_{i,j+1,\mathrm{S}}^{\mathrm{L}})^n$, to obtain the Riemann fluxes $\boldsymbol{f}_{i-1/2,j}^n$, $\boldsymbol{f}_{i+1/2,j}^n$, $\boldsymbol{g}_{i,j-1/2}^n$ and $\boldsymbol{g}_{i,j+1/2}^n$, respectively.

5. Calculate an intermediate state $\boldsymbol{u}^{n+1/2}$ given by

$$\boldsymbol{u}_{i,j}^{n+1/2} = \boldsymbol{u}_{i,j}^n + \frac{\Delta t}{\Delta x}(\boldsymbol{f}_{i-1/2,j}^n - \boldsymbol{f}_{i+1/2,j}^n) + \frac{\Delta t}{\Delta y}(\boldsymbol{g}_{i,j-1/2}^n - \boldsymbol{g}_{i,j+1/2}^n) + \Delta t \boldsymbol{q}_{i,j}^n, \tag{41}$$

13

6. Compute the half-states $\boldsymbol{u}_{i,j,\mathrm{S}}^{n+1/2}$, $\boldsymbol{u}_{i,j,\mathrm{N}}^{n+1/2}$, $\boldsymbol{u}_{i,j,\mathrm{W}}^{n+1/2}$ and $\boldsymbol{u}_{i,j,\mathrm{E}}^{n+1/2}$ using Eqs. (10)–(13) based on $\boldsymbol{u}_{i,j}^{n+1/2}$ and the total source terms $\boldsymbol{q}_{x,i,j}^{n}$ and $\boldsymbol{q}_{y,i,j}^{n}$ given by (40).

7. Calculate the limited states $(\boldsymbol{u}_{i,j,\mathrm{N}}^{\mathrm{L}})^{n+1/2}$ and $(\boldsymbol{u}_{i,j,\mathrm{E}}^{\mathrm{L}})^{n+1/2}$ according to Eq. (14). The limited states $(\boldsymbol{u}_{i,j,\mathrm{S}}^{\mathrm{L}})^{n+1/2}$ and $(\boldsymbol{u}_{i,j,\mathrm{W}}^{\mathrm{L}})^{n+1/2}$ are then given by Eqs. (10) and (11), respectively.

8. Solve the Riemann problems defined by the limited values $(\boldsymbol{u}_{i-1,j,\mathrm{E}}^{\mathrm{L}})^{n+1/2}$ and $(\boldsymbol{u}_{i,j,\mathrm{W}}^{\mathrm{L}})^{n+1/2}$, $(\boldsymbol{u}_{i,j,\mathrm{E}}^{\mathrm{L}})^{n+1/2}$ and $(\boldsymbol{u}_{i+1,j,\mathrm{W}}^{\mathrm{L}})^{n+1/2}$, $(\boldsymbol{u}_{i,j-1,\mathrm{N}}^{\mathrm{L}})^{n+1/2}$ and $(\boldsymbol{u}_{i,j,\mathrm{S}}^{\mathrm{L}})^{n+1/2}$, $(\boldsymbol{u}_{i,j,\mathrm{N}}^{\mathrm{L}})^{n+1/2}$ and $(\boldsymbol{u}_{i,j+1,\mathrm{S}}^{\mathrm{L}})^{n+1/2}$, to obtain the Riemann fluxes $\boldsymbol{f}_{i-1/2,j}^{n+1/2}$, $\boldsymbol{f}_{i+1/2,j}^{n+1/2}$, $\boldsymbol{g}_{i,j-1/2}^{n+1/2}$ and $\boldsymbol{g}_{i,j+1/2}^{n+1/2}$, respectively.

9. Advance time by Δt to reach $\boldsymbol{u}_{i,j}^{n+1}$, i.e.

$$
\begin{aligned}
\boldsymbol{u}_{i,j}^{n+1} = \boldsymbol{u}_{i,j}^{n} + \frac{\Delta t}{2} \Bigg(& \frac{\boldsymbol{f}_{i-1/2,j}^{n+1/2} - \boldsymbol{f}_{i+1/2,j}^{n+1/2}}{\Delta x} + \frac{\boldsymbol{g}_{i,j-1/2}^{n+1/2} - \boldsymbol{g}_{i,j+1/2}^{n+1/2}}{\Delta y} + \boldsymbol{q}_{i,j}^{n+1/2} \\
& + \frac{\boldsymbol{f}_{i-1/2,j}^{n} - \boldsymbol{f}_{i+1/2,j}^{n}}{\Delta x} + \frac{\boldsymbol{g}_{i,j-1/2}^{n} - \boldsymbol{g}_{i,j+1/2}^{n}}{\Delta y} + \boldsymbol{q}_{i,j}^{n} \Bigg),
\end{aligned}
\tag{42}
$$

This scheme is quite similar to Heun's method, a two-stage Runge-Kutta method. In our scheme, however, the source terms $\boldsymbol{q}^{n}$, $\boldsymbol{q}_{x}^{n}$ and $\boldsymbol{q}_{y}^{n}$ are used in *both* stages, and are calculated based on the fluxes in the previous half time step, given by Eq. (40). An alternative to this scheme would have been a simple first-order forward Euler scheme, i.e. steps 1 to 5 above with half steps $n-1/2$ in (40) and $n+1/2$ in (41) replaced by the old and new time levels $n-1$ and $n+1$, respectively. However, the scheme presented above exhibits better stability properties and can handle larger time steps. Whenever a MUSCL scheme was used for comparison, the time integration was performed with a standard Heun's method. A CFL number of $C = 0.3$ was used for all the numerical computations, which was chosen as a safe value to avoid any possible instabilities in time, and since our focus was not on the time integration itself. The CFL number is defined as

$$
C = \Delta t \max_{p,k} \frac{|\lambda_{p,k}|}{\Delta x_k},
\tag{43}
$$

where $\lambda_{p,k}$ is the pth eigenvalue in the kth dimension of the hyperbolic system, and Δx_k is the grid spacing in the kth dimension.

The time stepping scheme presented above is not formally of second order for the RHR scheme, since the total source terms $\boldsymbol{q}_{x,i,j}^{n}$ and $\boldsymbol{q}_{y,i,j}^{n}$ depend on the fluxes in the previous time step. With this in mind, we may expect that the RHR scheme converges slower in time than e.g. a MUSCL scheme with a two-step second-order scheme like Heun's method. In addition, for the RHR solver each time step involves solving the RHR relations (10)–(13) which are not solved in the MUSCL scheme, hence we may expect that each time step may be more costly for the RHR scheme. We will discuss the computational expense of the RHR scheme for each system of equations in the following sections.

14

4.2. Method of manufactured solutions

To compute the exact error of a numerical solution, one needs to know the exact solution to the problem, given the boundary (and possibly initial) conditions. For more complex systems of PDEs, domains and boundary conditions, an exact solution may be out of reach. In these cases, the method of manufactured solutions can often be useful [21]. Instead of searching for the exact solution to the original problem (38), one rather makes the ansatz that the solution is $\boldsymbol{u}^*$, which can be an arbitrary sufficiently smooth function, preferably close to an exact solution. We then assume that the ansatz solves the modified equation

$$\frac{\partial \boldsymbol{f}(\boldsymbol{u}^*)}{\partial x} + \frac{\partial \boldsymbol{g}(\boldsymbol{u}^*)}{\partial y} = \boldsymbol{q}(\boldsymbol{u}^*, \boldsymbol{x}) + \boldsymbol{R}(\boldsymbol{u}^*, \boldsymbol{x}), \tag{44}$$

where $\boldsymbol{R}$ is the residual, caused by the fact that $\boldsymbol{u}^*$ is not an exact solution to the original problem. This residual is simply calculated by inserting $\boldsymbol{u}^*$ into Eq. (44) and solving for $\boldsymbol{R}$. If $\boldsymbol{R}$ were zero, $\boldsymbol{u}^*$ would be an exact solution to Eq. (2) or the steady version of Eq. (38). This problem has essentially the same structure as the steady version of the original problem (38), and can thus be used to investigate the accuracy properties of the numerical method. We solve Eq. (44) numerically using the modified source term $\boldsymbol{q}^* = \boldsymbol{q} + \boldsymbol{R}$, and since we now know that the manufactured solution $\boldsymbol{u}^*$ is the exact solution to the modified problem, we can compute the numerical error exactly. The method of manufactured solutions will be used to calculate the numerical error for an isothermal Euler case in Section 4.4 and a shallow water case in Section 4.5.

In the following sections we will present a number of numerical cases, each of which has either a known exact solution or a manufactured solution. Knowing the solution, we can set the boundary conditions to the exact solution, avoiding any possible issues of employing characteristic or non-reflecting boundary conditions. The characteristic Riemann solvers will automatically take the characteristic variables from the exterior, i.e. the given boundary conditions, or from the interior, i.e. from the solution in the adjacent cell at the previous time level or previous stage, depending on whether the characteristic is entering or leaving the domain.

4.3. Advection of a scalar

In this section we present some findings with the RHR solver applied to a two-dimensional scalar linear advection case with constant velocity, which in the steady case is given by

$$a\frac{\partial u}{\partial x} + b\frac{\partial u}{\partial y} = 0. \tag{45}$$

The simplicity of this equation makes it suitable to illustrate some important properties of the RHR solver.

4.3.1. Numerical order of convergence

As shown in Section 3.1, the RHR solver is expected to be of second order for a smooth solution. To confirm this numerically, we consider a cosine shaped solution,

$$u(x, y) = \cos(\omega_0(-bx + ay)) \tag{46}$$

15

where $\omega_0 = \pi/9$, $a = 1.0$, $b = 0.5$, and the grid has dimensions $[0, 36] \times [0, 36]$. The solution (46) is used to set the boundary conditions at $x = 0$ and $y = 0$. We solve the equation using the time integration scheme in Section 4.1 and wait for the solution to reach steady state. The numerical solution is then compared to the exact solution to determine the error. For illustration, Figure 7 shows the solution for the RHR solver with and without limiter and a MUSCL upwind solver with van Albada limiter for a grid of 20×20 cells. We recognize that the RHR solver with limiter does a significantly better job than MUSCL in resolving the problem on this grid, while the RHR solver without limiter is even more accurate. The plot in Figure 8 shows the L^2 errors for the RHR solver with and without
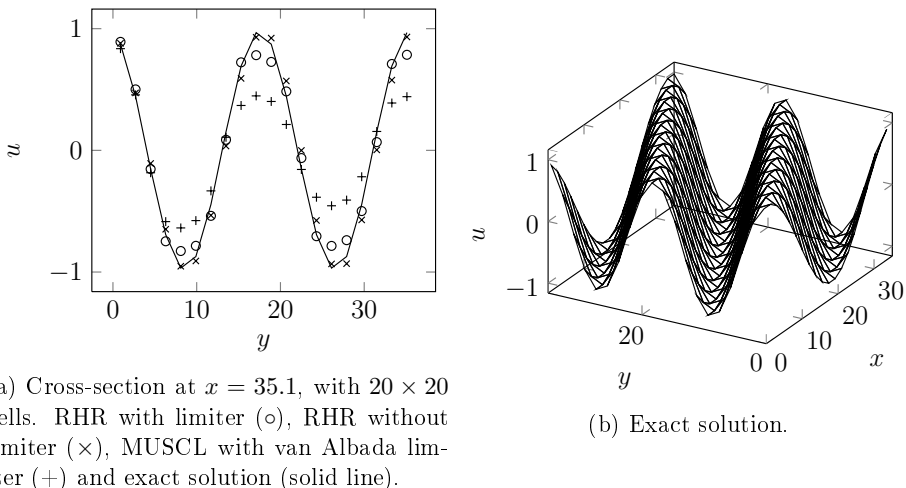
(a) Cross-section at $x = 35.1$, with 20×20 cells. RHR with limiter ($\circ$), RHR without limiter ($\times$), MUSCL with van Albada limiter ($+$) and exact solution (solid line).

(b) Exact solution.

Figure 7: Advection of a scalar cosine-shaped boundary condition (46) with velocity $(a, b)^\top = (1, 0.5)^\top$, on a 20×20 grid with $\Delta x = \Delta y = 1.8$.

limiter, and the MUSCL upwind solver with minmod and van Albada limiters, as functions of grid size $n_x = n_y$, where n_x and n_y are the number of grid cells in x- and y-direction, respectively. As seen in the figure, the RHR solver has an error significantly smaller than that of a MUSCL solver with van Albada limiter, while the RHR solver without limiter is even more accurate.

Figure 9 shows the L^1 norm of the residual as a function of the number of time steps, given by

$$R^n = \sum_{i,j,k} |(\boldsymbol{u}_{i,j}^n)_k - (\boldsymbol{u}_{i,j}^{n-1})_k|, \tag{47}$$

where $(\boldsymbol{u}_{i,j}^n)_k$ is the kth component of $\boldsymbol{u}^n$ at the grid point i, j. We see that all methods converge to machine precision, although the RHR solver with limiter converges slightly slower. This may be due to the non-standard time integration method used for the RHR solver, where the fluxes depend not only on the solution $\boldsymbol{u}$, but also on the fluxes in the previous time step, giving a method which is not formally second order in time.

16
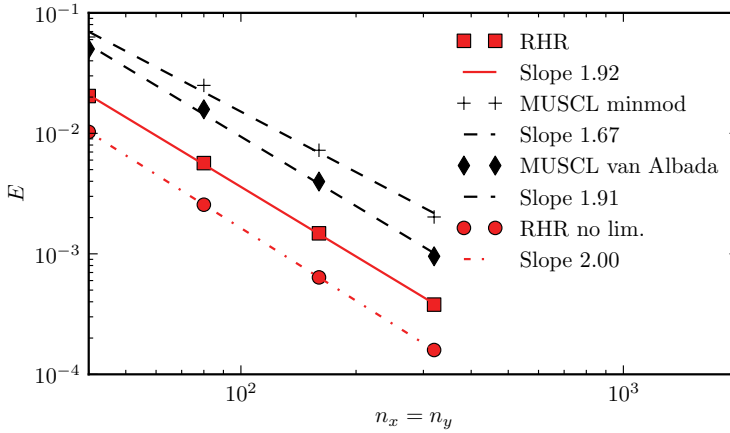
Figure 8: L^2 error E as a function of grid size $n_x = n_y$ for a case with advection of a cosine shaped scalar profile.
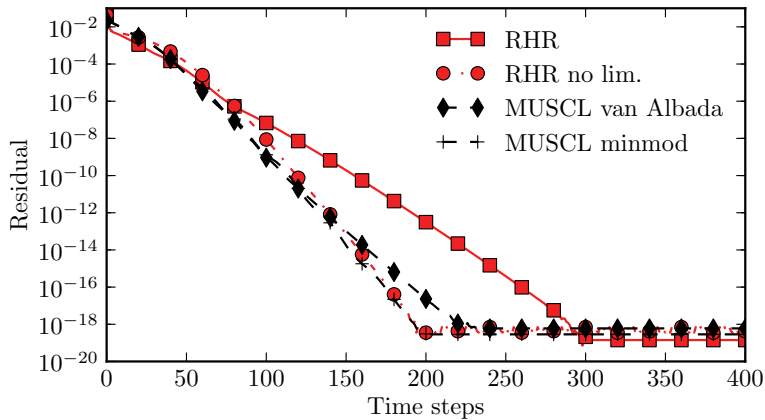
Figure 9: L^1 norm of the residual as a function of the number of time steps for a case with advection of a cosine shaped scalar profile, for a 10×10 grid, $C = 0.3$.

4.3.2. RHR compared to upwind and MUSCL

In this section we present results for scalar linear advection of a Gaussian curve, given by Eq. (16), in order to illustrate the good properties of the RHR solver when it comes to transport in directions oblique to the grid lines. Figure 10 shows results calculated with a first-order upwind method, a MUSCL upwind scheme with van Albada limiter, and the RHR solver with limiter. The RHR solver is seen to be less diffusive than the other two methods, which is also illustrated by the scalar cross-section profiles shown in Fig. 10d.

(a) Upwind.

(b) MUSCL with van Albada limiter.

(c) RHR solver with limiter.

(d) Cross-section at $x = 35.1$ for the three numerical solutions, together with the exact solution.
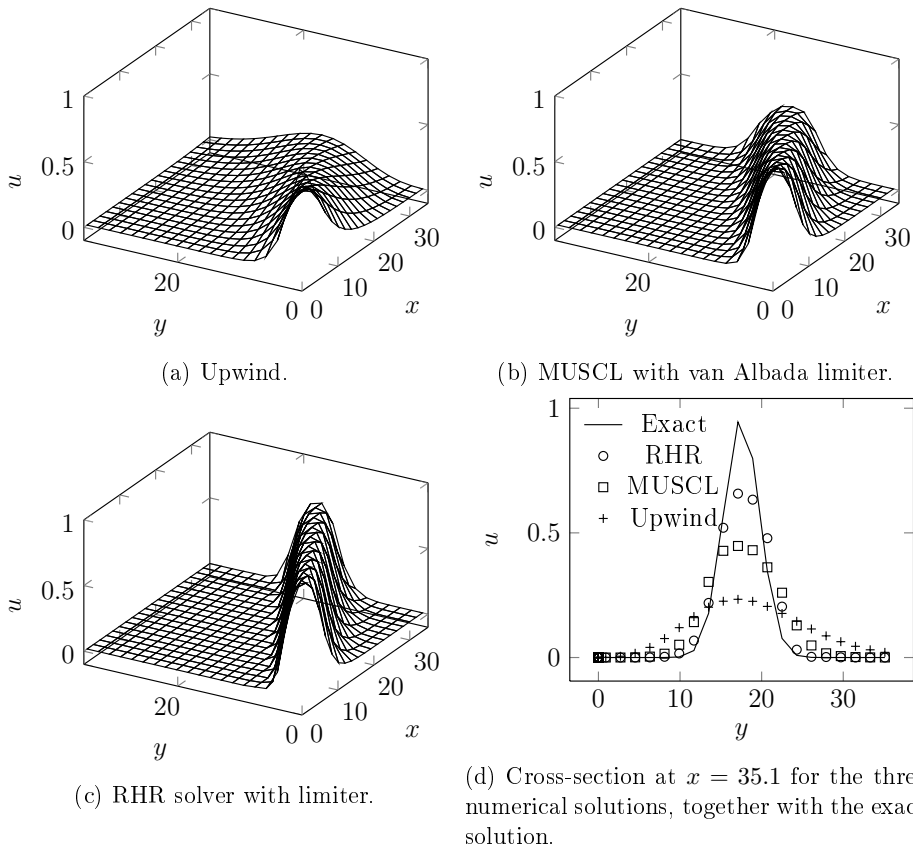
Figure 10: Advection of a scalar Gaussian profile (16) with velocity $(a, b)^\top = (1, 0.5)^\top$, on a 20×20 grid with $\Delta x = \Delta y = 1.8$.

When it comes to the computational cost of each time step for the RHR scheme, it is not expected to be significantly bigger than for the MUSCL scheme, as solving the RHR relations (10)–(13) only involves solving two simple linear equations.

4.4. Isothermal Euler

As a slightly more complex numerical example, we now present results for the two-dimensional isothermal Euler equations,

$$\frac{\partial}{\partial t} \begin{bmatrix} \rho \\ \rho u \\ \rho v \end{bmatrix} + \frac{\partial}{\partial x} \begin{bmatrix} \rho u \\ \rho u^2 + p \\ \rho u v \end{bmatrix} + \frac{\partial}{\partial y} \begin{bmatrix} \rho v \\ \rho u v \\ \rho v^2 + p \end{bmatrix} = \mathbf{0}, \tag{48}$$

where ρ is the density, and u and v are velocity components in the x- and y-directions, respectively. We close the system with a simple equation of state, $p = \rho c^2$, where c is the constant speed of sound. In the following we first show how the RHR relations are solved for the isothermal Euler equations, followed by a derivation of the characteristic solver used to solve the resulting Riemann problems. Finally, we present numerical results for a manufactured steady solution demonstrating second order.

4.4.1. Solving the RHR relations

To calculate the half-states $\boldsymbol{u}_{i,j,\mathrm{E}}$, $\boldsymbol{u}_{i,j,\mathrm{W}}$, $\boldsymbol{u}_{i,j,\mathrm{S}}$ and $\boldsymbol{u}_{i,j,\mathrm{N}}$ based on $\boldsymbol{q}_{x,i,j}$ and $\boldsymbol{q}_{y,i,j}$, we need to solve the RHR relations given by Eqs. (10)–(13). This is a straightforward process for the advection equation we have considered so far, but slightly more complex for the isothermal Euler equations.

In the following, we only consider the solution procedure for $\boldsymbol{u}_{i,j,\mathrm{E}}$, as the procedure for $\boldsymbol{u}_{i,j,\mathrm{N}}$ is completely analogous. The states $\boldsymbol{u}_{i,j,\mathrm{W}}$ and $\boldsymbol{u}_{i,j,\mathrm{S}}$ are then given by Eqs. (10)–(11). Using Eq. (10), we replace $\boldsymbol{u}_{i,j,\mathrm{W}}$ in Eq. (12), which then reads

$$\frac{1}{\Delta x}(\boldsymbol{f}(\boldsymbol{u}_{\mathrm{E}}) - \boldsymbol{f}(2\boldsymbol{u} - \boldsymbol{u}_{\mathrm{E}})) = \boldsymbol{q}_x, \tag{49}$$

where we have omitted the spatial indices i and j. The flux function $\boldsymbol{f}$ is given by

$$\boldsymbol{f}(\boldsymbol{u}) = \begin{bmatrix} \rho u \\ \rho(u^2 + c^2) \\ \rho u v \end{bmatrix} = \begin{bmatrix} u_2 \\ u_2^2/u_1 + u_1 c^2 \\ u_2 u_3/u_1 \end{bmatrix}, \tag{50}$$

where $u_1 = \rho$, $u_2 = \rho u$ and $u_3 = \rho v$. Substitution into Eq. (49) leads to

$$\begin{bmatrix} u_{2,\mathrm{E}} \\ u_{2,\mathrm{E}}^2/u_{1,\mathrm{E}} + u_{1,\mathrm{E}} c^2 \\ u_{2,\mathrm{E}} u_{3,\mathrm{E}}/u_{1,\mathrm{E}} \end{bmatrix} - \begin{bmatrix} 2u_2 - u_{2,\mathrm{E}} \\ (2u_2 - u_{2,\mathrm{E}})^2/(2u_1 - u_{1,\mathrm{E}}) + (2u_1 - u_{1,\mathrm{E}})c^2 \\ (2u_2 - u_{2,\mathrm{E}})(2u_3 - u_{3,\mathrm{E}})/(2u_1 - u_{1,\mathrm{E}}) \end{bmatrix} = \Delta x \boldsymbol{q}_x. \tag{51}$$

The first component of Eq. (51) is easily solved for $u_{2,\mathrm{E}}$, i.e.

$$u_{2,\mathrm{E}} = \frac{\Delta x}{2} q_{x,1} + u_2. \tag{52}$$

Next, we solve the second component of Eq. (51) for $u_{1,\mathrm{E}}$. After substituting $\xi = u_1 - u_{1,\mathrm{E}}$ one obtains the cubic equation

$$\xi^3 + \frac{\Delta x q_{x,2}}{2c^2}\xi^2 + \frac{2u_{2,\mathrm{E}}^2 - 2u_1^2 c^2 + 4u_2(u_2 - u_{2,\mathrm{E}})}{2c^2}\xi + \frac{-4u_2 u_1(u_2 - u_{2,\mathrm{E}}) - \Delta x q_{x,2} u_1^2}{2c^2} = 0 \tag{53}$$

19

for ξ. This equation may be solved either exactly using an analytical approach, or numerically using Newton's method. Having found ξ and thus $u_{1,\mathrm{E}}$, one can calculate $u_{3,\mathrm{E}}$ using the third component of Eq. (51) and obtains

$$u_{3,\mathrm{E}} = \frac{\frac{(2u_2 - u_{2,\mathrm{E}})2u_3}{2u_1 - u_{1,\mathrm{E}}} + \Delta x q_{x,3}}{\frac{u_{2,\mathrm{E}}}{u_{1,\mathrm{E}}} + \frac{(2u_2 - u_{2,\mathrm{E}})}{2u_1 - u_{1,\mathrm{E}}}}. \tag{54}$$

In summary, Eqs. (52)–(54) yield $\boldsymbol{u}_{i,j,\mathrm{E}}$, and similarly $\boldsymbol{u}_{i,j,\mathrm{N}}$ can be calculated.

4.4.2. Characteristic solver

Here a characteristic-based Riemann solver, similar to the one by Sesterhenn et al. [22, 23], is employed, which is explained next. To derive the characteristic quantities, we consider the isothermal Euler equations in one dimension, written in the quasi-linear form

$$\begin{bmatrix} \rho \\ \rho u \end{bmatrix}_t + \underbrace{\begin{bmatrix} 0 & 1 \\ c^2 - u^2 & 2u \end{bmatrix}}_{\boldsymbol{J}} \begin{bmatrix} \rho \\ \rho u \end{bmatrix}_x = 0. \tag{55}$$

We now rewrite this system to formulate it using the primitive variables $\boldsymbol{v} = [\rho, u]^\top$,

$$\begin{bmatrix} \rho \\ u \end{bmatrix}_t + \underbrace{\begin{bmatrix} u & \rho \\ \frac{c^2}{\rho} & u \end{bmatrix}}_{\boldsymbol{J}'} \begin{bmatrix} \rho \\ u \end{bmatrix}_x = 0. \tag{56}$$

The eigenvalues of the Jacobian matrix $\boldsymbol{J}'$ are $\lambda_1 = u - c$ and $\lambda_2 = u + c$. Solving for the eigenvectors of $\boldsymbol{J}'$ yields the right eigenvector matrix

$$\boldsymbol{R}(u) = \begin{bmatrix} \rho & \rho \\ -c & c \end{bmatrix}. \tag{57}$$

We then determine the inverse (left eigenvector) matrix $\boldsymbol{R}^{-1}$ and multiply $\boldsymbol{R}_0^{-1} = \boldsymbol{R}^{-1}(\boldsymbol{v}_0)$ by the primitive variables $\boldsymbol{v} = [\rho, u]^\top$, which yields the characteristic variables

$$\boldsymbol{w} = \boldsymbol{R}_0^{-1}\boldsymbol{u} = \frac{1}{2\rho_0 c} \begin{bmatrix} c & -\rho_0 \\ c & \rho_0 \end{bmatrix} \begin{bmatrix} \rho \\ u \end{bmatrix} = \frac{1}{2\rho_0 c} \begin{bmatrix} \rho c - \rho_0 u \\ \rho c + \rho_0 u \end{bmatrix}, \tag{58}$$

where we have evaluated the matrix $\boldsymbol{R}_0^{-1} = \boldsymbol{R}^{-1}(\boldsymbol{v}_0)$ at some point of linearization $\boldsymbol{v} = \boldsymbol{v}_0$.

In the context of Fig. 11, we calculate the state in the region C by assuming that the characteristic variables are constant along the solid lines from the regions L and R to region C. The dashed lines are the waves resulting from the Riemann problem. From Eq. (58) we then derive the approximate relations

$$\rho_\mathrm{R} c - \rho_\mathrm{C} u_\mathrm{R} = \rho_\mathrm{C} c - \rho_\mathrm{C} u_\mathrm{C}, \tag{59}$$

$$\rho_\mathrm{L} c + \rho_\mathrm{C} u_\mathrm{L} = \rho_\mathrm{C} c + \rho_\mathrm{C} u_\mathrm{C}, \tag{60}$$
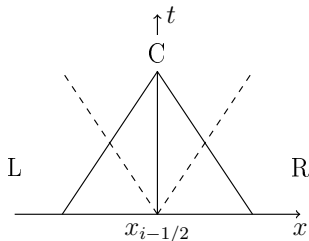
Figure 11: A Riemann problem at $x_{i-1/2}$ giving rise to two waves, shown by dashed lines. The characteristics are shown by solid lines.

which follows from the fact that the characteristic variables (58) are constant along the characteristics, shown by solid lines in Figure 11. Here we have chosen to linearize w_1 and w_2 around $\boldsymbol{u}_0 = \boldsymbol{u}_{\mathrm{C}}$. Solving these two relations for u_{C} and ρ_{C} yields

$$\rho_{\mathrm{C}} = \frac{c(\rho_{\mathrm{R}} + \rho_{\mathrm{L}})}{2c + u_{\mathrm{R}} - u_{\mathrm{L}}}, \tag{61}$$

$$u_{\mathrm{C}} = \frac{c(\rho_{\mathrm{L}} - \rho_{\mathrm{R}}) + \rho_{\mathrm{C}} u_{\mathrm{R}} + \rho_{\mathrm{C}} u_{\mathrm{L}}}{2\rho_{\mathrm{C}}}. \tag{62}$$

In two dimensions, the velocity component parallel to the face is simply advected from the upwind side, i.e. $v_{\mathrm{C}} = v_{\mathrm{L}}$ if $u_{\mathrm{C}} > 0$, and $v_{\mathrm{C}} = v_{\mathrm{R}}$ if $u_{\mathrm{C}} < 0$. The Riemann flux is then given by $\boldsymbol{f}(\boldsymbol{u}_{\mathrm{C}})$.

We have now derived a characteristic Riemann solver for the isothermal Euler equations. This works well for small Mach numbers, but can be replaced with an exact Riemann solver or e.g. Roe's approximate Riemann solver for higher Mach numbers.

4.4.3. Order of convergence

To check the order of convergence of the RHR solver for the isothermal Euler equations, we apply the solver to a problem with a manufactured solution. For the solution we make the ansatz

$$\rho = \rho_0 \exp[\frac{-\frac{1}{2}(x^2 + y^2)B^2}{c^2}], \tag{63}$$

$$u = Bx, \tag{64}$$

$$v = -By, \tag{65}$$

where B and ρ_0 are some constants; here we chose $B = 0.1$ and $\rho_0 = 1.0$. For the speed of sound, we chose $c = 1.0$. We then insert this into the (steady) isothermal Euler equations to find the source terms that result from the presented ansatz.

$$\frac{\partial}{\partial x} \begin{bmatrix} \rho u \\ \rho(u^2 + c^2) \\ \rho uv \end{bmatrix} + \frac{\partial}{\partial y} \begin{bmatrix} \rho v \\ \rho uv \\ \rho(v^2 + c^2) \end{bmatrix} = \begin{bmatrix} \rho \\ \rho u \\ \rho v \end{bmatrix} \frac{B}{c^2}(v^2 - u^2) \equiv \boldsymbol{q}. \tag{66}$$

21

We have now derived a manufactured solution with a corresponding source term, which we use to analyze the order of convergence. The potential flow field specified by Eqs. (64)–(65) is illustrated in Figure 12. When we solve this case numerically, the solution in Eqs. (63)–(65) is used to set the boundary conditions exactly on all boundaries, while the source term $\boldsymbol{q}$ is computed from Eq. (66) in all cells. The numerical solution is then compared with the exact solution to calculate the error.
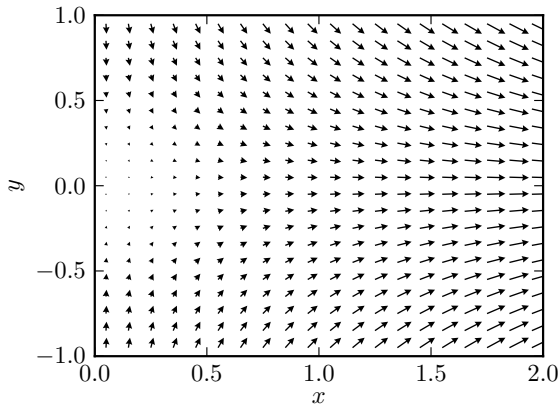
Figure 12: Velocity field for the 2D isothermal Euler case.

Figure 13 shows the L^2 error for density, $\|\rho - \rho_{\text{exact}}\|_2$, as function of grid size n for a $n \times n$ grid, which demonstrates second order convergence for both the MUSCL upwind scheme with minmod and MC limiters, and the RHR solver with limiter. The error of the RHR solver is clearly smaller that the error of the MUSCL MC scheme, and almost one order of magnitude smaller than that of the MUSCL minmod scheme.

Figure 14 shows the L^1 norm of the residual as a function of the number of time steps for the same case, which shows that all the schemes converge to machine accuracy. The RHR scheme converges slower than the MUSCL scheme, which can (at least in part) be explained by the fact that the time-stepping scheme for the RHR solver is not formally of second order.

When it comes to the computational cost of each time step, the RHR scheme is expected to be slightly more costly than a MUSCL scheme, since solving the RHR relations (10)–(13) involves (among other operations) solving a cubic equation (53), which may be costly. One might be able to linearize this cubic equation in some way, thereby reducing the cost for solving it.

4.5. Shallow water

The shallow water equations may include source terms due to bottom topography and bottom friction. Those source terms have been an important motivation to develop well-balanced methods. In this section, however, we will focus on solving the homogeneous
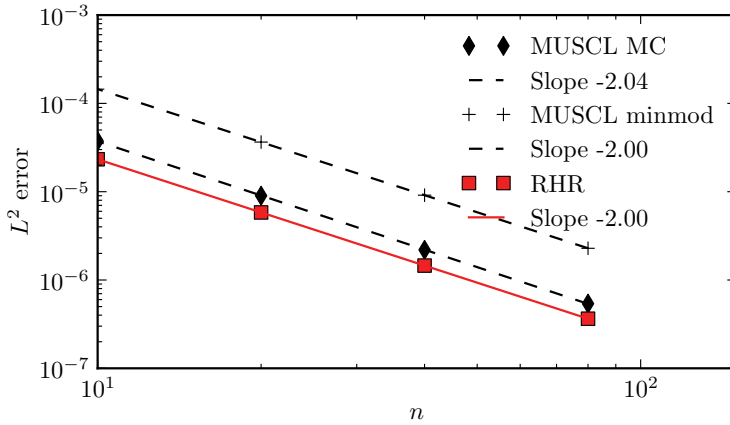
Figure 13: Grid convergence of the L^2 error of density for the 2D isothermal Euler equations.
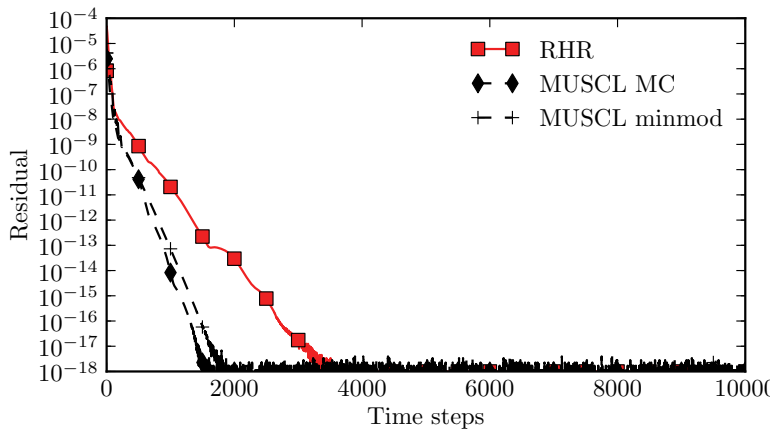
Figure 14: L^1 norm of the residual as the function of the number of time steps for the 2D isothermal Euler equations, 10×10 grid, $C = 0.3$.

shallow water equations to demonstrate how the RHR solver performs to maintain a flux balance in the steady state. The homogeneous shallow water equations read

$$\frac{\partial}{\partial t} \begin{bmatrix} h \\ hu \\ hv \end{bmatrix} + \frac{\partial}{\partial x} \begin{bmatrix} hu \\ hu^2 + \frac{1}{2}gh^2 \\ huv \end{bmatrix} + \frac{\partial}{\partial y} \begin{bmatrix} hv \\ huv \\ hv^2 + \frac{1}{2}gh^2 \end{bmatrix} = \mathbf{0}. \tag{67}$$

where h is the water height above the bottom surface, and u and v are velocity components in the x- and y-directions, respectively. In the following we first show how the RHR relations are solved, derive a characteristic solver, and then present numerical results for a steady case demonstrating the order of convergence.

4.5.1. Solving the RHR relations

To calculate the half-states $\boldsymbol{u}_{i,j,\mathrm{E}}$, $\boldsymbol{u}_{i,j,\mathrm{W}}$, $\boldsymbol{u}_{i,j,\mathrm{S}}$, $\boldsymbol{u}_{i,j,\mathrm{N}}$, we need to solve the RHR relations (10)–(13). For the shallow water equations we choose to linearize these relations. By writing $\boldsymbol{u}_\mathrm{E} = \boldsymbol{u} + \boldsymbol{\epsilon}$ and replacing $\boldsymbol{u}_\mathrm{W}$ using Eq. (10), we can write Eq. (12) as

$$\boldsymbol{f}(\boldsymbol{u} + \boldsymbol{\epsilon}) - \boldsymbol{f}(\boldsymbol{u} - \boldsymbol{\epsilon}) = \Delta x \boldsymbol{q}_x. \tag{68}$$

We then linearize this equation, which yields

$$\boldsymbol{f}'(\boldsymbol{u})\boldsymbol{\epsilon} = \frac{\Delta x}{2} \boldsymbol{q}_x \tag{69}$$

where $\boldsymbol{f}'(\boldsymbol{u})$ is the Jacobian of $\boldsymbol{f}(\boldsymbol{u})$,

$$\boldsymbol{f}'(\boldsymbol{u}) = \begin{bmatrix} 0 & 1 & 0 \\ -\frac{u_2^2}{u_1^2} + gu_1 & 2\frac{u_2}{u_1} & 0 \\ -\frac{u_2 u_3}{u_1^2} & \frac{u_3}{u_1} & \frac{u_2}{u_1} \end{bmatrix} = \begin{bmatrix} 0 & 1 & 0 \\ -u^2 + gh & 2u & 0 \\ -uv & v & u \end{bmatrix} \tag{70}$$

The first component of the equation system (69) can easily be solved for ϵ_2,

$$\epsilon_2 = \Delta x \frac{q_{x,1}}{2}. \tag{71}$$

We then solve for ϵ_1 from the second component of (69),

$$\epsilon_1 = \frac{1}{-u^2 + gh}(\Delta x \frac{q_{x,2}}{2} - 2u\epsilon_2) \tag{72}$$

Finally, the third component of (69) can be solved for ϵ_3,

$$\epsilon_3 = \frac{1}{u}\Delta x \frac{q_{x,3}}{2} + v\epsilon_1 - \frac{v}{u}\epsilon_2. \tag{73}$$

Should u be zero, the Jacobian matrix $\boldsymbol{f}'(\boldsymbol{u})$ is singular, and this final equation cannot be solved, in which case we assume ϵ_3 to be zero. The same applies to $u = \pm\sqrt{gh}$, in which case we must assume $\epsilon_1 = 0$. Having solved for $\boldsymbol{\epsilon}$, we can then calculate $\boldsymbol{u}_\mathrm{E}$ and $\boldsymbol{u}_\mathrm{W}$, and a similar procedure is used to calculate $\boldsymbol{u}_\mathrm{N}$ and $\boldsymbol{u}_\mathrm{S}$.

4.5.2. Characteristic solver

For the shallow water equations, we employ a characteristic based Riemann solver, similar to the one presented in Section 4.4.2. To derive the characteristic quantities, we consider the shallow water equations in one dimension, written in the quasi-linear form

$$\begin{bmatrix} h \\ hu \end{bmatrix}_t + \underbrace{\begin{bmatrix} 0 & 1 \\ gh - u^2 & 2u \end{bmatrix}}_{\boldsymbol{J}} \begin{bmatrix} h \\ hu \end{bmatrix}_x = 0. \tag{74}$$

We then rewrite this system to a one formulated using the primitive variables $\boldsymbol{v} = [h, u]^\top$,

$$\begin{bmatrix} h \\ u \end{bmatrix}_t + \underbrace{\begin{bmatrix} u & h \\ g & u \end{bmatrix}}_{\boldsymbol{J}'} \begin{bmatrix} h \\ u \end{bmatrix}_x = 0. \tag{75}$$

The eigenvalues of the Jacobian matrix $\boldsymbol{J}'$ are $\lambda_1 = u - \sqrt{gh}$ and $\lambda_2 = u + \sqrt{gh}$. We recognize that the quasi-linear formulation of the shallow water equations is identical to that of the isothermal Euler equations if we only replace c by $\sqrt{gh}$. As in Section 4.4.2, we derive the characteristic variables

$$\boldsymbol{w} = \boldsymbol{R}_0^{-1}\boldsymbol{v} = \frac{1}{2h_0\sqrt{gh_0}} \begin{bmatrix} \sqrt{gh_0} & -h_0 \\ \sqrt{gh_0} & h_0 \end{bmatrix} \begin{bmatrix} h \\ u \end{bmatrix} = \frac{1}{2h_0\sqrt{gh_0}} \begin{bmatrix} h\sqrt{gh_0} - h_0u \\ h\sqrt{gh_0} + h_0u \end{bmatrix}, \tag{76}$$

where we have evaluated the matrix $\boldsymbol{R}_0^{-1} = \boldsymbol{R}^{-1}(\boldsymbol{v}_0)$ at some point of linearization $\boldsymbol{v} = \boldsymbol{v}_0$. From Eq. (76) we then derive the approximate relations

$$h_{\mathrm{C}}\sqrt{gh_{\mathrm{R}}} - h_{\mathrm{R}}u_{\mathrm{C}} = h_{\mathrm{R}}\sqrt{gh_{\mathrm{R}}} - h_{\mathrm{R}}u_{\mathrm{R}}, \tag{77}$$

$$h_{\mathrm{C}}\sqrt{gh_{\mathrm{L}}} + h_{\mathrm{L}}u_{\mathrm{C}} = h_{\mathrm{L}}\sqrt{gh_{\mathrm{L}}} + h_{\mathrm{L}}u_{\mathrm{L}}, \tag{78}$$

where we have linearized w_1 and w_2 at the right and left state, $\boldsymbol{v}_{\mathrm{R}}$ and $\boldsymbol{v}_{\mathrm{L}}$, respectively. We solve Eqs. (77) and (78) for h_{C} and u_{C},

$$h_{\mathrm{C}} = \frac{\sqrt{h_{\mathrm{L}}h_{\mathrm{R}}}(u_{\mathrm{L}} - u_{\mathrm{R}} + \sqrt{gh_{\mathrm{R}}} + \sqrt{gh_{\mathrm{L}}})}{\sqrt{gh_{\mathrm{R}}} + \sqrt{gh_{\mathrm{L}}}}, \tag{79}$$

$$u_{\mathrm{C}} = \frac{gh_{\mathrm{L}} - gh_{\mathrm{R}} + \sqrt{gh_{\mathrm{R}}}u_{\mathrm{R}} + \sqrt{gh_{\mathrm{L}}}u_{\mathrm{L}}}{\sqrt{gh_{\mathrm{R}}} + \sqrt{gh_{\mathrm{L}}}}. \tag{80}$$

In two dimensions, the velocity component parallel to the face is simply advected from the upwind side, i.e. $v_{\mathrm{C}} = v_{\mathrm{L}}$ if $u_{\mathrm{C}} > 0$, and $v_{\mathrm{C}} = v_{\mathrm{R}}$ if $u_{\mathrm{C}} < 0$. The Riemann flux is then given by $\boldsymbol{f}(\boldsymbol{u}_{\mathrm{C}})$.

4.5.3. Order of convergence

To demonstrate the order of convergence of the RHR solver for the shallow water equations, we apply the solver to a manufactured solution. We make the ansatz

$$h = h_0 - \frac{B^2 x^2}{2g} - \frac{B^2 y^2}{2g}, \tag{81}$$

$$u = Bx, \tag{82}$$

$$v = -By, \tag{83}$$

where B and h_0 are some constants; here we chose $B = 0.1$ and $\rho_0 = 1.0$. By inserting this ansatz into the steady shallow water equations, we find the source terms associated with this manufactured solution.

$$\frac{\partial}{\partial x} \begin{bmatrix} hu \\ hu^2 + \frac{1}{2}gh^2 \\ huv \end{bmatrix} + \frac{\partial}{\partial y} \begin{bmatrix} hv \\ huv \\ hv^2 + \frac{1}{2}gh^2 \end{bmatrix} = \begin{bmatrix} 1 \\ Bx \\ -By \end{bmatrix} \frac{B^3}{g}(y^2 - x^2) \equiv \boldsymbol{q}. \tag{84}$$

We will now use the given manufactured solution with the corresponding source term to investigate the order of convergence. We use the exact solution (81)–(83) to set the boundary conditions on all boundaries, while the source term $\boldsymbol{q}$ is computed from Eq. (84) in all cells. The numerical solution is then compared with the exact solution to calculate the error.

Figure 15 shows the L^2 error for height, $\|h - h_{\text{exact}}\|_2$, as a function of grid size n for a $n \times n$ grid, which demonstrates a second order convergence for both the MUSCL scheme with MC and minmod limiter, and the RHR solver with limiter. The picture is very similar to that in Fig. 13: The error of the RHR solver is systematically smaller than that of the MUSCL MC scheme, and almost one order of magnitude smaller than that of the MUSCL minmod scheme.

Figure 16 shows the L^1 norm of the residual as a function of the number of time steps for the same case. The RHR converges slower than the MUSCL scheme, similar to what was seen in Fig. 14. We assume this to be due to the fact that the time stepping scheme is not formally of second order for the RHR solver, since the fluxes depend on the fluxes in the previous time step.

When it comes to the computational cost of each time step, the RHR scheme is expected to be only slightly more expensive than the MUSCL scheme, since the RHR solver has the extra cost of solving the RHR relations (10)–(13), which involves solving the three linear equations (71)–(73) for the eastern/western states, and three equivalent ones for the northern/southern states.

5. Conclusion and further work

We have developed a *Rankine-Hugoniot-Riemann* (RHR) solver for steady multidimensional conservation laws with source terms. The cross fluxes are treated as source terms, which are distributed as singular sources in the middle of each cell, leading to a jump in

26
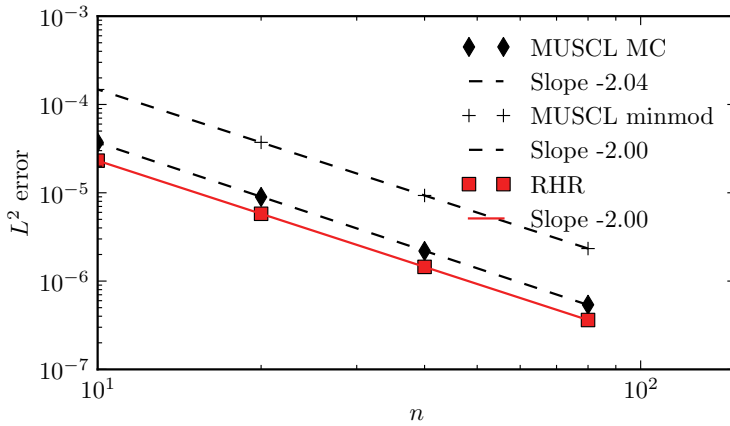
Figure 15: Grid convergence of the L^2 error of height for the 2D shallow water equations.
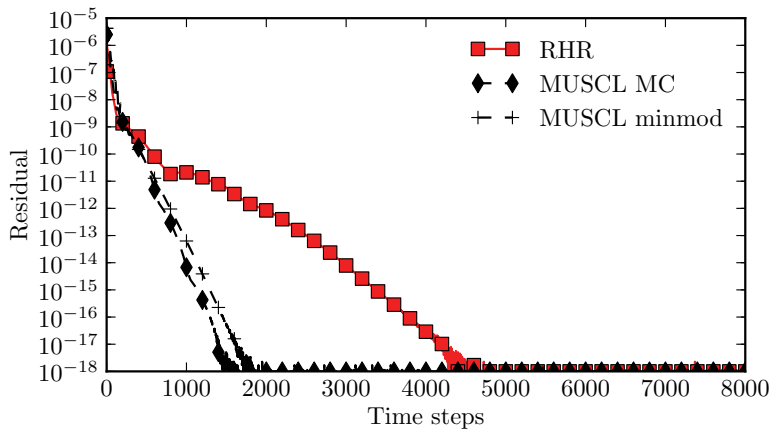
Figure 16: Residual as a function of number of time steps for the 2D shallow water equations.

the solution given by a Rankine-Hugoniot condition. The resulting Riemann problems at the cell faces are then solved using a standard Riemann solver. In contrast to many other schemes treating multidimensionality and source terms, there is no need for special Riemann solvers. We introduced a limiting procedure similar to a total variation diminishing (TVD) enforcement, to avoid instabilities.

We were able to prove that on rectangular grids, the RHR solver yields a second order accurate numerical solution for the 2D linear advection equation with a linear source term, and that the solution can be advected exactly if the advection velocity is diagonal on the grid. We have also investigated the properties of the RHR solver numerically, which confirmed that the scheme is of second order both for the 2D linear advection equation, the 2D isothermal Euler equations and the 2D shallow water equations. Furthermore, the RHR solver has an error which is smaller than that of a second-order MUSCL scheme for these cases.

The stencil of the RHR scheme has the advantage of being compact, as the numerical fluxes of a cell only depend on the numerical solutions of the cell and its neighbours which have a face or a corner in common with the cell. The basic ideas outlined here for the isothermal Euler equations and shallow water equations should carry over to other conservation laws with source terms, such as the full Euler equations or two-phase flow equations.

Acknowledgements

References

[1] P. Jenny, B. Müller, Rankine–Hugoniot–Riemann solver considering source terms and multidimensional effects, J. Comput. Phys. 145 (1997) 575–610.

[2] H. B. Stewart, B. Wendroff, Two-phase flow: Models and methods, J. Comput. Phys. 56 (1984) 363–409.

[3] H. Lund, P. Aursand, Two-phase flow of CO_2 with phase transfer, Energy Procedia 23 (2012) 246–255.

[4] L. Gosse, A well-balanced flux-vector splitting scheme designed for hyperbolic systems conservation laws with source terms, Comput. Math. Appl. 39 (2000) 135–159.

[5] R. Saurel, F. Petitpas, R. Abgrall, Modelling phase transition in metastable liquids: application to cavitating and flashing flows, J Fluid Mech 607 (2008) 313–350.

[6] R. J. LeVeque, Balancing source terms and flux gradients in high-resolution Godunov methods: The quasi-steady wave-propagation algorithm, J. Comput. Phys. 146 (1998) 346–365.

[7] D. S. Bale, R. J. LeVeque, S. Mitran, J. Rossmanith, A wave-propagation method for conservation laws and balance laws with spatially varying flux functions, SIAM J. Sci. Comput. 24 (3) (2002) 955–978.

[8] R. J. LeVeque, D. S. Bale, Wave propagation methods for conservation laws with source terms, in: International Series of Numerical Mathematics, Vol. 130, Birkhäuser, 1999.

[9] R. J. LeVeque, Finite Volume Methods for Hyperbolic Problems, Cambridge University Press, 2002.

[10] A. Bermudez, M. E. Vazquez, Upwind methods for hyperbolic conservation laws with source terms, Comput. Fluids 23 (8) (1994) 1049–1071.

[11] R. Donat, A. Martinez-Gavara, Hybrid second order schemes for scalar balance laws, J. Sci. Comput. 48 (2011) 52–69.

[12] M. E. Hubbard, P. García-Navarro, Flux difference splitting and the balancing of source terms and flux gradients, J. Comput. Phys. 165 (2000) 89–125.

[13] R. J. LeVeque, A well-balanced path-integral f-wave method for hyperbolic problems with source terms, J. Sci. Comput. 48 (2011) 209–226.

[14] J. Murillo, P. García-Navarro, Weak solutions for partial differential equations with source terms: Application to the shallow water equations, J. Comput. Phys. 229 (2010) 4327–4368.

[15] S. Noelle, N. Pankratz, G. Puppo, and J. R. Natvig, Well-balanced finite volume schemes of arbitrary order of accuracy for shallow water flows. J. Comput. Phys. 213 (2006) 474–499.

[16] S. Noelle, Y. Xing, and C.-W. Shu. High-order well-balanced finite volume WENO schemes for shallow water equation with moving water. J. Comput. Phys. 226 (2007) 29–58.

[17] S. Noelle, Y. Xing, and C.-W. Shu. High-order well-balanced schemes. In G. Puppo and G. Russo, editors, Numerical Methods for Balance Laws. Quaderni di Matematica 24 (2010), pages 1–66.

[18] Y. Xing, C.-W. Shu, and S. Noelle. On the advantage of well-balanced schemes for moving-water equilibria of the shallow water equations. J. Sci. Comput. 48 (2011) 339–349.

[19] R. J. LeVeque, M. Pelanti, A class of approximate Riemann solvers and their relation to relaxation schemes, J. Comput. Phys. 172 (2001) 572–591.

[20] F. Müller, Rankine-Hugoniot-Riemann solver for two-dimensional conservation laws, Master's thesis, ETH Zürich (2010).

[21] P. J. Roache, Verification and Validation in Computational Science and Engineering, Hermosa Publishers, Albuquerque, USA, 1998.

[22] J. Sesterhenn, B. Müller, H. Thomann, A simple characteristic flux evaluation for subsonic flow, in: 2nd ECCOMAS CFD Conf., Wiley, Chichester, 1994, p. 57.

[23] J. Sesterhenn, Zur numerischen Berechnung kompressibler Strömungen bei kleinen Mach-Zahlen, Ph.D. thesis, ETH Zürich, diss. ETH Nr. 11334 (1995).